2012

A Study On Thermal Stability Of Palladiumcomposite Membrane Fabricated By Surfactant Induced Electroless Plating (Siep)

Syed Zahadul Islam
North Carolina Agricultural and Technical State University

A STUDY ON THERMAL STABILITY OF PALLADIUM-COMPOSITE MEMBRANE FABRICATED BY SURFACTANT INDUCED ELECTROLESS PLATING (SIEP)

by

Syed Zahadul Islam

A thesis submitted to the graduate faculty
in partial fulfillment of the requirements for the degree of
MASTER OF SCIENCE

Department: Chemical & Bioengineering
Major: Chemical Engineering
Major Professor: Dr. Shamsuddin Ilias

North Carolina A&T State University
Greensboro, North Carolina
2012

School of Graduate Studies
North Carolina Agricultural and Technical State University

This is to certify that the Master's Thesis of

Syed Zahadul Islam

has met the thesis requirements of
North Carolina Agricultural and Technical State University

Greensboro, North Carolina
2012

Approved by:

_____	_____
Dr. Shamsuddin Ilias	Dr. Leonard C. Uitenham
Major Professor	Committee Member
_____	_____
Dr. Dhananjay Kumar	Dr. Leonard C. Uitenham
Committee Member	Department Chairperson

_____
Dr. Sanjiv Sarin
Associate Vice Chancellor for Research and Dean of Graduate Studies

DEDICATION

To

My Mother Fazilotunnasa

and

My Father Syed Abdul Mannan

BIOGRAPHICAL SKETCH

Syed Zahadul Islam was born on November 1, 1984, in Comilla, Bangladesh. He received his Bachelor of Science degree in Chemical Engineering in 2009 from Bangladesh University of Engineering and Technology (BUET). In fall 2010, Syed came to North Carolina A&T State University to pursue his Master of Science degree in Chemical Engineering. Upon completion of his MS degree, he plans to continue his PhD in Chemical Engineering at University of Kentucky, Lexington, KY.

ACKNOWLEDGMENT

I would like to take this opportunity to express my sincere appreciation and gratitude to my advisor Dr. Shamsuddin Ilias for his excellence in scientific guidance, insight and continuous support. It has been rewarding experience and I had tremendous personal and professional growth under Dr. Ilias' supervision.

I am also thankful to the thesis committee members Drs. Leonard C. Uitenham and Dhananjay Kumar for their support and valuable suggestions.

Analytical support from the Engineering Research Center (ERC), NCAT, is greatly appreciated with special thanks to Drs. Jag Sankar, Ram Gupta, and Zhigang Xu.

The financial support received from the US DOE-NETL grant, Award No. DE-FG08-NT000143 (Mr. Richard Dunst, DOE Program Manager) is gratefully acknowledged. I am really indebted to North Carolina A&T State University for giving me the opportunity for graduate education and research. It has been a rewarding and learning experience.

Technical supports from former graduate students of Dr. Ilias' lab, particularly Dr. Mohammad Azhar Islam, Md. Mizanur Rahman and Md. Saiful Islam were very helpful and I gratefully acknowledge that.

I am grateful to my family for the help and understanding they have granted me during school years and before. Thank you.

TABLE OF CONTENTS

LIST OF FIGURES

FIGURES **PAGE**

LIST OF TABLES

TABLES **PAGE**

LIST OF SYMBOLS

N_H	Flux (mol/m^2-s)
Q_H	Permeability (mol/m-s-psi^n)
Q_{Ho}	Pre-exponent factor (mol/m-s-psi^n)
P_f	Feed side pressure (psi)
P_p	Permeate side pressure (psi)
t	Membrane thickness (μm)
n	Pressure exponent (power index)
E	Activation energy (KJ/mol)
R	Universal gas constant (KJ/mol-K)
2θ	X-ray beam incident angle
d	Lattice spacing (Å)
a	Lattice parameter (Å)
nm	Nanometer (10^{-9} meter)
μm	Micrometer (10^{-6} meter)
Å	Angstrom (10^{-10} meter)
P_{H_2}	Partial pressure of hydrogen (MPa)
η	Hydrogen to palladium ratio (H_2:Pd)
wt%	Weight percent
L	Liquid phase
α-Fe	α Iron phase

β-Fe	β Iron phase
γ-Fe	γ Iron phase
K	1000 X magnification
kV	Kilo electron volt
KJ	Kilo joule
MPa	Mega pascal

ABSTRACT

Islam, Syed Zahadul. A STUDY ON THERMAL STABILITY OF PALLADIUM-COMPOSITE MEMBRANE FABRICATED BY SURFACTANT INDUCED ELECTROLESS PLATING (SIEP). **(Major Advisor: Dr. Shamsuddin Ilias)**, North Carolina Agricultural and Technical State University.

Thermal stability of the palladium membrane is a major challenge in hydrogen separation from mixture of gases at high temperature. To study the long term thermal stability of palladium membrane, thin, dense, and defect free Pd composite membranes on microporous stainless steel (MPSS) substrate were prepared by surfactant induced electroless plating (SIEP). Dodecyl trimethyl ammonium bromide (DTAB), a cationic surfactant was used in the Pd EP-bath. Permeability tests were carried out with hydrogen and nitrogen at temperatures and pressures in the range of 523 - 823 K and 20 - 100 psi respectively. The membranes showed good hydrogen flux and selectivity. Pd MPSS composite membrane was subject to test for long term performance and thermal cycling (573 - 723 - 573 K) at 15 psi pressure drop for 1200 hours. In another test, a Pd MPSS composite membrane with an oxide layer as an intermetallic diffusion barrier was tested for long term performance and thermal cycling (623 - 723 - 623 K) at 15 psi pressure drop for 408 hours. Both Pd membranes showed excellent hydrogen permeability and infinite selectivity during the operation period. The physical and morphological features of the membranes at pre- and post-annealing, post permeability test, and post long term thermal stability test were studied by SEM, XRD, EDS, and AFM analysis.

CHAPTER 1

INTRODUCTION

The demand for hydrogen in the application of fuel cells, petroleum refining, petrochemical operations, metallurgical processing, and semiconductor processing has been rapidly increasing. Hydrogen is used for ammonia synthesis in fertilizer industries. Hydrodealkylation, hydrodesulfurization and hydrocraking require hydrogen to upgrade the more viscous oil fractions into fuel products. Electronics manufacturing industries such as semiconductor processing use high purity hydrogen. One of the major global concerns is the impact of carbon dioxide emission on climate change. Hydrogen is an important source of energy having no gas emission [1]. Hydrogen has tremendous potential to become environmental friendly fuel in the fuel cell technologies. Electricity can be produced at over 50% efficiency in the fuel cell using hydrogen as the fuel whereas water is the only by product [2]. For automotive and stand-alone power-generation applications, PEMFC (Proton-Exchange Membrane Fuel Cell) technology is being considered a serious contender. In PEMFC, hydrogen is used as a fuel. In the aforementioned application, availability of high-purity hydrogen at a competitive price has to be assured. This has intrigued researchers all over the world in developing technologies for production and separation of hydrogen with high purity (>99.99%).

Steam reforming reaction, partial oxidation, electrolysis, and coal gasification produce hydrogen. Reforming reactions, such as steam reforming of methane, methanol, ethanol and logistic fuels, are considered important reactions for large-scale production of

hydrogen. The product of these reactions contains H_2, CO, CO_2, CH_4, and N_2 from where hydrogen needs to be separated before end use [3]. Various techniques, such as pressure swing adsorption (PSA), cryogenic distillation, or membrane separation can be used to purify hydrogen. Among those techniques, the commercially available separation techniques are PSA and cryogenic distillation processes [4]. However, these membranes are energy intensive and expensive. Membrane technology has become one of the most promising separation processes for production of ultra-high pure hydrogen (99.9999%) [2, 5-8]. Depending upon the purity and scale of production, membrane separation can provide an attractive alternative to PSA and cryogenic distillation. One of the most important advantages of using membrane separation processes is the consumption of less energy with the possibility of continuous operation [4].

Membrane can be of different metals such as palladium (Pd), nickel (Ni), platinum (Pt) and some other metals from Group III-V of the periodic table. Hydrogen can be associated, dissolved and dissociated into these metals. Among them, Pd-based membranes show high hydrogen selectivity and permeability because of high solubility and diffusivity of hydrogen into Pd lattice over wide range of temperatures [6, 7, 9-11]. Palladium membrane can be used as reactor and separator for the hydrogen producing reactions such as hydrogenation and dehydrogenation, methoxymethane reforming, methane steam reforming, water–gas shift, hydroxylation of benzene, and hydrogen peroxide synthesis [10, 12-16]. In this reactor-separator configuration, hydrogen productivity can be significantly enhanced by shifting equilibrium.

For successful commercial application of palladium based membranes, the membrane must meet several requirements. Reasonable membrane cost, high hydrogen permeance, high hydrogen selectivity over other gases, and steady and predictable performance over a long period of time under harsh conditions, resistance to poisoning by hydrogen sulfide, chlorine, carbon monoxide, and hydrocarbons, and thermal stability under thermal cycling are the major requirements. It is reported that researchers have expended much effort to acquire the requirements for the commercial application of various palladium based membranes supported on ceramic and metallic materials with high hydrogen permeance and selectivity. According to a National Energy Technology Laboratory (NETL) report, Pd membranes are stable for 10 months. Preparation of thermally and chemically stable, dense, thin, and defect free Pd-based membranes with high hydrogen permeability and selectivity still remains a challenge [10].

Many research groups have worked on numerous synthesis procedures over the period. However, membranes end up with few defects such as pinholes which reduce the hydrogen selectivity. Sometimes the Pd-films peel off from the substrate. Synthesis of dense and pinhole free Pd membrane requires thick Pd-film which eventually reduces the hydrogen throughput. To address all these issues, the control over the microstructure (grain size distribution) of Pd membrane is most important for the future success of membrane application in hydrogen production and separation. The control over the microstructure will allow one to synthesize pinhole free dense membrane with relatively thinner films [3]. Our research group has patented a process called surfactant induced electroless plating (SIEP) process in fabricating thin Pd-film in the development of

defect free Pd and Pd-alloy membranes for hydrogen separation and membrane reactor application [17]. The use of a surfactant in SIEP has provided a superb control on the grain size distribution as well as its reproducibility. It is now necessary to test the Pd membrane for thermal stability and estimate lifetime of the membrane in hydrogen separation applications. The major objectives of this study are:

Pd composite membranes on MPSS substrate were fabricated using SIEP process. The microstructure of the Pd membrane was thoroughly examined in terms of grain distribution, grain agglomeration and film characteristics. The use of a surfactant in electroless plating enhances the uniformity of the deposited film and produces finer grains. It is expected that SIEP process should achieve thinner film thickness for Pd membrane than conventional EP process. In this work, the thickness of Pd membrane fabricated by SIEP process has been investigated and found thinner in comparison with that of Pd membrane fabricated by the conventional EP process.

1. Fabricate Pd membranes on microporous stainless steel (MPSS) substrate by SIEP
2. Examine the membrane microstructure at pre- and post-annealing conditions using SEM, EDS, XRD and AFM analytical tools.
3. Test the membranes for hydrogen transport behavior at the temperature range of 250 – 550 °C and at the transmembrane pressure range of 20 – 100 psi.
4. Perform long term thermal cycling test to evaluate the membrane performance in terms of hydrogen perm-selectivity and membrane stability.

This thesis is divided into of five chapters with CHAPTER 1 as introduction. A critical review of pertinent literature is presented in CHAPTER 2. In CHAPTER 3,

materials and methods for membrane synthesis is presented. Results and discussions are presented in CHAPTER 4. Conclusions and recommendations for future works are presented in CHAPTER 5.

CHAPTER 2

LITERATURE REVIEW

2.1 Introduction

Hydrogen has been a valuable material since first artificially produced by Hohenheim via mixing of metals and strong acids and is consumed on the order of billions of cubic meters per day in various industrial fields. The use of hydrogen includes hydrodealkylation, hydrodesulfurization, and hydrocracking. Recently hydrogen got tremendous research interest because of its use as an energy carrier. Environmental problems and energy conversion efficiency has shifted the need from using fossil fuel to clean energy carrier hydrogen. Proton exchange fuel cell uses hydrogen as raw material and produces water as a byproduct which does not have environmental impact. The increasing demand of hydrogen is met from various sources such as methane steam reforming reaction, water electrolysis, partial oxidation of oil and natural gas and coal gasification.

The trends in global hydrogen production is shown in Figure 2.1 which shows a growing demand for the future [10]. Hydrogen needs to be separated from mixture of gases before its end use. There are various hydrogen separation technologies such as solvent extraction, pressure swing adsorption, cryogenic separation and membrane technology. The choice of the separation processes depends on the requirement of hydrogen purity, percent recovery, feed gas compatibility and flexibility of processes.

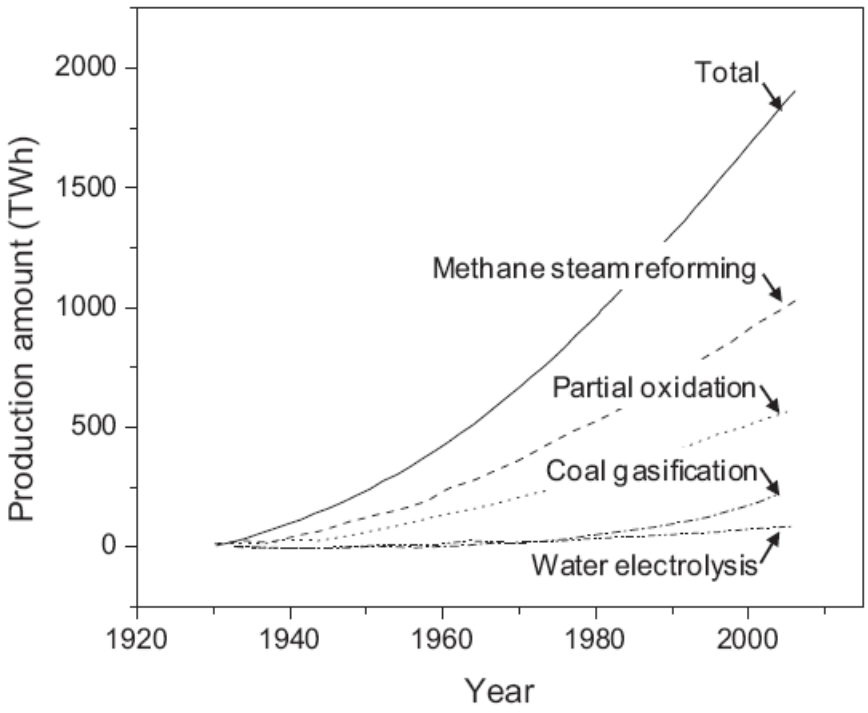

Figure 2.1. Annual global production of hydrogen [10].

A comparison of different separation processes is summarized in Table 2.1 [18]. Membranes are dominated by palladium and its alloys. Palladium has long been recognized to possess the characteristics of a membrane. It is also probably the first well-studied and documented inorganic membrane. Thomas Graham (1866) first observed the unusually high hydrogen-absorption ability of metallic palladium. It is permeable only to hydrogen. The most important property that makes palladium unique from the other metals is its ability to take large quantity of hydrogen into solid solution. Figure 2.2 shows the solubility of hydrogen in palladium along with some others [10]. At the same time, it retains a high degree of ductility. Most significantly, hydrogen has a very high diffusion rate through the lattice of palladium.

Table 2.1. Comparison of H_2 separation technologies [18]

Comparison of Hydrogen Purification Techniques						
Technique	**Principle**	**Typical Feed Gas**	**Hydrogen Output Percent**		**Scale of Use**	**Comments**
			Purity	**Recovery**		
Cryogenic Separation	Partial condensation of gas mixture at low temperatures	Petrochemical and refinery off-gases	90-98	95	Large scale	Pre purification step necessary to remove CO_2, H_2S and water
Polymer Membrane Diffusion	Differential rate of diffusion of gases through a permeable membrane	Refinery off-gases and ammonia purge gas	92-98	>85	Small to large	He, CO_2 and H_2O may also permeate the membrane
Metal Hydride Separation	Reversible reaction of hydrogen with metals to form hydrides	Ammonia purge gas	99	75-95	Small to medium	Hydrogen absorption poisoned by O_2, N_2, CO and S
Solid Polymer Electrolyte Cell	Electrolyte passage of hydrogen ions across a solid polymer membrane	Purification of H_2 by thermochemical cycles	99.8	95	Small	Sulfur-containing compounds poison the electro-catalysts
Pressure Swing Adsorption	Selective adsorption of impurities from gas stream	Any hydrogen rich gas	99.999	70-85	Large	The recovery is relatively low as hydrogen is lost in the purging step
Catalytic Purification	Removal of oxygen by catalytic reaction with hydrogen	Hydrogen streams with oxygen impurity	99.999	Up to 99	Small to large	Upgrading electrolytic H_2, organics, Pb-, Hg-, Cd- and S-compounds poison the catalyst. H_2O produced
Palladium Membrane Diffusion	Selective diffusion of hydrogen through a palladium alloy membrane	Any hydrogen containing gas stream	≥99.9999	Up to 99	Small to medium	Sulfur-containing compounds and unsaturated hydrocarbon impair permeability

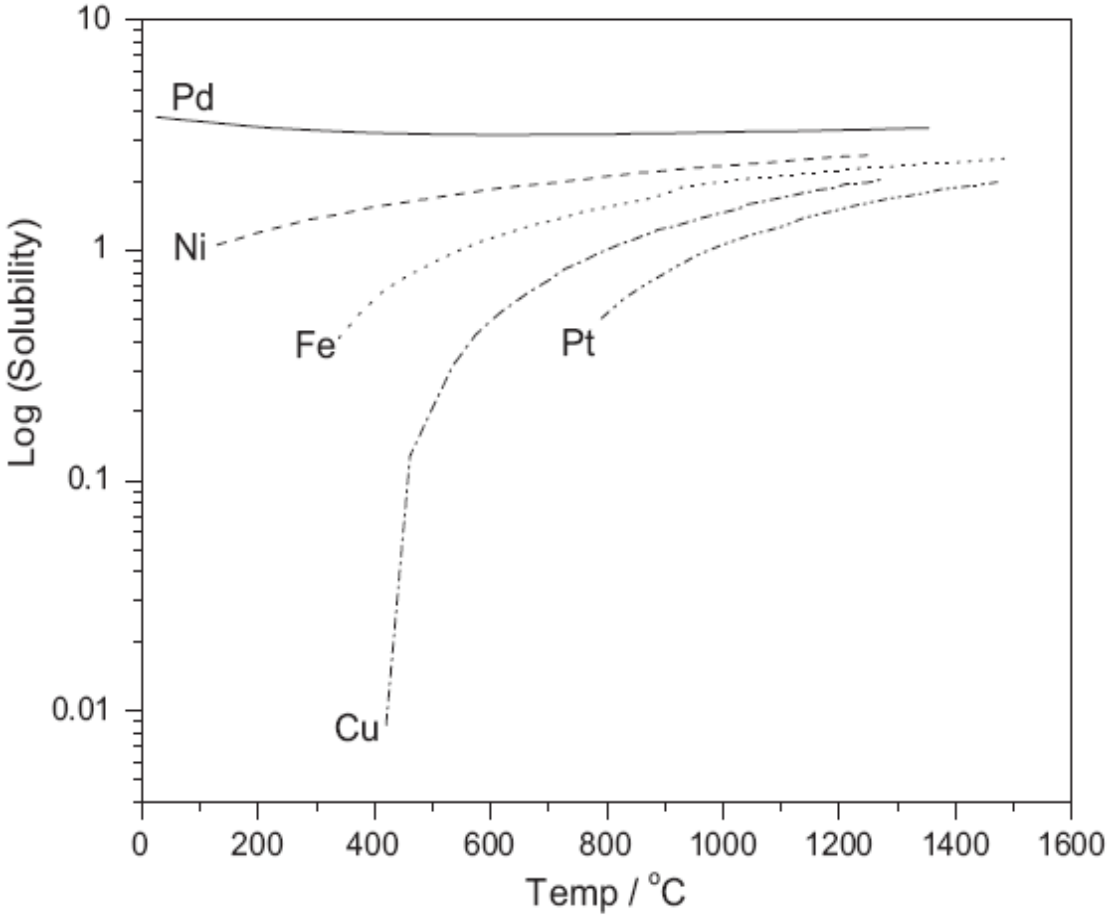

Figure 2.2. Comparison of hydrogen solubility in several metals at a pressure of 1 atm. Solubility is given in units of standard cm^3 of H_2 per 100 g of metal [10].

Palladium properties help palladium or palladium based membranes to be used as a separation unit for separating hydrogen from mixed process gases. Apart from hydrogen permeability in Pd- and Pd-alloy membranes, the permeability of all other gases (CO, CO_2, CH_4, and N_2) is so low that they are negligible in practice. Therefore, these membranes act as a highly specific filter for the production of ultra-pure hydrogen. Hydrogen transport through the Pd membranes takes place via solution diffusion mechanism. When H_2 comes in contact with the Pd-film of the membrane, Pd acts as a

catalyst and H_2 dissociates to hydrogen atom. Molecular hydrogen chemisorptions take place on the membrane surface followed by reversible dissolution of atomic hydrogen in the bulk layers of the metal. Due to the trans-membrane partial pressure gradient atomic hydrogen diffuses through the bulk metal to the other side of the membrane and reassociates to H_2 molecule. The H_2 transport mechanism through the membrane is depicted in Figure 2.3 [1, 3].

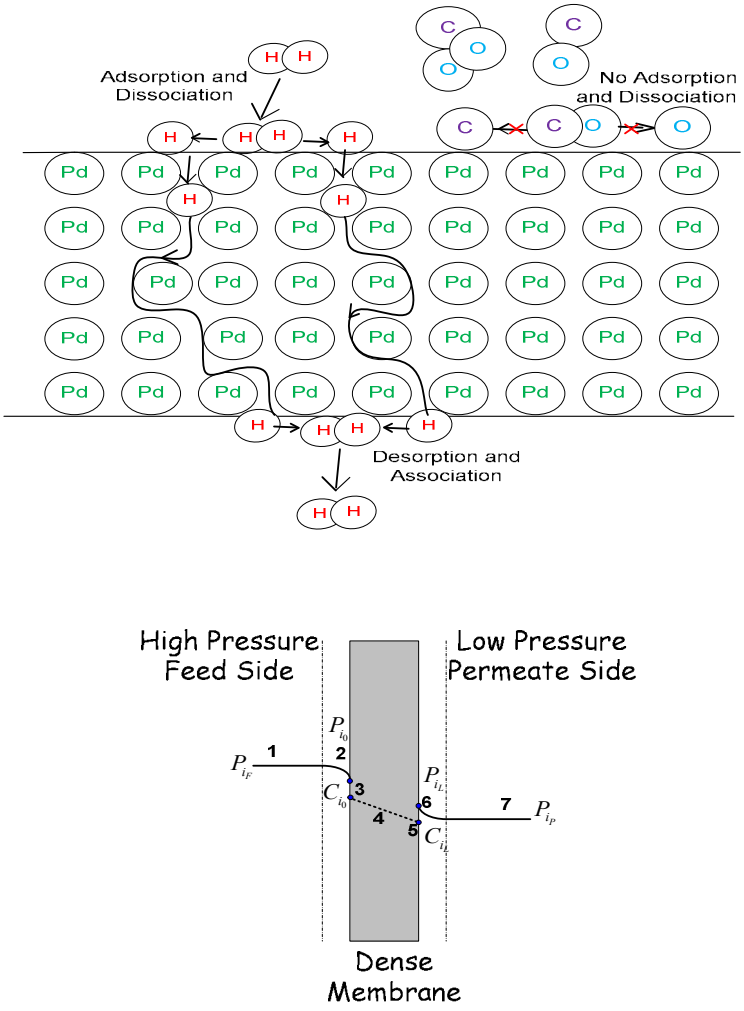

Figure 2.3. Principle of hydrogen separation through a metal membrane [3].

It is very important to understand several aspects of membrane technology, namely: I) the metallurgical properties of palladium, II) selection criteria of support material, III) the interaction of support material components with H_2 perm-selective Pd-film, IV) the effect of heat treatment on membrane film, V) the role of external mass transfer resistance and different approaches to overcome this resistance, VI) the effect of grain size on the permeability, and VII) different fabrication approaches and their effect on the membrane characteristics. The following sections give a brief discussion on the aforementioned topics.

2.2 Membrane and Membrane Processes

A membrane process requires two bulk phases physically separated by a third phase, the membrane. The membrane is an interphase between the two bulk phases. It is either a homogeneous phase or a heterogeneous collection of phases. The membrane phase is almost always thinner compared with the dimensions of the bulk phases in at least two other directions. The membrane phase controls the exchange of mass between the two bulk phases in a membrane process. In membrane separation processes, the bulk phases are mixtures of gases or liquids. One of the species in the mixture is allowed to be exchanged in preference to others. The membrane is selective to one of the species. One bulk phase is enriched in one of the species while the other is depleted of it. A membrane process then allows selective and controlled transfer of one species from one bulk phase to another bulk phase separated by the membrane [19]. The current status of membrane technology is given in Table 2.2. The merits and demerits of using different types of membrane technologies are depicted in this table.

Table 2.2. Current status of membrane technology [20]

Process	Problems			Comments
	Major	Minor	Mostly Solved	
Microfiltration	Reliability (fouling)	Cost	Selectivity	Better fouling controls could improve membrane lifetime significantly
Ultrafiltration	Reliability (fouling)	Cost	Selectivity	Fouling remains the principal operational problem. Current fouling control techniques are a substantial portion of process cost.
Reverse osmosis	Reliability	Selectivity	Cost	Incremental improvements in membrane and process design will gradually reduce costs.
Gas separation	Selectivity flux	Cost	Reliability	Membrane selectivity is the principal problem in many gas separation systems. Higher permeation rates would help to reduce costs.
Electro-dialysis	Fouling temperature Stability	Cost	Selectivity Reliability	Process reliability and selectivity are adequate for current uses. Improvements could lead to cost reduction, especially in newer applications
Pervaporation	Selectivity Reliability	Cost	-	Membrane selectivity must be improved and systems developed that can reliably operate with organic solvent feeds before major new applications are commercialized

2.3 Organic and Inorganic Membranes

The advantages of inorganic membranes have been recognized for a long time. The thermal stabilities of organic polymers, inorganic polymers and inorganic materials as membrane materials can be conveniently classified as <100 - 150 ºC, 100 - 350 °C and >350 °C, respectively. The operable temperature limits of inorganic membranes are obviously much higher than those of organic polymeric membranes. The majority of organic membranes begin to deteriorate structurally around 100 °C. A comparison of polymeric and inorganic membranes is placed in Table 2.3 where the current status, and advantages and disadvantages of using organic and inorganic membranes are described. Inorganic membranes generally can withstand organic solvents, chlorine and other chemicals better than organic membranes. Many organic membranes are susceptible to microbial attack during applications. This is not the case with inorganic types, particularly ceramic membranes. In addition, inorganic membranes in general do not suffer from the mechanical instability. It is obvious that in a high temperature or harsh chemical environment, inorganic membranes could become the only recourse to many challenging separation applications. Some inorganic membranes such as microporous alumina membranes and surface treated porous glass membranes are more fouling resistant due to their low protein adsorption. Many inorganic membranes are less susceptible to biological and microbial degradation. With ceramic and metallic membranes, it is possible to apply short bursts of permeate streams in the reverse direction through the membrane to dislodge some clogged pores of the membrane. This is referred to as backflush [21].

Table 2.3. Comparison of polymeric and inorganic membranes [22]

Membrane	Advantages	Disadvantages	Current Status
Inorganic	Long term durability	Brittle (Pd)	Small scale applications
	High thermal stability (> 200 °C)	Expensive	Surface modifications to improve hydrothermal
	Chemical stability in wide pH	Some have low hydrothermal stability	
	High structural integrity		
Polymeric	Cheap	Structurally weak, not stable	Wide applications in aqueous phase, and some gas separations
	Mass production (larger scale)	Temperature limited	
	Good quality control	Prone to denature & be contaminated (short life)	

2.4 Structure of Inorganic Membranes

Inorganic membranes have significant potential for use in a variety of processes such as gas separation, purification, and membrane reactors [23]. Membranes can be divided into two categories according to their structural characteristics which can have significant impacts on their performance as separators or reactors shown below:

1. Dense membranes
2. Porous membranes
    i) Meso porous
    ii) Micro porous.

There are two major types of dense inorganic membranes:

1. Metal membranes

2. Solid electrolyte membranes.

Structures of inorganic membranes are given in Figure 2.4. By the term dense, it is implied that there are no intentional interconnected pores in the membranes other than atomic interstices, atomic vacancies and dislocations. Such void spaces are too small to accommodate even molecular hydrogen, and dense membranes transport hydrogen only in a dissociated form. Dense membranes block transport even of helium, and the absence of larger pores gives dense membranes hydrogen selectivity approaching 100 %. Transport of hydrogen in a dissociated form implies that dense membranes must possess adequate catalytic activity for the adsorption and dissociation of H_2 on the feed-side surface (retentate) as well as for the subsequent recombination and desorption from the permeate-side surface. Dense membranes are free of discrete, well-defined pores or voids [24]. The term composite membrane, as defined in membrane technology, refers to membranes with two or more distinct layers. Composite membranes have the advantage that the separating layer and the support layer(s) can be tailored with different materials.

When the separating layer and the bulk support designed for mechanical strength are indistinguishable and show an integral, homogeneous structure and composition in the direction of the membrane thickness, it is called a symmetric or isotropic membrane. Since the flow rate through a membrane is inversely proportional to the membrane thickness, it is very desirable to make the homogeneous membrane layer as thin as possible. However, very thin stand-alone membranes typically do not exhibit mechanical integrity to withstand the usual handling procedures and processing pressure gradients found in many separation applications.

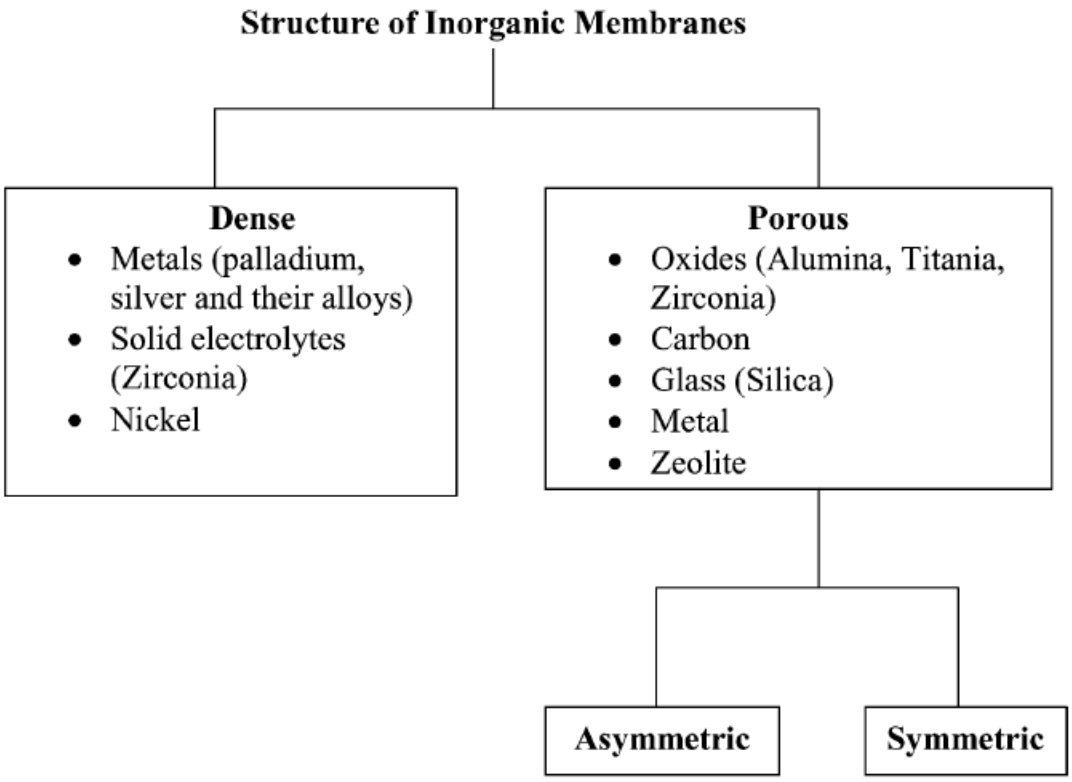

Figure 2.4. Structures of inorganic membranes [23, 25].

A practical solution to the dilemma has been the concept of an asymmetric or composite membrane where the thin, separating membrane layer and the open-cell mechanical support structure are distinctly different. In this anisotropic arrangement, separation of the species in the feed stream and ideally the majority of the flow resistance (or pressure drop) also take place primarily in the thin membrane layer. The underlying support should be mechanically strong and porous enough that it does not contribute to the flow resistance of the membrane element to any significant extent. A porous membrane can be asymmetric and symmetric. If a membrane has a graded pore structure

but is made in one processing step, frequently from the same material across its thickness, it is called an asymmetric membrane.

2.5 Gas Separation in Membranes

The transport mechanism of gas through membrane is very important since this transport mechanism is one of the determinants of the application of membrane. There are generally six possible gaseous mixtures transport mechanisms through membranes as summarized below: (a) viscous flow, (b) Knudsen diffusion, (c) surface diffusion, (d) multi-layer diffusion, (e) capillary condensation, and (f) molecular sieving. Viscous flow through the membrane is not effective for gas separation and basically no separation is achieved [22]. Knudsen diffusion is based on the mean free path of the molecules. In this mechanism, the pore radius is smaller than the gas molecule's mean free path [22]. If the mean free path of the molecules increases or the pore diameter decreases, lighter molecules will move faster than their counter heavier molecules, resulting in separation. In practice, when the pore diameter becomes less than 5 to 10 nm under pressure, Knudsen diffusion becomes the dominant transport mode.

Surface diffusion becomes important when the gas molecules are adsorbed into the surface in a significant amount. As the surface is being covered by adsorbed molecules, the molecules diffuse through the bulk of the surface due to the concentration gradients. This phenomenon is dominant when the surface area becomes large. In solution diffusion mechanism, gas is separated based on the solubility and diffusivity of the gases. Solubility selectivity favors the most condensable molecule and diffusivity selectivity favors the smallest molecule. Hydrogen transport through dense metallic

membrane follows solution diffusion mechanism. Capillary condensation occurs for some gases at relatively low temperatures when gases adjacent to the pore become liquid. If the other gases (non-condensed) cannot dissolve in the condensed gases, separation occurs. Molecular sieving occurs when the pore size is smaller than the size of any molecules present in the gases. Currently, zeolite and some carbon molecular sieves have narrow pore sizes that are capable of separating gases that differ by only about 0.02 nm [21]. In molecular sieving or activated diffusion, separation is based on the much higher diffusion rates of the smallest molecule. However, when the molecular size of the species are similar, adsorption capacities become dominant factor [22].

2.6 Metallurgical Properties of Palladium

It is important to understand the metallurgy of metal/alloy-hydrogen system for the fabrication and successful application of Pd-based membrane as a commercial separation unit. A good understanding of the metallurgy of metal/alloy-hydrogen system will lead us to know better about hydrogen diffusion technology for palladium membrane. Sieverts and his associates were the earlier researchers who pioneered the work to determine isotherms in the palladium-hydrogen system [18]. Sometime later, these data were then extended to include higher pressure and lower temperature. More recently, Shu et al. studied pressure-composition isotherm in 1991 [26]. The palladium-hydrogen phase diagram shown in Figure 2.5 describes the equilibrium pressure and temperature for bulk Pd as a function of hydrogen content [10, 27]. This Pd-H diagram is comprised of two major regions. These regions are of low and high hydrogen concentrations, which are defined as the α- and β-phases of the Pd hydride, respectively.

In the Pd-H system, α-phase increases with the equilibrium pressure at low hydrogen to palladium ratio.

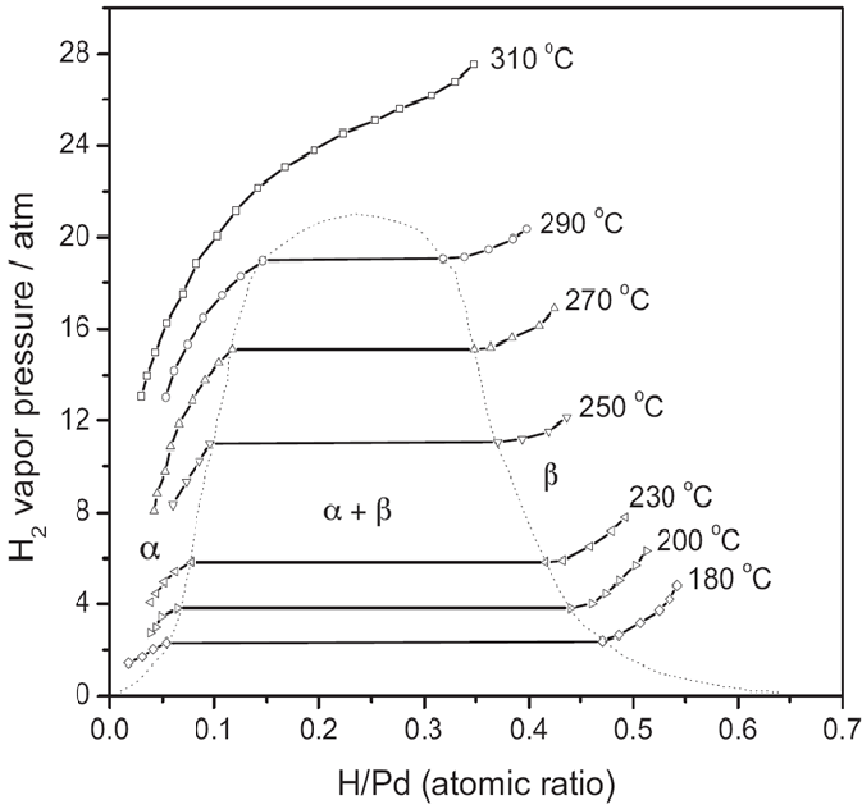

Figure 2.5. Phase diagram of palladium-hydrogen system [10, 27].

The maximum solubility of hydrogen in the α-phase is called α_{max} which is the beginning of another hydride phase, β-phase. Before certain hydrogen concentration, both the α- and β-phase co-exist in the invariant pressure region or plateau region where transformation from α- to β- phase occurs. In the plateau region, hydrogen vapor pressure does not increase with hydrogen to palladium ratio. Co-existing the α-phase and β-phase is the miscibility gap of the two phases. Both the hydrides have face center cubic (FCC)

crystal structure but differences in lattice parameters. The lattice parameter in β-phase is 10% larger than the α-phase for hydrogen to palladium ratio of 0.5.

After the complete transformation from α- to β- phase, equilibrium pressure starts to increase with the increase in hydrogen concentration in the solution. The hydrogen concentration at or above equilibrium pressure starts to increase with adding more hydrogen is called β_{min}. The miscibility gap disappears where α_{max} and β_{min} coincide. In this Pd-H system, the critical temperature, critical pressure and H/Pd ratio at which miscibility gap disappears are 298 ºC, 20 atmospheres and 0.27, respectively [18]. The curve for 310 °C does not have miscibility gap. The increase in lattice parameter due to the transformation from α- to β-phase hydrides causes lattice strain. As a result, the Pd-film goes through distortion, dislocation multiplication and hardening during hydrogen permeation through Pd membrane at or below the critical temperature and pressure. This phenomenon is called hydrogen embrittlement which makes the membrane loss of complete selectivity. The mechanism of occurring hydrogen embrittlement was described by various theories such as pressure theory, the reduced surface energy theory, the de-cohesion theory, the H_2 phase change theory and H_2 enhanced local plasticity theory [28].

Hydrogen embrittlement can be avoided by operating the membrane in single phase region. This can be avoided by operating the membrane above 300 °C in hydrogen atmosphere or by ensuring that cooling takes place only when it is in a dehydrogenated condition. However, this approach will really narrow down its application [18].

The other method is to change the metallurgy of the palladium membrane rather than changing the operational regulation. It is necessary to suppress the β- to α- phase

transition in order to avoid distortion. Adding a number of elements to palladium can suppress the transition sufficiently, which significantly reduces or eliminates distortion. These elements include transition metals of group VB (tantalum, vanadium and niobium), VIIIB (nickel, rhodium, ruthenium, iridium, platinum) and group IB (copper, silver and gold) [3, 28]. Figure 2.6 shows the rate of diffusion of hydrogen in palladium and different palladium binary alloys at 813 K temperature and 50 psi pressure. Typically palladium is alloyed with Ag, Au, Cu, and Ni for hydrogen separation. Palladium with 25 percent silver shows the maximum permeability and palladium with 5 percent iron shows minimum permeability among the palladium binary alloys shown in Figure 2.6.

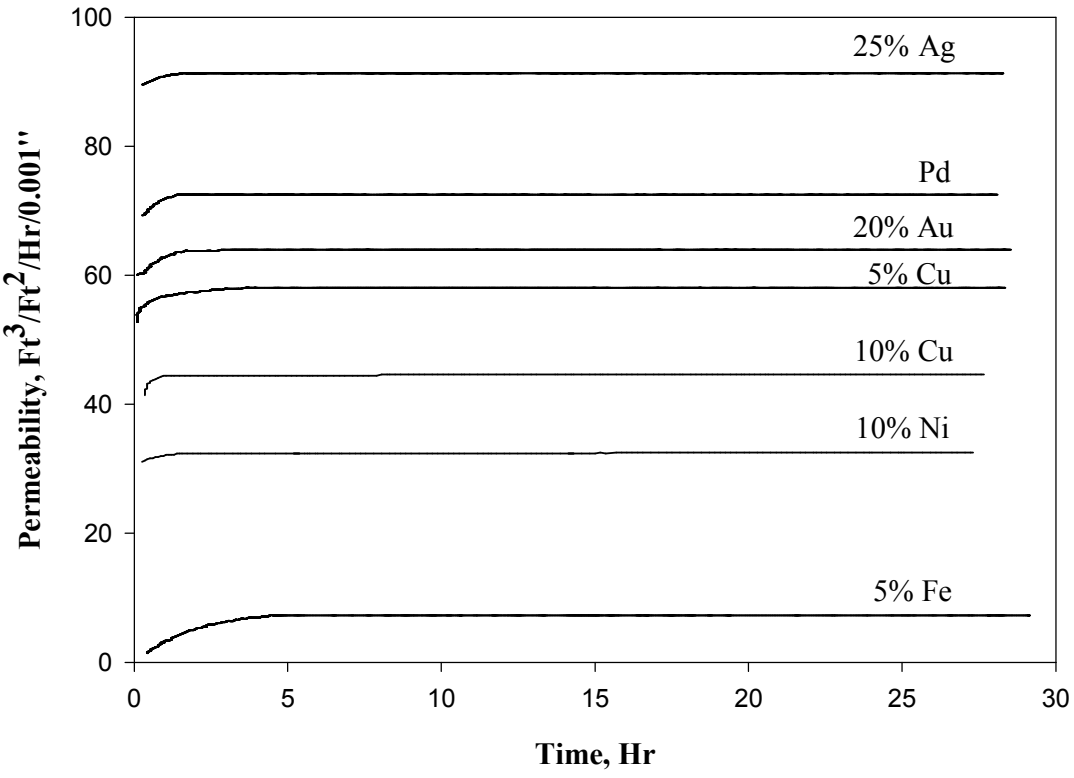

Figure 2.6. Rate of diffusion of hydrogen in palladium and number of palladium binary alloys (T = 813 K and P = 50 psi) [18].

2.7 Phase Diagram of Palladium and Stainless Steel

The understanding of phase diagrams for alloy systems is extremely important because there is a strong correlation between microstructure and mechanical properties, and the development of microstructure of an alloy is related to the characteristics of its phase diagram. In addition, phase diagrams provide valuable information about melting, casting, crystallization, and other phenomena [29]. It is of paramount importance to understand the phase diagram for palladium and its alloying materials for membrane application. An understanding of the phase diagram will allow us to find the limit for the annealing temperature. This will furnish a clear pathway for the post fabrication treatment for the membrane. The phase diagram of palladium and stainless steel is discussed below.

The binary phase diagram of the Pd/Fe system [30] is given in Figure 2.7. The main features of the phase diagram of the Pd/Fe system are characterized by the phase separation in the Fe rich region (>90 wt % Fe) due to the size mismatch among αFe, δFe and γFe phases [31] and the appearance of the two ordered phases , namely PdFe and $FePd_3$, in the Pd rich region (>62 wt% Pd). The Pd/Fe binary phase diagram shows a continuous region of solid solution with FCC structure existing over the entire composition range at high temperatures (>700 °C). However, the FCC phase is still stable at lower temperatures above 90 wt% of Pd.

Detail studies were done on the Pd/PSS, Ag/PSS and Pd/Ag/PSS by Yi Hua Ma et al. in 2007. They showed the effect of the annealing temperature on the alloying phases. In addition, one important feature they noticed is the impact of the annealing temperature

on the lattice size of the Pd-Fe alloy [32]. The lattice parameters for the pure Pd, porous stainless steel (PSS, composition in wt %: $Cr_{0.19}Fe_{0.70}Ni_{0.11}$) and Fe are 3.89, 3.59 and 2.87 Å, respectively as reported in the powder diffraction data base File Nos. 46-1043, 33-0397 and 06-0696 [JADE4.0: A program for powder diffraction data analysis; Materials Data, Inc.: Livermore, CA, 2001].

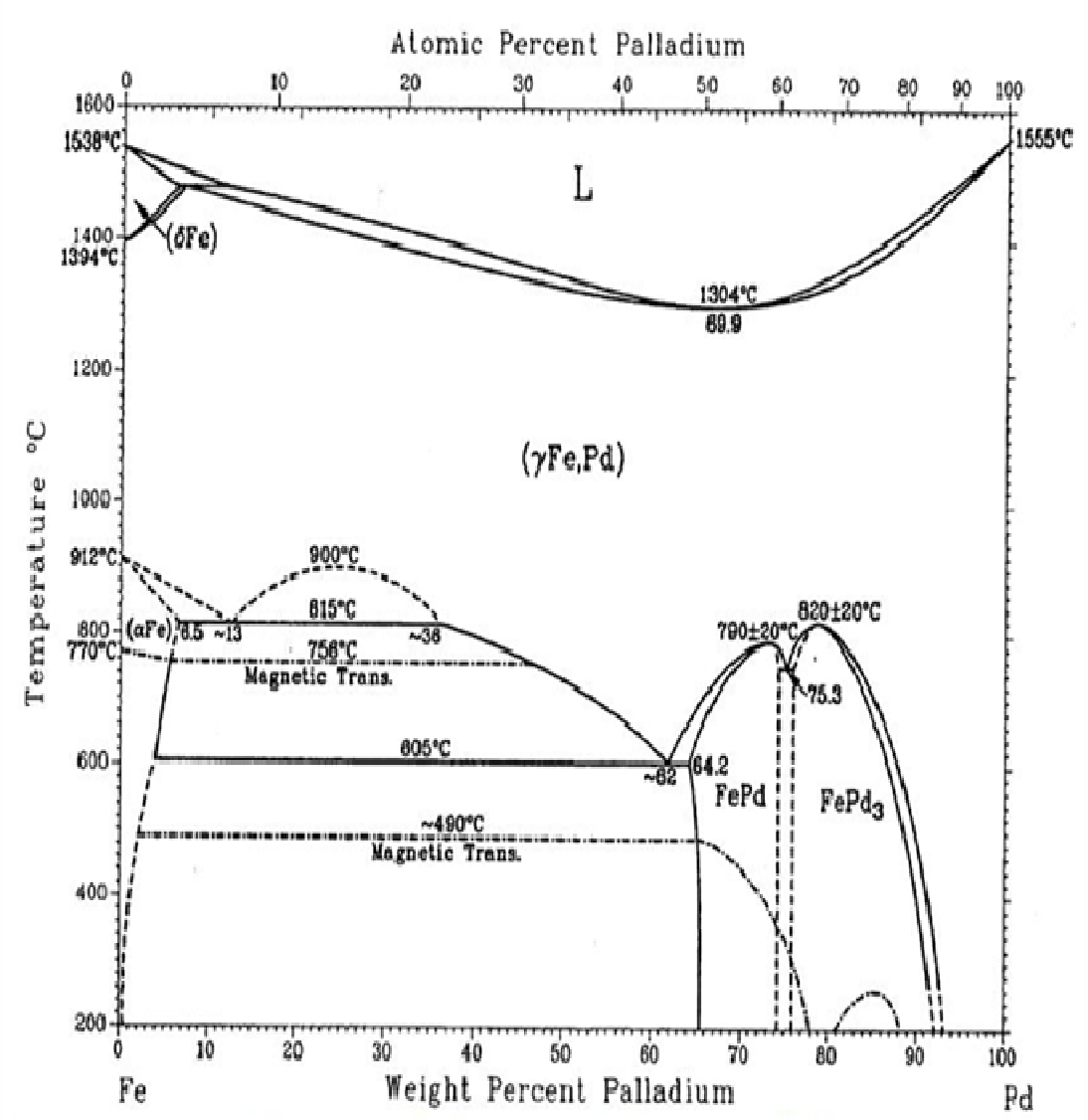

Figure 2.7. Phase diagram of palladium/porous stainless steel system [3].

After annealing the samples at 500 °C, 600 °C and 800 °C, they found the Pd lattice parameters as 3.89, 3.87 and 3.76 Å, respectively. Since the intermetallic diffusion is a temperature activated process, the Fe diffusion into the Pd layer with the increasing temperature apparently reduced the Pd lattice. Since increasing the Fe content would shrink the metal lattice and reduce the H_2 solubility and diffusivity [33], the intermetallic diffusion of the PSS components into the Pd matrix and the formation of undesirable alloy phases during the high temperature diffusion treatment might significantly alter the hydrogen permeance for Pd/ PSS composite membrane [3].

2.8 Membrane Support Materials Selection

Self-supporting palladium membranes need to be thick enough to have sufficient mechanical strength. If the palladium membrane is too thick, it will have a high cost and low hydrogen flux. Also exposure of the palladium foil in the H_2 environment results in severe distortion. Supported membranes can be prepared with much thinner palladium layers leading to lower expense, so considerable efforts have been expended to develop methods of preparation using supports. Different supports and deposition methods have been tried so as to obtain thin palladium films with good membrane integrity along with high hydrogen permeance and selectivity [10]. An economical route was chosen by using palladium based films on top of a substrate as a composite membrane. This approach significantly improved the hydrogen flux and reduced the investment level. In general, palladium based composite membranes are composed of a thin palladium film for separation and a substrate for its mechanical support. It is not only the mechanical

property but there are few other selection criteria for the selection of the desired support material. The ideal support materials should have the following features:

- Support should be chemically inert in reactions with Pd at any operating temperatures or pressures.
- Support should not allow any crystal migration.
- The pore size and pore size distribution of the support should be very fine and narrow, respectively. Significant interconnection of the pores is desirable.
- There should not be any blind pores present in the support. Pore size and morphology should not damage the top surface smoothness.

Supported palladium membranes are divided into three broad categories based on the supporting materials used: vycor glass, ceramics and stainless steel. Every type of membrane supports has both performance and commercial tradeoffs. At the early age of palladium membrane technology, porous vycor glass was used as support materials in the fabrication of composite Pd membranes. Porous vycor glass supports can endure thermal shock and are stable at high temperature along with high porosity but are mechanically fragile [10]. Porous ceramic supports have been considered as a promise substrate for Pd membrane. Ceramic substrate can be formed into a variety of shapes with controllable pore sizes. Pd attachment and has high hydrogen permeability. Alumina is used as ceramic supports material. Alumina can be formed in different compositions. Alumina is thermally and mechanically stable. In addition, alumina can be modified with intermediate layer which is very needed for good selective and high throughput membrane.

Metals are good candidates for substrate for the preparation of Pd membrane. These conductive materials can be formed into various shapes with convenient pore size. The advantages of using metallic support such as stainless steel are sturdiness and weldability.

The thermal expansion coefficient of stainless steel is very closer to that of palladium than ceramic supports. Closer thermal expansion coefficients give less stress during long term performance and thermal cycling of palladium membrane on stainless steel support [34]. Furthermore, stainless steel can be easily sturdy sealed in industrial assemblies than with fragile ceramic supports [35]. Among the porous metals, stainless steel is the most frequently used material due to its ease of fabrication, chemical resistance, and low cost [10]. Metal properties of film and support are summarized in Table 2.4.

Table 2.4. Physical properties of palladium, silver, copper, stainless steel and its constituent elements [3]

Material	Thermal Expansion Coefficient, K^{-1}	Tamman Temperature, °C	Lattice Parameter, Å	Density, gm/cc
Iron, Fe	1.2×10^{-5}	632	2.87	7.874
Nickel, Ni	1.3×10^{-5}	590	3.52	8.903
Chromium, Cr	2.3×10^{-5}	817	2.88	7.19
SS 316L	1.7×10^{-5}	550 - 560	3.59	8
Palladium, Pd	1.2×10^{-5}	640	3.89	12.023
Silver, Ag	1.9×10^{-5}	345	4.08	10.5
Copper, Cu	1.7×10^{-5}	405	3.6	8.96

Although the Pd and Pd/alloy deposition technique on PSS support is popular means of synthesis, one of the problems associated with the electroless plating is the difficulty in forming uniform alloys. Alloying is most commonly achieved by annealing under inert (i.e. He, Ar) or reducing (i.e. H_2) atmospheres prior to the hydrogen permeation testing. At high temperature ($\geq$ 500 °C), the intermetallic diffusion of support metals (Fe, Cr, Ni) takes place into the dense Pd or Pd/alloy separation layer resulting in deterioration in hydrogen permeation and non-uniform alloy layer. In order to achieve uniform alloy layers with electroless deposition, a substantial amount of studies has been done on a wide variety of support material [34, 36-44]. Most of the metallic support leads to intermetallic diffusion above 300 °C. Ceramic or vycor glass does not show any migration of its constituent element into the film at all.

In order to avoid metal migrations, many researchers attempted to develop intermetallic diffusion barrier in between metal support and membrane layer. Ma et al. have introduced a controlled in situ oxidation technique for producing an oxide layer on top of porous sintered metal tubes before plating [45]. They oxidize the membrane in air at 600 °C for 10-12 hours. It produces very thin stable Cr_2O_3 and Fe_2O_3 layer which reduces permeability in some extent. The oxide layer formed acts as a diffusion barrier between the hydrogen selective dense Pd and the PSS [38]. Membranes produced by these methods have been shown to be stable for over 6000 hours in the temperature range of 350 – 800 °C. Very negligible amount of iron, chromium and Nickel were found in the perm-selective Pd and Pd/Ag layer. In their recent work, Ma et al. have developed a method to produce a porous Pd/Ag intermetallic diffusion barrier layer on the surface of

the support by the bimetal multilayer (BMML) deposition technique prior to the application of the dense hydrogen selective layer [46]. The BMML acts as an extremely effective layer against intermetallic diffusion of the support metals and the membrane itself showed to be stable for several hundred hours at temperature 500 °C and above.

Recently, Tong et al. have reported that a 0.3 μm thick electroplated Ag on PSS support functions as a diffusion barrier [47]. Nam & Lee, 2001 reported the fabrication of Pd-composite membrane with 3 to 4 μm γ-Al_2O_3 layer as intermetallic diffusion barrier [35]. In this work, nickel powder was used to improve the surface smoothness. The pore size of the microporous metallic support plays a significant role on the quality of the final Pd/Pd-alloy film deposited by EP process. The maximum pore size in a support is characterized by pore diameter. The support materials are graded by pore size, such as 0.1 μm, 0.2 μm, 0.5 μm or so. Mercury porosimetry can be used to determine the pore size distribution in support surface. It has been shown theoretically that for a defect free, stable film, the Pd-film thickness should be at least three times of the largest pore (diameter) on the surface [48].

2.9 Electroless Deposition of Palladium

Pd membrane can be fabricated using various methods. Among them, electroless plating (EP), chemical vapor deposition (CVD), physical vapor deposition (PVD), electrodeposition (EPD) magnetron sputtering are commonly used methods [10]. The most advantageous method in fabricating Pd-composite membranes for high temperature H_2-separation applications is the electroless plating method [49]. The advantages using EP over other methods include the deposition on both conducting and non-conducting

surfaces, uniform deposition on complex geometries and large surface areas, simple plating bath set-up, strong mechanical strength of the deposited film, good adhesion to the substrate, and low cost [3, 10].

Electroless plating (EP) is a method for plating metallic films on a substrate by the reduction of metal complex ions in solution with the aid of a reducing agent without the application of an external electric field, but using the metal formed as a catalyst [10]. Pd electroless plating is comprised of cathodic deposition of metal and anodic oxidation of reductant in an immersion potential [49]. The commonly used metal ion sources are $PdCl_2$, $Pd(NH_3)_4Cl_2$, $Pd(NH_3)(NO_3)_2$ and $Pd(NH_3)_4Br_2$ and reducing agents are NH_2NH_2, $NaH_2PO_2.H_2O$, and tri-methyl-amine-borane. The oxidant and reductant used in this work were $Pd(NH_3)_4Cl_2$ and NH_2NH_2, respectively. Other than oxidant and reductant, a complexing agent such as ethylene-di-amine tetra-acetic acid (EDTA), ethylene-di-amine (EDA), NH_4OH), stabilizer (NH_4OH) and accelerators are used in Pd plating bath. In order to shorten the induction period for the autocatalytic decomposition reaction of the metastable complexes of Pd salts on the target surface and to initiate the electroless plating process, the stainless steel substrate was seeded with palladium by being dipped successively in acidic $SnCl_2$ solution followed by acidic $PdCl_2$ solution. This activation and sensitization step can be described by the following reaction:

$$Pd^{2+} + Sn^{2+} \rightarrow Pd^{\circ} + Sn^{4+} \tag{2.1}$$

The reaction steps for Palladium deposition in electroless plating are shown here:

$$2Pd(NH_3)_4^{2+} + 4e^{-} \rightarrow 2Pd^{\circ} + 8NH_3 \tag{2.2}$$

$$H_2NNH_2 + 4OH^- \rightarrow N_2 + 4H_2O + 4e^- \quad (2.3)$$

$$\text{Overall reaction: } 2Pd(NH_3)_4Cl_2 + H_2NNH_2 + 4NH_4OH \rightarrow 2Pd^\circ + N_2 + 8NH_3 + 4NH_4Cl + 4H_2O \quad (2.4)$$

$NaH_2PO_2.H_2O$ based plating baths with EDA as the complexing agents have been frequently used. But the microstructures of the deposited films were significantly altered with the formation of cracks due to the evolving hydrogen gas during the reaction [50]. For this reason, hydrazine based electroless plating bath is very attractive. Rhoda was the first to develop this type of bath using $Pd(NH_3)_4Cl_2$ [51]. Rhoda observed a linear increase in the plating rate within the temperature range of 40 - 80 ºC and a spontaneous precipitation of the bath above 70 °C in the absence of stabilizer EDTA salt. Another observation reported by Rhoda was rapid decrease in the plating rate with time, which was due to the catalytic decomposition of hydrazine by palladium. Over the years from Rhoda onwards, hydrazine based electroless plating was well established and successfully employed in the fabrication of dense hydrogen selective Pd-composite membrane on various substrate such as porous glass, ceramics, and porous sintered metal. In the past two decades, the bath parameters have been established for the effective plating of metals.

2.10 Modifications in Pd Electroless Deposition Techniques

For the economic viability of the membrane technology, some specific requirements such as high hydrogen permeation rates, high selectivity, long term thermal and chemical stability, and defect free (pinhole, cracks) film have to be achieved. The synthesis procedures for achieving the above mentioned requirements as well as their

reproducibility were a long deadlock. For finding a single synthesis procedure that will optimize the membrane properties as well as the durability, it is of utter importance to understand the solution chemistry, reaction mechanism of the electroless deposition, influence of the processing parameters on the properties of the deposited layer, and the ways and means for reducing mass transfer resistances. Thus, the effects of temperature, initial metal ion concentration and initial reducing agent concentration on electroless plating rates of Pd and Ag deposit on porous sintered metal were thoroughly studied [52]. It is now well established that the plating rate and conversion are heavily dependent with the initial concentration of metal ion and reducing agents. Apart from the metal ion and the reducing agent, it has been provided enough evidences on the effect of temperature in the plating technique. However, the plating rate and the efficiency differ from metal to metal such as the deposition rate for Ag is faster than Pd as well as the efficiency.

It is interesting that most of the previous investigators ignored the mass transfer limitations. Ma et al. observed that external mass transfer has a pronounced effect on the deposition kinetics. They found that the electroless plating of both Pd and Ag were strongly affected by the external mass transfer in the absence of bath agitation. The external mass transfer limitations for Pd depositions have been minimized at or above an agitation rate of 400 rpm. The result is a maximum conversion of the plating reaction at 60 °C and dramatically shortens the plating time. The plating yielded a uniform morphology. Ayturk et al. 2007 applied agitation through internal rotation in EP solution bath as an external driving force which improved reaction rate as well as grain size [53].

Their experiments demonstrated that plating efficiency can be as high as 90 %, if the rotation rate is set at 500 rpm during the electroless deposition process.

Varma et al. investigated EP of Pd in presence of osmotic pressure field [23, 54]. It was reported that osmosis helps to fabricate thinner and denser palladium films in shorter period of time. The osmotic pressure field improves metal penetration into the pores. The resulting membranes were found to be better quality in terms of mechanical and thermal stability compare to conventional EP [54]. This study also showed that agglomeration of Pd grains also increases with osmotic pressure.

The membrane characteristics are strongly influenced by the metal deposition methods [55]. In conventional EP process, the resulting Pd-film is formed by columnar grain growth [56] and there is little control on the grain size distribution for the deposited film. The grain size and its distribution are important parameters for the uniformity of the deposited film as well as for making it pinhole free. Apart from that, the grain size distribution and microstructure of the deposited film have a pivotal role in the hydrogen permeability. According to Kirchhiem et al., the diffusivity of hydrogen in nano-crystalline Pd is lower than that of single crystal at low hydrogen concentrations [57]. The diffusivity of hydrogen is significantly higher in nanocrystalline Pd than its single crystal counterpart at higher hydrogen concentrations. According to Gleiter et al., nanocrystalline palladium has almost 10 times higher diffusivity than conventional polycrystalline Pd [58]. In small nanocrystalline metal, at least 20 to 50 % of its atom located in the grain boundaries act as a network for faster diffusion. Therefore, it is of absolute importance to achieve the control on microstructure of the Pd-film by gaining

control over grain size distribution. The control on grain size distribution will eventually make the process reliable and yield a perm-selective film having desired characteristics.

2.11 Surfactant Induced Electroless Plating (SIEP)

Chen et al. 2002 studied Effects of added surfactants in the acidic hypophosphite plating baths on the properties of the resulting electroless nickel-phosphorus (Ni-P) deposits on the brass substrates [59]. It was observed that the addition of suitable amounts of surfactants can increase the deposition rate up to twenty five percent and reduce the formation of the pores on the surface of Ni-P alloys [59]. During the electroless plating process, the released N_2 gas bubbles get adsorbed by the support surface and eventually create micro-porosity in the deposited film and surfactant helps to remove the nitrogen gas bubbles from the substrate surface.

Ilias et al. investigated the palladium deposition on micro-porous stainless steel (MPSS) substrate in presence of anionic, cationic and nonionic surfactants in EP process [11, 17, 20, 49]. It was found that cationic surfactant with active polar group participates in the reaction or deposition process and effectively activates the process of grain nucleation and agglomeration in electro-crystallization. The membranes with agglomerated grains fabricated using surfactant possess relatively higher permeability and selectivity. To emphasize the role of surfactant in EP, Ilias and coworkers introduced the term Surfactant Induced Electroless Plating (SIEP) process which can provide greater control of over grain size distribution with enhanced deposition rate [11, 17, 20, 49].

A surfactant with suitable charge and concentration can be used to tailor the Pd grain size and subsequent agglomeration. Ilias et al. used a balance between micelles

collapse and retention as a control to facilitate uniform nucleation and agglomeration of Pd grains in dense Pd-film fabrication on MPSS [17]. The presence of surfactant helps in continuous removal of the evolved gases (NH_3, N_2 etc.). The interaction of surfactant in solid-liquid and solid-gas interface during grain coarsening helps in removing gas bubbles making almost entire substrate surface available for deposition. It was also concluded that the surfactant took part in the reduction reaction enhancing the plating process. As a result, the equilibrium shifts to the right which increases the rate of production of Pd°. The other advantage of this process is the preparation of an extremely dense thin film.

The concentration of the surfactant was chosen as a function of critical micelle concentration (CMC). It appears that during electro-crystallization, the driving force between newly formed crystallite and original coarse grains depends on the relative size and crystalline configuration of the newly formed crystallite. On the other hand, the crystallites are affected by the localized over potential, presence of active nucleating particles, texture of MPSS surface and operating conditions. The size of the newly formed grain is smaller when the concentration of surface active agents is relatively higher. It suggests that, surfactant active polar group inherently participates in deposition process and effectively activates the process of grain nucleation and agglomeration in electro-crystallization. By fabricating Pd membrane with different grain size by using different concentrations of surfactant, they have finally proved the control over deposited Pd-film microstructure.

Surfactants are amphiphilic molecules that possess a hydrophobic hydrocarbon tail and a hydrophilic polar head. Surfactants have both polar and apolar group. When surfactants are added in different phases, they always tend to accumulate at the interfaces of the phases. The accumulation of this surfactant at the interfaces reduces the interfacial energy present at the boundaries of the phases. As a result, the liquid in contact with solid spreads uniformly over the solid surface [60].

There are three kinds of surfactant such as cationic surfactant carrying positive charge, anionic surfactant carrying negative charge and nonionic surfactant or amphoteric surfactant, also known as zwitterionic surfactant which may exhibit either negative or positive charges depending on solution conditions but never shows no charge. The amount of surfactant added to the solution is expressed in terms of critical micelle concentration (CMC). Critical micelle concentration is the concentration of surfactant above which micelles which is the aggregation of surfactant molecules are just formed. The critical micelle concentration of dodecyl trimethyl ammonium bromide (DTAB) is 15 mM [61] . Micelles can be in different forms such as laminar, cylindrical and spherical with different number of molecules. The criteria for choosing a surfactant are that a surfactant should be partially soluble and stable in the medium and possess substantial adhesion tension and have good leveling power. The surfactant selection criteria are given below.

The paramount criteria for selecting a surfactant for a solution is the compatibility of that surfactant with the solution which means the ability of a surfactant to achieve adequate solubility in the solution. The molecular structure of the surfactant determines

whether it is compatible with a solution or not. A surfactant consists of a hydrophobic group which is a long chain hydrocarbon and hydrophilic group. The longer the hydrocarbon chain of surfactant, the surfactant will be more insoluble in the solution. On the other hand, if the hydrocarbon chain is smaller, this surfactant becomes more soluble in the solution resulting in poor performance due to poor surface activity.

There is Traube's rule which states that each methylene unit added will result in a reduction of the CMC of the surfactant by a factor of 3 [62]. One of the ways to find a suitable surfactant for a solution is the hydrophilic lipophilic balance (HLB) number which is used to optimize a compatible surfactant. Temperature is another factor in selecting suitable surfactant along with compatibility because the solubility of a surfactant depends on temperature. A surfactant may be poorly soluble in a solution at low temperature but micelle cannot be formed at that solubility and the surfactant cannot perform its job properly. The temperature below which a surfactant ordinarily soluble in a solution exhibits poor solubility and cannot form micelles, is known as the Krafft temperature [60]. The surfactant needs to be stable in the solution before performing its activity. The surfactant has to interact with the solution having charges to be stable in the solution. Positively charged cationic surfactants are generally compatible with metallic cations. In an electroless plating bath, presence of surfactant promotes the deposition reaction between the bath solution and the immersed substrate surface.

CHAPTER 3

MATERIALS AND METHODS

The electroless plating technique was used to obtain a dense Pd layer on the porous stainless steel supports. The supports were microporous stainless steel disc of grade 0.2 μm average pore size, 1 inch in diameter and 0.062 inch in thickness as per the manufacturer, Mott metallurgical Corporation (Farmington, CT). The entire process included the following steps: cleaning of the substrate, substrate's surface activation (pre-seeding), electroless plating, post plating treatment, and characterization.

3.1 Cleaning

The substrates need to be cleaned thoroughly prior to activation. The surface cleaning also has certain steps. Firstly, the surface of the substrate was cleaned by a metal brush to remove the external dust. Then the substrate was cleaned with alkaline cleaning solution (prepared in our lab) kept in ultrasonic bath for 40-60 minutes at 60 °C temperature to remove the grease, oil, dirt, corrosion products and other contaminants impregnated in the top surface of the substrate [38, 63]. The composition of the alkaline cleaning solution is given in Table 3.1. The substrate was washed with de-ionized water to make the surface pH 7. The substrate was dipped into isopropanol (Fisher Scientific) solution for 10 minutes and then it is dried for 2 hours at 120 °C in an oven.

3.2 Sensitization and Activation

The activation procedure consisted of immersion of the substrate for 5 minutes in an acidic $SnCl_2$ (Sigma-Aldrich, 98%) bath called sensitization followed by 5 minutes in

an acidic $PdCl_2$ (Sigma-Aldrich, 99.9%) bath called activation with rinsing in de-ionized water for 4-5 minutes between baths. Rinsing prevented drag out (transfer of activator or sensitizer into the plating bath) which caused precipitation of Pd metal particles. The composition of the sensitization and activation solutions prepared in our lab is given in Table 3.2. The activated substrate was rinsed with 0.01 M HCl in order to prevent hydrolysis of Pd^{2+}. From sensitization to rinsing with HCl completes one cycle. This cycle was repeated 6-10 times until the substrate surface became completely activated when the color of the surface looked like a uniform dark brown [5, 38, 63].

Table 3.1. Chemical composition of cleaning solution

Name of Chemicals	Supplier	Composition
$Na_3PO_4.12H_2O$ (ACS Reagent grade, 99.4%)	Alfa Aesar	45 g/L
Na_2CO_3 (ACS Grade, ≥ 99.5%)	Alfa Aesar	65 g/L
NaOH (ACS Grade, 97%)	Alfa Aesar	45 g/L
Industrial Detergent (Liqui-Nox^R)	Alconox	5 mL/L

Table 3.2. Chemical composition of sensitization and activation solutions

Name of Chemicals	Supplier	Sensitization Solution	Activation Solution
$SnCl_2.2H_2O$ (ACS Reagent grade, 98%)	Sigma-Aldrich	1 g/L	-
$PdCl_2$ (ACS Reagent grade, 99.9%)	Alfa Aesar	-	0.1 g/L
HCl (ACS Reagent grade, 37%)	Sigma-Aldrich	1 mL/L	1 mL/L
Temperature		20 °C	20 °C
Time		4-6 minutes	4-6 minutes
pH		4-5	4-5

3.3 Development of Pd-Bath

After impregnating the surface with Pd nuclei on the substrate surface, Pd-film was deposited by surfactant induced electroless plating (SIEP) process. The deposition

was carried out in an electroless plating bath at a constant temperature of 55 °C. The membranes were cleaned thoroughly with de-ionized water so that the entrapped salts and other chemicals in the Pd-film pores could be removed [64]. The operating condition and composition of the Pd plating bath are given in Table 3.3.

Table 3.3. Chemical composition of Pd-bath solution

Name of Chemicals	Supplier	Pd-bath
Pd $(NH_3)_4Cl_2.H_2O$ ($\geq$ 99.99%)	Sigma-Aldrich	4 gm/L
Na_2EDTA ($\geq$ 99%)	Acros Organics	40.1 gm/L
NH_4OH (ACS grade, 29.17%)	Fisher Scientific	198 mL/L
NH_2-NH_2 (1.0 M)	Sigma-Aldrich	5.6 mM
DTAB (~ 99%)	Sigma-Aldrich	4×CMC
Time		1 hour
Temperature		60 °C
pH		10-11

Sodium salts of EDTA and analytical grade ammonium hydroxide were obtained from Acros Organic and Fisher Scientific, respectively. Hydrazine (1.0 M) and tetra-amine palladium chloride were supplied by Sigma-Aldrich. De-ionized water was supplied by Milli-Q purification system (Millipore^{TM}) with conductivity as high as 18.2 mho-cm for sample preparation and rinsing of the glassware as well as experimental setup. All chemicals were used as received. The surfactant used in this work was DTAB (dodecyl trimethyl ammonium bromide, MW 308.35) obtained from Sigma Aldrich. The DTAB concentration was expressed in critical micelle concentration (CMC). In this SIEP process, the best performed concentration of DTAB is 4×CMC [49]. In this work, 4×CMC of DTAB for 5 membrane samples (Pd 26, Pd 28, Pd 30, Pd 31 and Pd 32),

1×CMC of DTAB for 2 membrane samples (Pd 21 and Pd 22), and no CMC of DTAB for membrane sample Pd 19A were used in the Pd plating bath [65]. The amount of Pd deposition was calculated by gravimetric method. The Pd-film thickness was calculated using both gravimetric method and from SEM images. The deposition plating process was continued until the surface was deactivated. After each cycle, helium leak test was carried out and flux was measured. The completion of fabrication was determined when the helium flow was found to be zero at room temperature and 20 psi pressure.

3.4 Post Treatment

Annealing is the heat treatment in which a material is exposed to a higher temperature for an extended time period and then slowly cooled. After the preparation of Pd membrane, the membranes were annealed for 18 hours at 500 °C temperature and 15 psi pressure under hydrogen atmosphere to coalesce the deposited Pd crystals to form a continuous, smooth, uniform and impervious membrane [64]. The membranes were first heated to 550 °C at a low temperature gradient under nitrogen atmosphere and then hydrogen gas was introduced in the membrane removing the nitrogen gas switch. The Tamman temperature of a metal is equal to one half of its melting point (in Kelvin) and is a temperature at or above which the atoms of the metals start to vibrate in a considerable extent [66]. The annealing temperature was chosen based on the tamman temperatures of Pd and stainless steel substrate's constituents. The tamman temperatures are 640 °C for Pd, 632 °C for Fe, 817 °C for Cr and 632 °C for Ni. The annealing temperature of the Pd membrane should be below enough the tamman temperature of substrate's constituent so that no elements of the substrate can diffuse into the Pd-film and vice versa which is

called intermetallic diffusion. Intermetallic diffusion reduces hydrogen flux. After 18 hours of heat treatment, nitrogen gas was again introduced in the membrane removing the hydrogen gas switch and temperature was brought down to room temperature at a very slow rate. Annealing for this membranes helps to produce specific microstructure, relieve stresses and increase softness, ductility, and toughness [29].

3.5 Characterization

Finally, the surface microstructure characterizations of the deposited films were conducted using scanning electron microscope (SEM) (HITACHI SU 8000), energy dispersive spectroscopy (EDS) (BRUKER AXS Microanalysis Gmbtt XFlash Detector 5030), X-ray diffractometer (XRD) (Bruker AXS (D8 Discover)) using the 2θ-θ scan with CuK_{α} (λ = 1.5405 Å) radiation and atomic force microscopy (AFM) (NT-MDT Integra-Prima). Using point to point measurements from SEM images, grain sizes were measured. The statistical distributions were estimated considering a minimum 500 no. of grains in a constant cross-section area. The membranes were characterized by permeability and selectivity tests. The experimental set-up is presented in Figure 3.1. The cross-sections of these membranes were investigated by SEM after cutting the membranes into pieces. EDS mapping and line scanning were used to investigate the composition of the palladium membrane layer to determine if any detectable levels of substrate component metals such as Fe, Cr and Ni migrated into the palladium film. Two membranes, Pd 31 and Pd 32 were tested for long term thermal stability study. Pd 31 performed 1200 hours with infinite selectivity at the temperature range of 300 – 450 – 300 °C and at 15 psi transmembrane pressure.

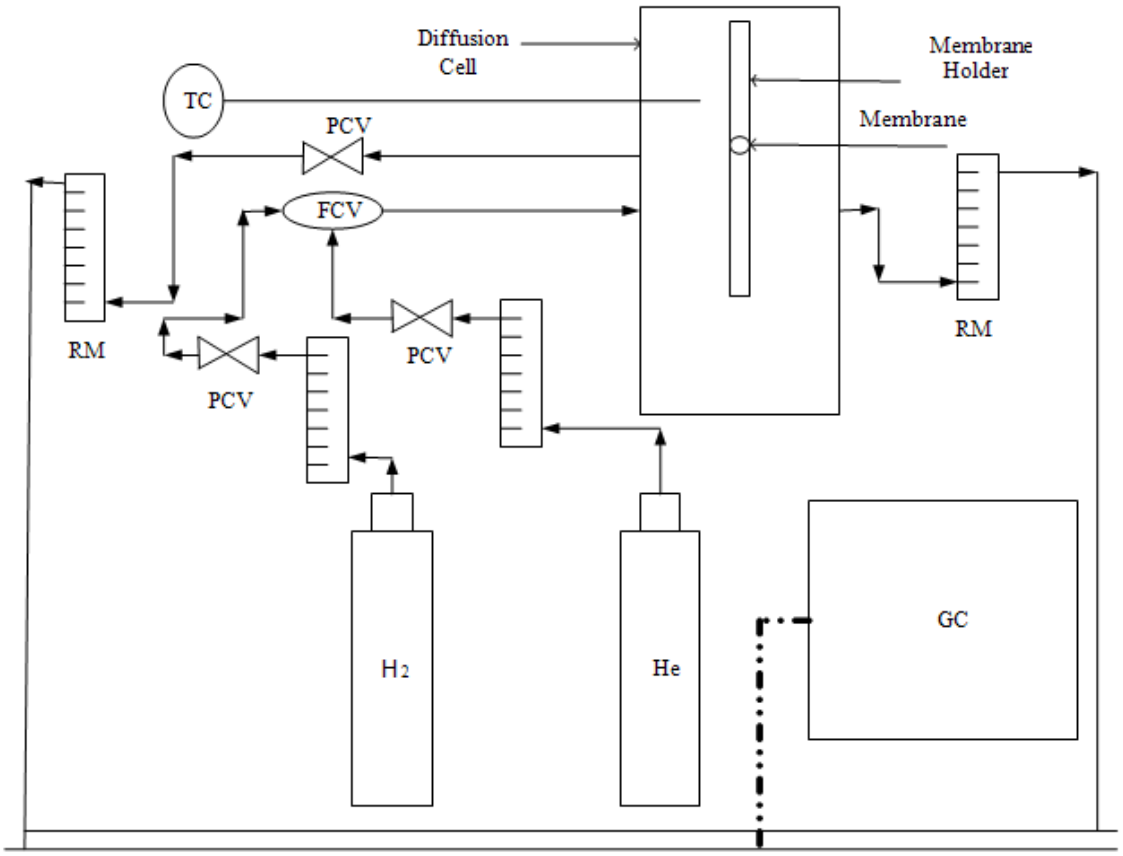

Figure 3.1. Experimental set-up for gas permeation through membrane at high temperature (FCV - flow control valve, TC - thermocouple (K - type), GC - gas chromatograph, PCV - pressure control valve, RM - rotameter) [3, 20].

Pd 32 was tested for 408 hours at the temperature range of 350 – 450 – 350 °C and at 15 psi transmembrane pressure. Pd 32 membrane also showed excellent permeability and infinite selectivity throughout the operation period. In this study, each of the thermal cycles were in few hours of duration. For example, in 350 – 450 – 350 °C cycle, the diffusion cell temperature was ramped from 350 °C to 450 °C (@ 1°C/minute) and after three to four hours operation, the temperature was slowly decreased to 350 °C and left it overnight or started a new cycle.

CHAPTER 4

RESULTS AND DISCUSSION

4.1 Introduction

Pd-composite membranes on microporous stainless steel were fabricated by SIEP process. Fabrication of thin, dense, and defect free palladium membrane depends on the microstructure of the palladium layer. Microstructure of the palladium film varies with several factors such as substrate surface roughness, pore dimension, fabrication technique, bath composition and operating conditions.

In conventional electroless (CEP) plating process, grain size distribution of Pd-film is controlled by various factors such as agitation and mixing of the plating bath solution, rotation of the substrate, osmotic pressure field, etc. To make a dense and defect free membrane using CEP process, membrane needs a thick palladium layer which reduces the hydrogen throughput. A cationic surfactant, dodecyl trimethyl ammonium bromide (DTAB) used in the SIEP process has great influence on the dense film microstructure of palladium composite membrane. Surfactant helps to form dense, uniform and defect free palladium film on MPSS substrate. Pd-composite membrane fabricated by SIEP process gives higher hydrogen throughput and permselectivity than that of membrane fabricated by CEP process. Using surfactant DTAB in SIEP process, the particle size distribution can be reduced significantly. The reduction of grain size helps to make a robust membrane of microstructure having desired grain agglomeration.

This was demonstrated by our research group previously. A brief introduction of the SIEP process is presented below [3].

Electroless plating is comprised of cathodic metal deposition and anodic oxidation of reductant on MPSS substrate. In conventional electroless plating, reduction of metal salt such as palladium tetra ammonium chloride monohydrate produces Pd-film on the substrate. Along with Pd° nitrogen and ammonia gases are produced from anodic and cathodic reactions. These gas bubbles adhere on the solid-liquid interface. As a result these gases hinder further deposition on the solid surface which creates dendrite growth. This dendritic growth of Pd crystalline results in non-uniform morphology and pinholes in the Pd-film. Pd grains and degree of agglomeration depend on the surface morphology. The crystalline distribution and microstructure characteristics of the deposited Pd-film have great effect on the long term performance and thermal stability of Pd-composite membrane. In SIEP process, surface active agent such as DTAB is added in the plating bath solution keeping bath composition, operating conditions same as for conventional electroless plating. The surfactant molecules form micelle with bath solution which helps to remove adhered gases from the solid-liquid interfaces. Most likely, the active Br^- in the head group of DTAB participate in the reduction process of the complex salt and favorably take part in Pd grain formation and subsequent grain coarsening, which helps in formation of uniform, defect free Pd-film on the substrate. The deposited Pd grain size and grain agglomeration are controlled by using this surfactant [49]. Our previous studies demonstrated that the best suited surfactant for Pd-composite membrane on MPSS substrate is dodecyl trimethyl ammonium bromide (DTAB) and the best performed

concentration of DTAB is 4×critical micelle concentration (CMC). SIEP process helps to enhance both hydrogen permeability and selectivity. In this work, using SIEP process, Pd-composite membrane on MPSS substrate has been fabricated, characterized; and long term performance and thermal cycling tests were carried out.

Instrumental analyses such as scanning electron microscopy (SEM), energy dispersive spectroscopy (EDS), X-ray diffraction (XRD), and atomic force microscopy (AFM) were carried out to characterize the membrane for the structure, grain size distribution, grain agglomeration and metal composition. Permeability measures were performed for the fabricated membrane. The long term performance of a SIEP membrane was observed for 1200 hours at temperatures ranging from 300 to 450 °C and at 15 psi pressure. Another SIEP membrane with intermetallic barriers was studied for 408 hours at temperatures ranging from 350 to 450 °C and at 15 psi pressure passing pure hydrogen. Both membranes showed excellent permeability and infinite selectivity over the performance period.

4.2 Microstructure Analysis

Pd-composite membrane's thickness, robustness, permeability, permselectivity, durability, and performance depend on the microstructure of the Pd-film on the substrate. Researchers have worked on film deposition methods to control grain size, adhesion, and film porosity [55]. The substrate surface roughness, fabrication technique, bath parameters, and operating conditions have great influence on the microstructure of Pd-composite membrane. The Pd-film microstructure also depends on the use of different reducing agent in different concentration which basically manipulates the reaction

kinetics. In this work, Pd-composite membranes were fabricated using SIEP process where a surfactant was used along with other parameters such as bath composition, bath parameters, operating conditions used in CEP process to demonstrate the role of surfactant in grain size, grain agglomeration, microstructure of Pd-film and the long term thermal durability and thermal cycling of the Pd-composite membrane. The substrate used here is microporous stainless steel from Mott Metallurgical Corporation. According to the manufacturer's data, the average pore size of the substrate was 0.2 μm and the physical dimensions of the substrate were 1 inch in diameter and 0.062 inch in thickness.

4.2.1 Helium Gas-tightness and Thickness Analysis of Pd Membranes

Pd-composite membranes on MPSS substrate were prepared using the cationic surfactant, DTAB at the concentration of 4×CMC, 1×CMC and no CMC. Both gravimetric method and SEM analysis of Pd-composite membrane cross section were used to measure the thickness of the membranes. Both methods gave consistent results. Thinner Pd-composite membrane can be prepared with shorter plating time by using surfactant [49]. The gas-tightness of these membranes was performed by passing helium gas through these membranes at transmembrane pressure of 20 psi and temperature of 27 °C. Pd deposition on the MPSS substrate was carried out layer by layer in electroless plating bath. When we observed, no helium flow through the membrane in the gas-tightness test, the membrane fabrication part was assumed to be complete. Helium was chosen for gas-tightness testing for being the smaller molecule (2.6 Å) compared to hydrogen (2.89 Å). In addition, helium is inert in reaction with palladium. In this work, several membranes were fabricated using 1×CMC and 4×CMC of DTAB, and without

DTAB. Hydrogen flux and selectivity data of four membrane samples are presented in Table 4.1 along with their fabrication processing variability and film thickness.

Table 4.1. Summary of Pd membranes characteristics fabricated by SIEP method

Membrane Sample	DTAB (CMC)	Film Thickness (μm)	H_2 Flux at 823K (mol/m^2-s)		Selectivity at 823 K (H_2 Flux/N_2 Flux)	
		SEM Analysis	20 psig	100 psig	20 psig	100 psig
Pd 19A	0	16.5	0.044	0.2202	84	35
Pd 21	1	12.4	0.0794	0.4722	207	120
Pd 26	4	11	0.3542	1.7172	330	148
Pd 31	4	7.5	-	-	-	-

Membrane sample Pd 19A is fabricated by conventional electroless plating (CEP) method (no surfactant). Samples Pd 21 and Pd 26 were fabricated by SIEP method with 1×CMC and 4×CMC of DTAB concentrations, respectively. From our study, we observed that a thinner Pd-film that is helium gas-tight can be fabricated by SIEP with higher DTAB concentration. For example, as given in Table 4.1 the Pd-film thickness decreased from 16.5 μm (with no surfactant) to 12.4 μm at 1×CMC DTAB and further dropped to 11 μm at 4×CMC DTAB concentration. Our test data showed that with increased DTAB concentration (consequently thinner Pd-film), the membranes provide higher hydrogen flux with higher H_2-selectivity (Table 4.1). At times, Pd membranes develop pinholes during heat treatment which require repair-deposition. Sample Pd 31 was not heat treated and it was used for characterization as a membrane before heat treatment. This work also demonstrates the reproducibility of the membrane prepared by SIEP process in our lab. It can be seen from the Table 4.1 that the Pd membrane has a

thinner film of thickness 7.5 μm which is consistent and compares well with our previously reported Pd-film thickness of 8.5 μm [49]. Shu et al. reported that at least 15 μm thick Pd-film deposition by CEP method is required to obtain a dense and defect free film when using 0.2 μm porous stainless steel support [34].

4.2.2 Microstructure Analysis of Pd Membranes Fabricated by SIEP Process

The fabricated Pd-composite membranes were characterized using scanning electron microscopy (SEM). The surface topology of Pd-film of membranes was analyzed by SEM images. Figure 4.1(a, b & c) shows the top view of the stainless steel support with a pore size of 0.2 μm at magnification of 500 X and 1.00 K at two different locations at electron beam energy of 5 kV. Pores are seen clearly in the substrate. Figures 4.2 and 4.3 show the top view of the Pd-composite membrane plated on top of the substrate. From the Figure 4.2 and 4.3 , it is obvious that the Pd-film fabricated using DTAB at 4×CMC level has finer grains and the diffusion of grain boundaries results in a uniform, smooth, continuous and pinhole free surface. The use of nanometer-sized palladium grains was reported as an alternative method for minimizing the lattice distortion from the α-β Pd hydride phase transition [10]. This occurs because the concentration of hydrogen on the grain surface and subsurface significantly increases compared to that in the interior sites for the case of nanometer particles. To investigate the particle size, surface roughness and grain boundary diffusion, the SEM images were taken in different agglomerated site at the magnifications of 1.00 K, 5.00 K, 10.0 K, 15.0 K, 20.0 K and 50.0 K. The energy of the electron beam was chosen at 5 kV since lower beam energy gives finer surface characteristics.

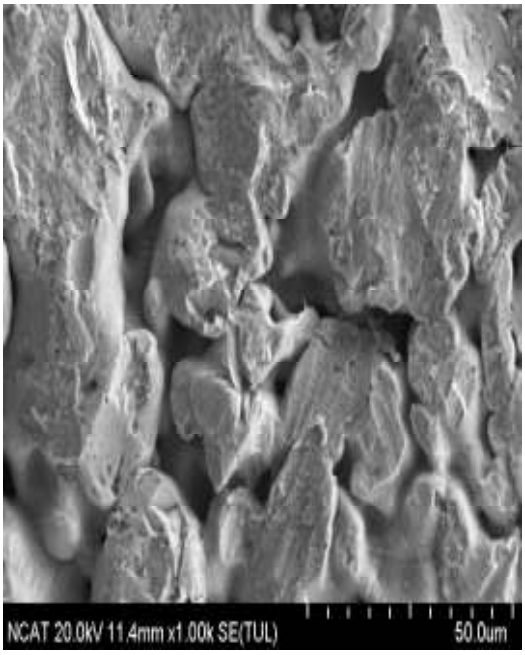

(a) MPSS substrate at 1.00 K (location 1)

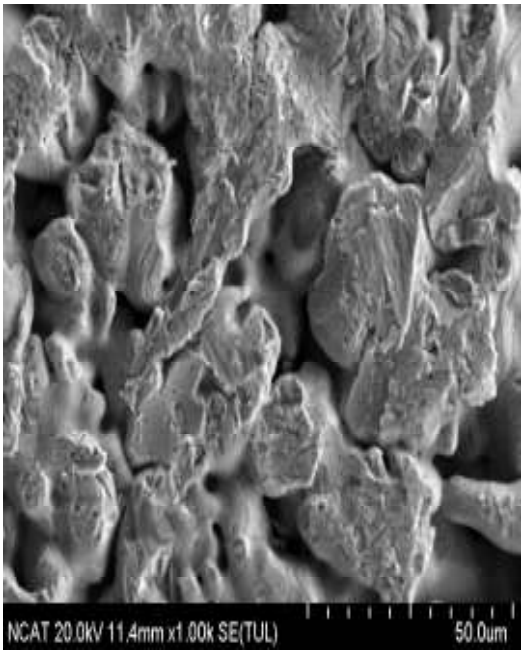

(b) MPSS substrate at 1.00 K (location 2)

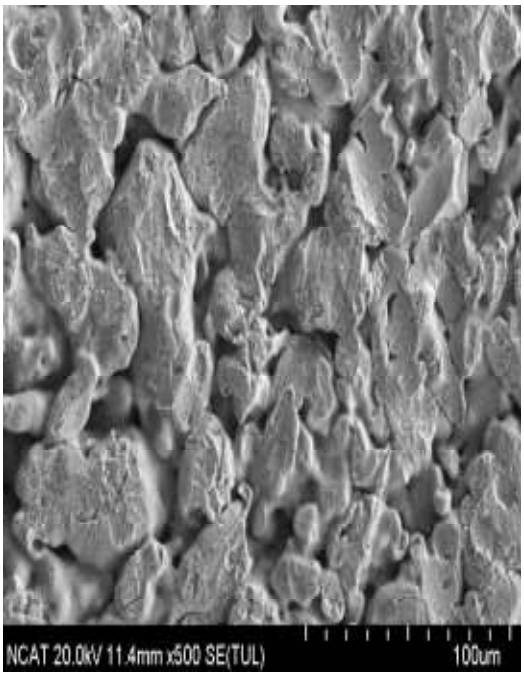

(c) MPSS substrate at 500 X

Figure 4.1. SEM images at different magnifications of the top surface of bare 316L microporous stainless steel (MPSS) substrate.

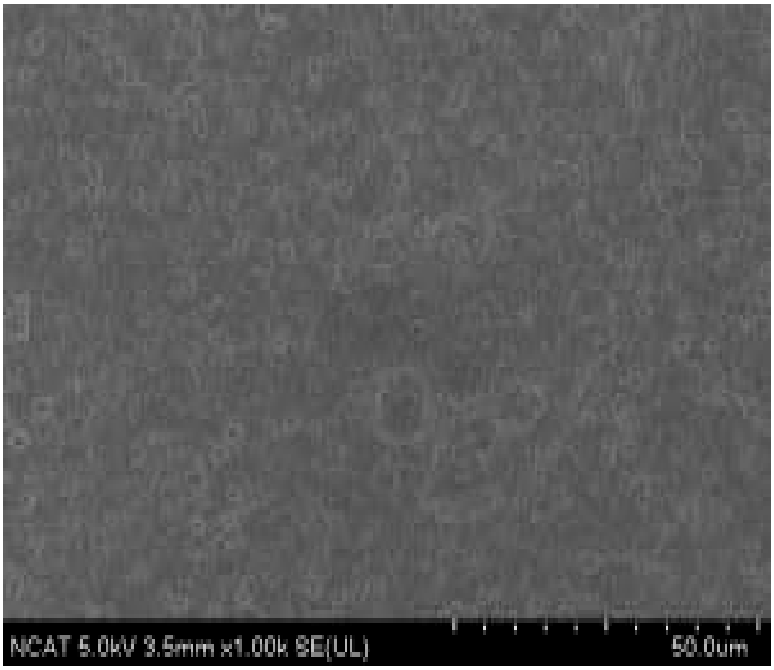

(a) Pd at 1.00 K

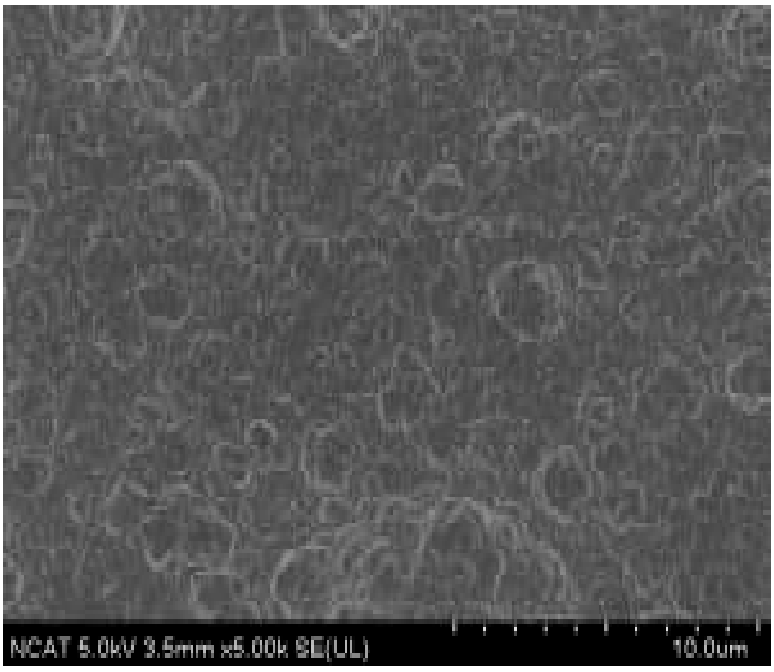

(b) Pd at 5.00 K

Figure 4.2. SEM images of Pd membrane top surface at 1.00 K and 5.00 K magnifications showing uniform agglomeration.

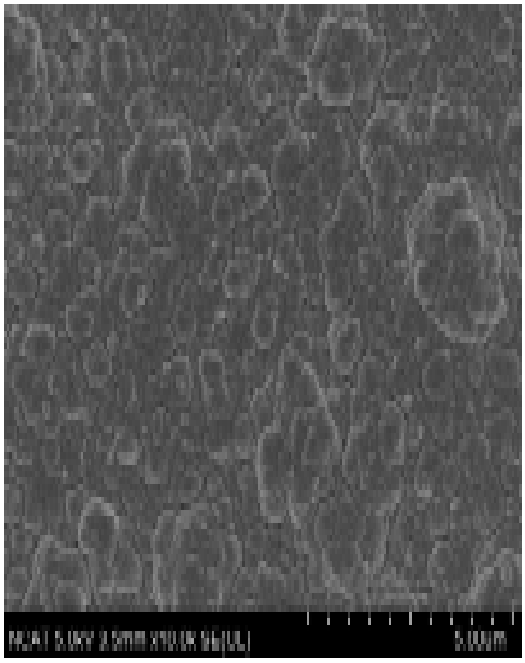

(a) Pd at 10.0 K

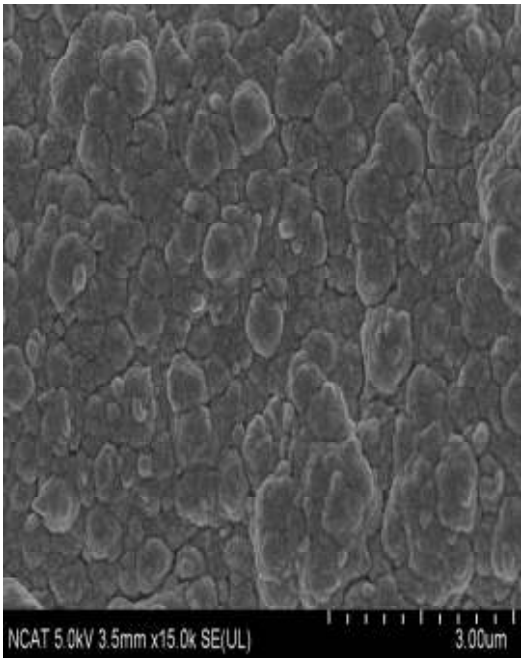

(b) Pd at 15.0 K

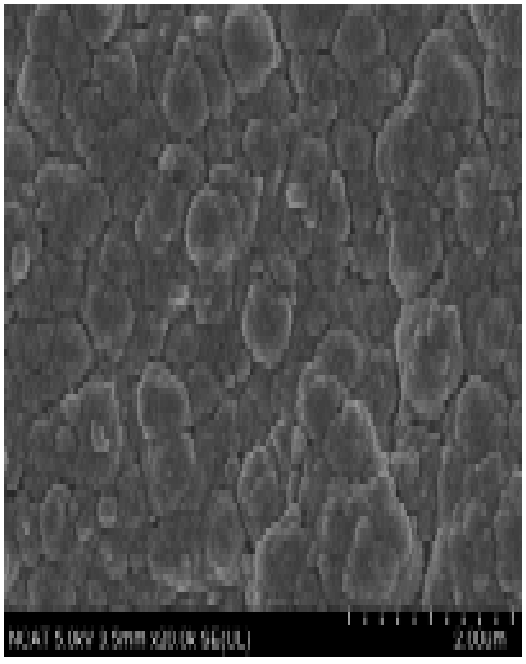

(c) Pd at 20.0 K

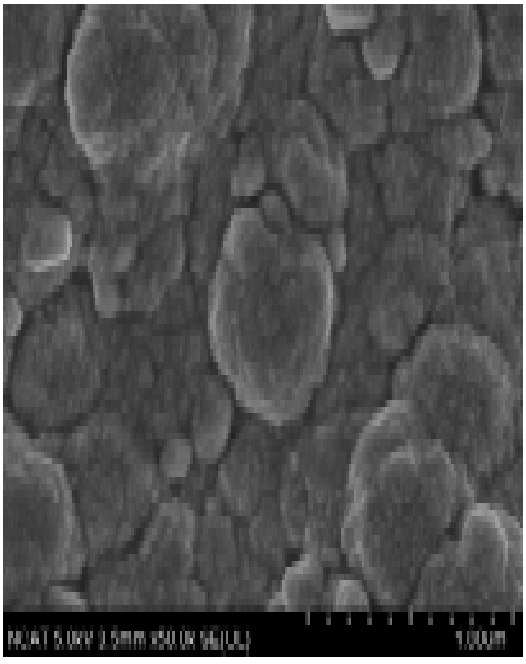

(d) Pd at 50.0 K

Figure 4.3. SEM images of Pd membrane top surface at different resolutions showing uniform agglomeration.

As we gradually move to the higher magnification images, it is clear that there is exactly similar grain boundary diffusion just beneath the top particle layer. Figure 4.4 shows the grain size distribution of Pd Membranes fabricated by SIEP process. From Figure 4.4, the average Pd grain size actually reduced to 0.47 μm in presence of DTAB at 4×CMC from an average particle size of 8 μm when DTAB was absent. The data for particle size distribution of Pd-film fabricated using no CMC of DTAB were taken from our previous work [49]. This result clearly suggests that the use of surfactant DTAB conclusively reduces the grain size considerably [49].

Surfactants are amphiphilic molecules that possess a hydrophobic hydrocarbon tail and a hydrophilic polar head. Surfactants have both polar and apolar group. When surfactants are added in different phases, they always tend to accumulate at the interfaces of the phases. The accumulation of this surfactant at the interfaces reduces the interfacial energy present at the boundaries of the phases. As a result, the liquid in contact with solid spreads uniformly over the solid surface [60]. Surfactant, DTAB is hydrophobic in nature and aligns itself around gas-liquid interfaces and forms various cylindrical and spherical cages like structure. Surfactant also tends to form meta-stable (cylindrical and spherical) structure in the solid - liquid interfaces that helps in finer grain formation and subsequent coarsening of the grain which was elucidated over a hydrophobic glass surface shown in Figures 4.5 and 4.6 in the scale of 1×1 μm scale and 2.5×2.5 μm scale, respectively. Figures 4.5 and 4.6 show that surfactant DTAB is forming a regular cage like structure after regular interval throughout the surface. These cages like structures support the idea of forming meta-stable structures in the solid-liquid interfaces by surfactant DTAB.

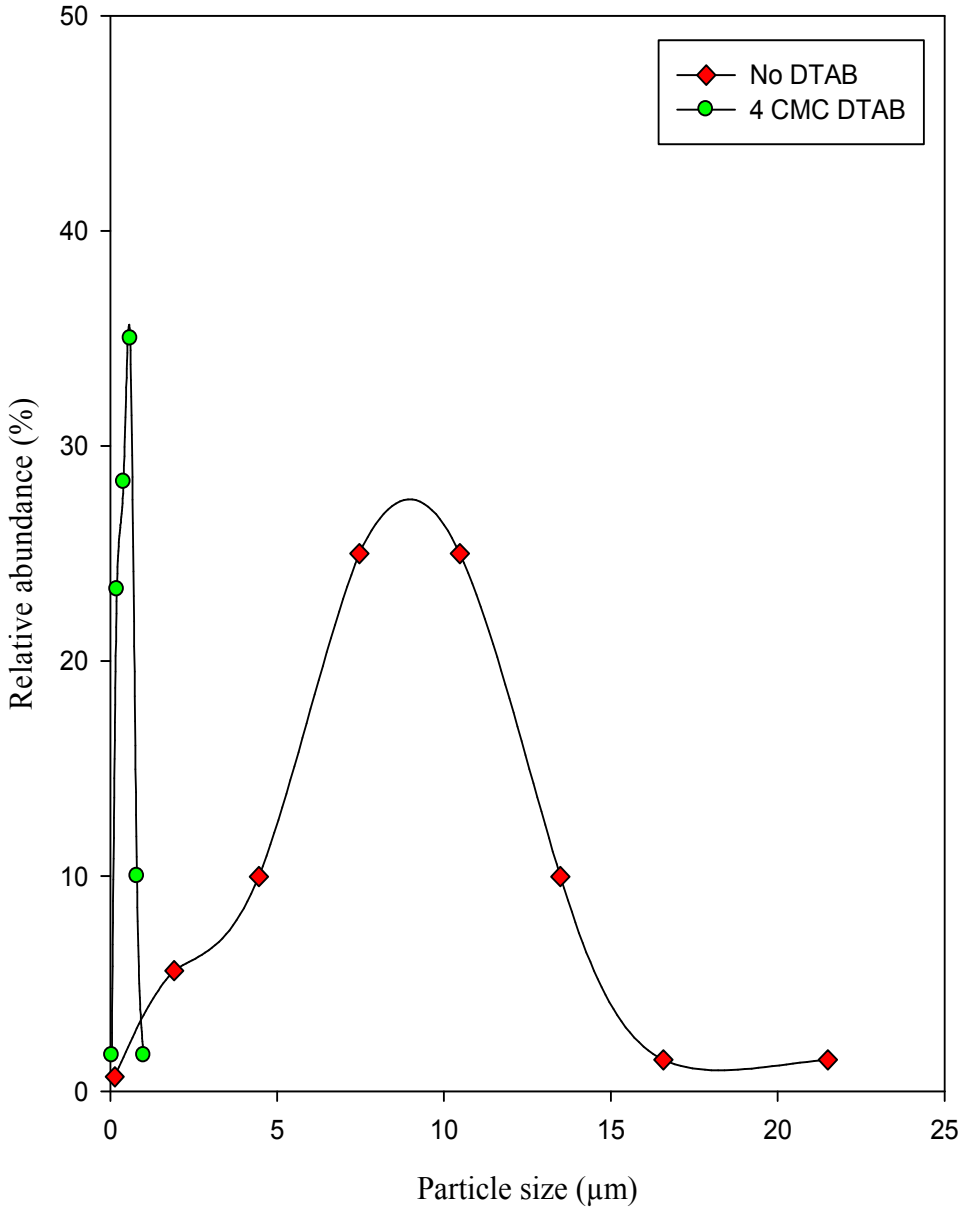

Figure 4.4. Pd grain size distribution observed in Pd membrane fabricated by SIEP process with DTAB at no CMC and 4×CMC.

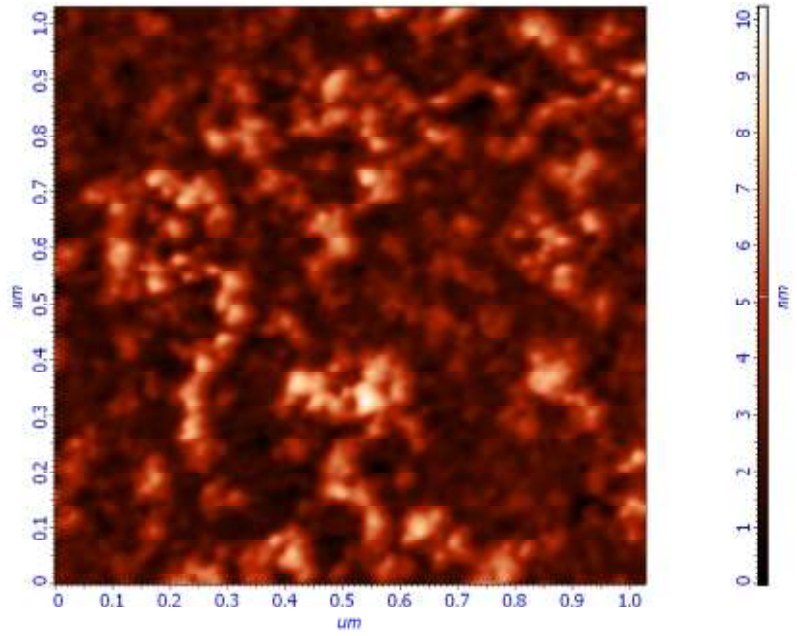

(a)

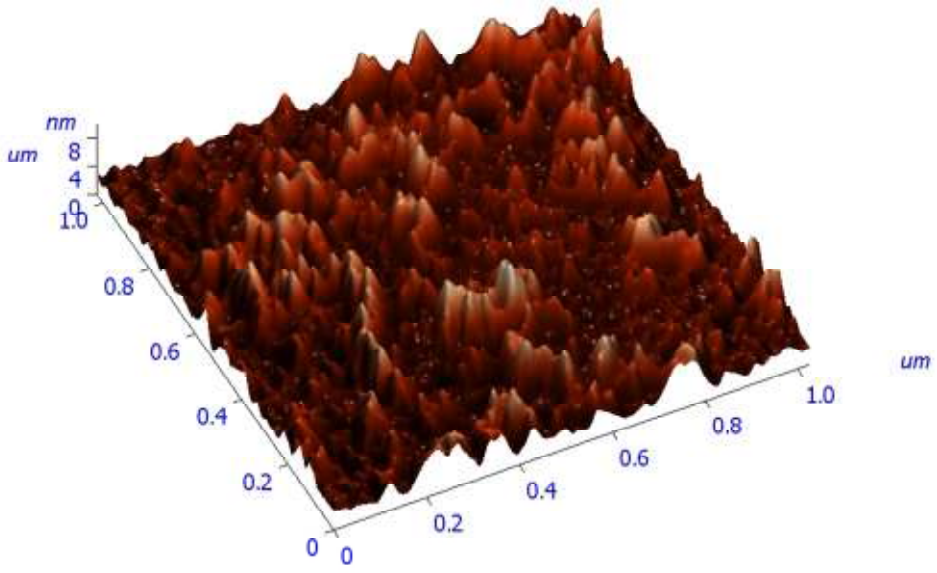

(b)

Figure 4.5. AFM images of Pd solid surface aggregation onto typical hydrophobic glass surface with DTAB in 1×1 µm scale.

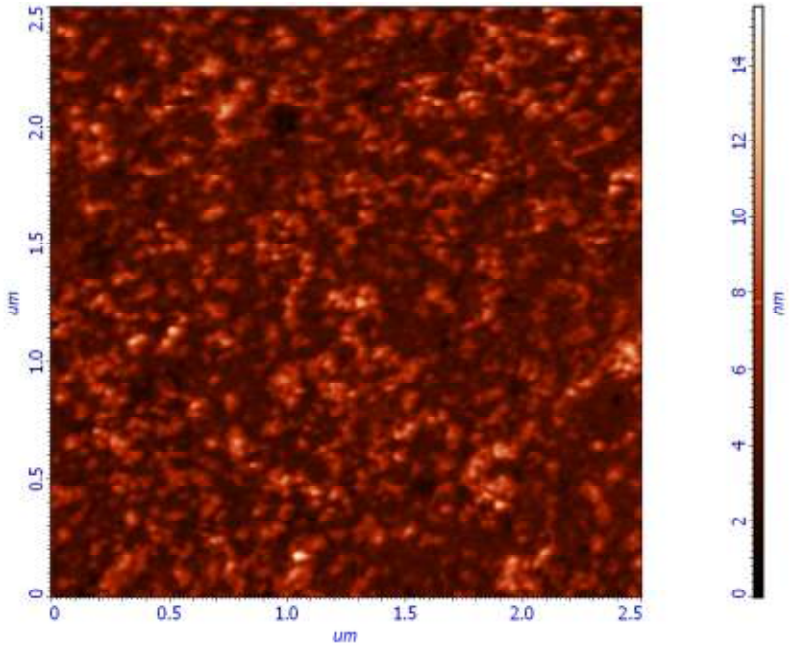

(a)

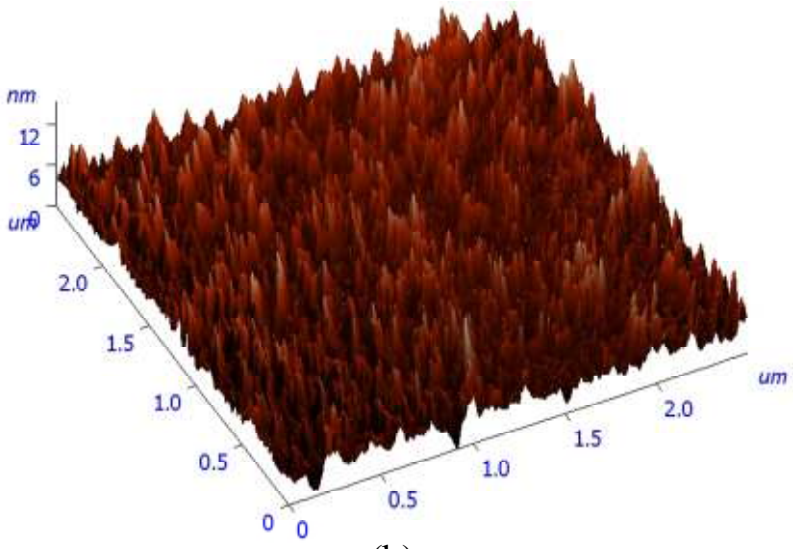

(b)

Figure 4.6. AFM images of Pd solid surface aggregation onto typical hydrophobic glass surface with DTAB in 2.5×2.5 µm scale.

It is also noticeable that using DTAB forms thinner layer as well. Figure 4.7 shows the surface topology of Pd-MPSS membrane examined by AFM study. The Pd-MPSS surface shows the presence of cage like structures but the grains are diffused one into another. Surface roughness is increased for Pd-MPSS top surface. Mean roughness of the surface was 16.59 nm.

One of the instruments for analyzing palladium films is X-ray diffraction (XRD). XRD is used to determine grain size, composition, and crystallographic orientation. X-ray diffraction was carried out for the structure analysis of the Pd-composite membrane fabricated by SIEP process. Figure 4.8 shows the XRD spectra of Pd peaks for Pd 31 membrane. XRD shows peaks in [111], [200], [220], and [311] characteristics planes, which implies the deposition of polycrystalline structure throughout the surface. The 2θ & d-spacing values corresponding to the three major reflection peaks in [111], [200] and [220] planes are presented in Table 4.2. No peak for the MPSS elements such as Fe, Cr, Ni and Mn were found in the XRD spectra.

Surface elemental analysis was carried out by energy dispersive spectroscopy (EDS). Figure 4.9 shows the typical EDS pattern of Pd-film fabricated using DTAB surfactant. It is observed from the figure that Pd peaks are intense. An escape peak for Pd at approximately 1.5 KeV X-ray energy is always observed when Pd is involved in the analysis. The EDS spectra did not show any peak for any elements other than palladium. So, the film contains only palladium metal. By adding the surfactant, DTAB in the SIEP, no contamination was added to the Pd-film structure as confirmed by the EDS and XRD results.

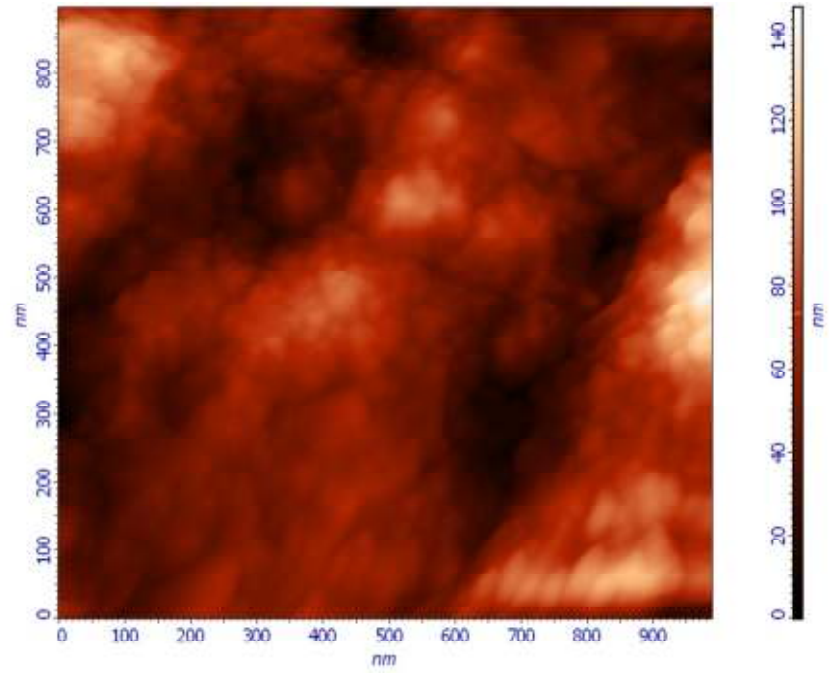

(a)

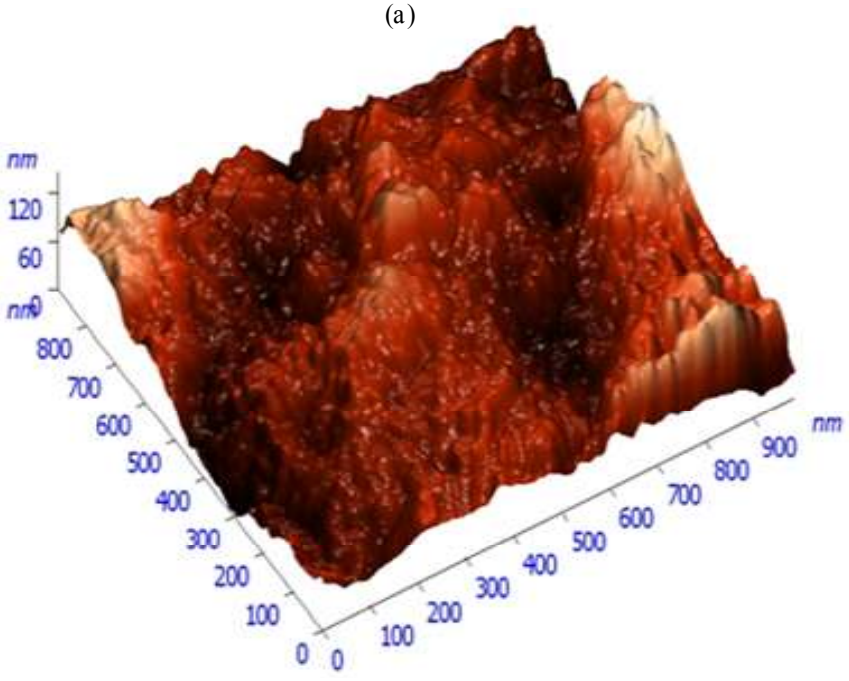

(b)

Figure 4.7. AFM images of Pd solid surface aggregation onto typical MPSS surface with DTAB in 1×1 µm scale.

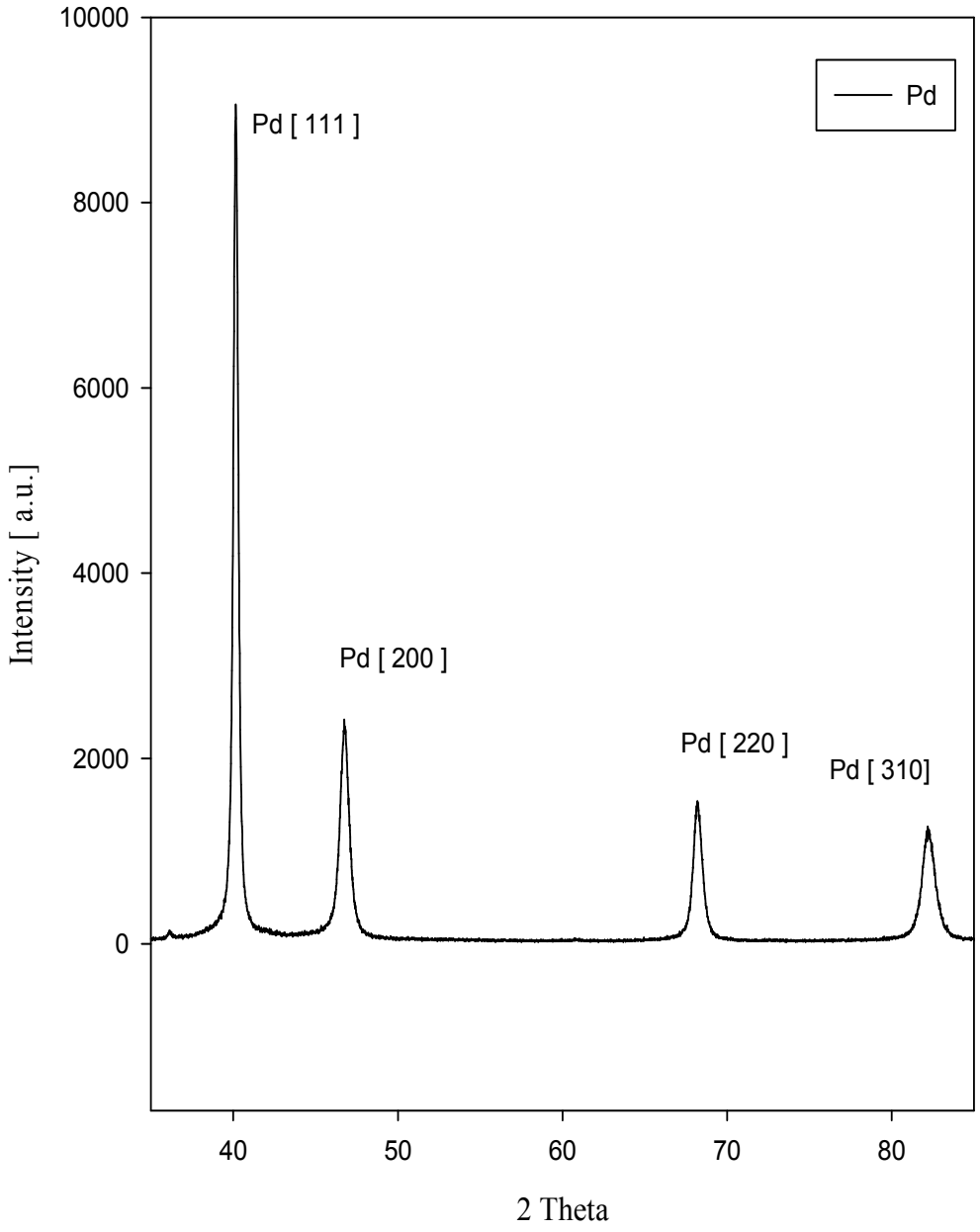

Figure 4.8. XRD pattern of Pd 31 membrane fabricated by SIEP process (before heat treatment).

Table 4.2. Comparison of high angle XRD reflection peaks of Pd-film fabricated by SIEP method

	Bravais Lattice	Pd (pre-annealed)	Pd (post-annealed)
2-theta	111	40.159	40.26
	200	46.924	46.693
	220	68.231	68.121
	311	82.212	81.981
d-spacing	111	2.2444	2.23885
	200	1.935	1.94428
	220	1.37378	1.37589
	311	1.171945	1.17472
Lattice parameter, a		3.8826	3.8885
Lattice Structure		FCC	FCC

4.3 Heat Treatment of Pd Membranes

The membranes were annealed for 18 hours at 500 °C temperature and 15 psi pressure under hydrogen atmosphere to coalesce the deposited Pd crystals to form a continuous, smooth, uniform and impervious membrane [64]. Although the Pd deposition technique on PSS support is popular means of synthesis, one of the problems associated with the electroless plating is the difficulty in forming uniform Pd-film. Uniform Pd-film is the most commonly achieved by annealing under inert (i.e. He, Ar) or reducing (i.e. H_2) atmospheres prior to the hydrogen permeation testing. At high temperature ($\geq$ 500 °C), the intermetallic diffusion of support metals (Fe, Cr, Ni) takes place into the dense Pd separation layer resulting in deterioration in hydrogen permeation and non-uniform Pd layer. Before annealing, the temperature of the membrane needs to rise up to 500 °C from room temperature. Cracks are produced during the transformation from α- to β-phase palladium hydride at 298 °C.

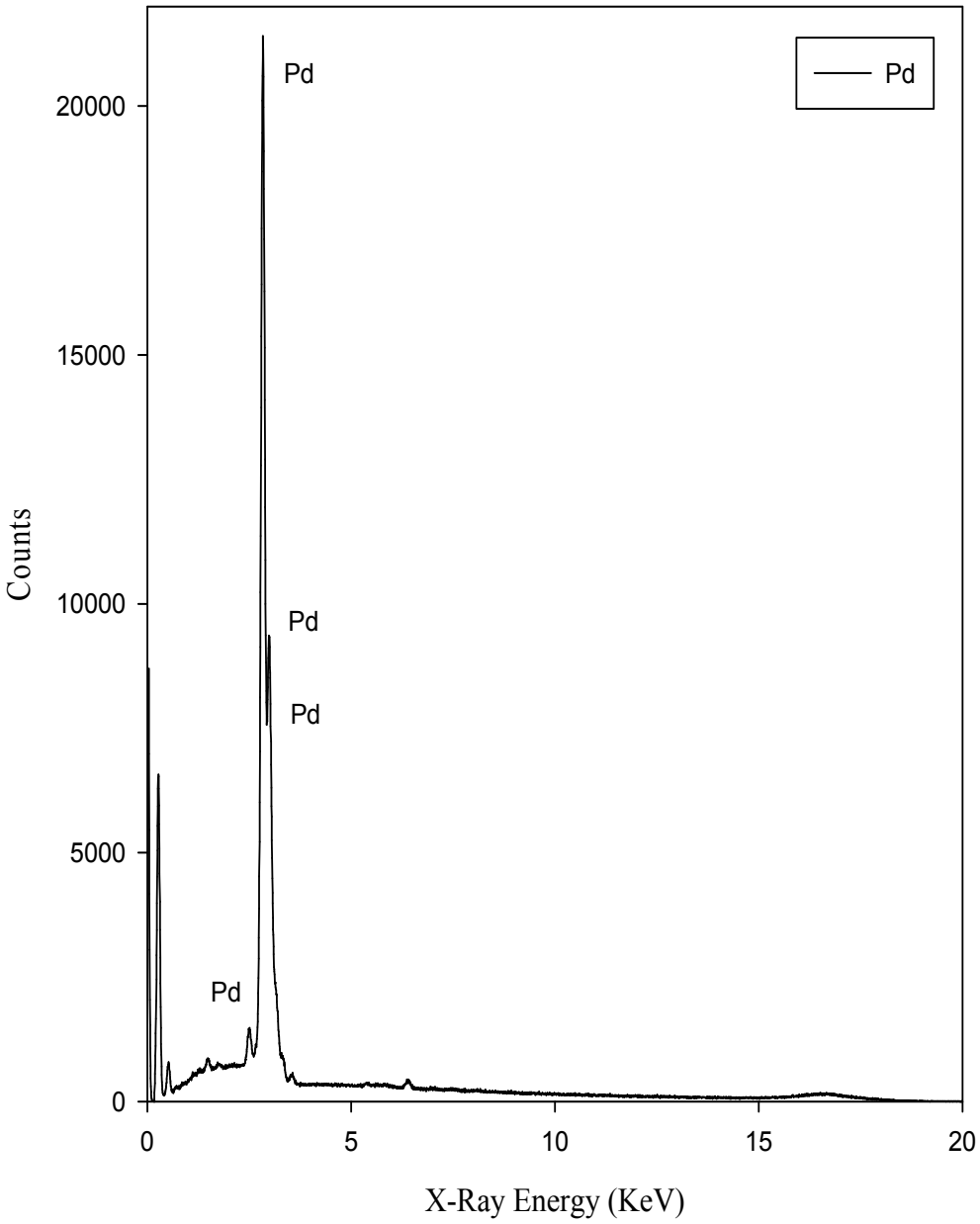

Figure 4.9. Typical EDS spectrum of Pd 31 membrane shows the presence of polycrystalline Pd deposition.

Pd membrane is heated from room temperature to annealing temperature and cooled from annealing temperature to room temperature under inert (e.g. He, Ar, N_2) atmosphere to avoid cracks. Figure 4.10 shows the change of helium flow rate with increasing temperature. For up to 200 °C, the helium flow rate did not increase significantly. From 200 to 400 °C, it was increasing to maximum at 80 ml/minute. During the increasing temperature, atomic movement of the palladium particles facilitated helium to pass through the membrane at an increasing rate. At 500 °C temperature, the helium flow rate came down to 26 ml/minute. At higher temperatures, palladium particles recrystallize themselves what reduced helium flow rate. It is seen from Figure 4.11 that hydrogen flux just immediately hydrogen introduced is very small. Hydrogen flux increased rapidly within 10 minutes of hydrogen permeation when hydrogen diffusion occurred through the palladium layer faster. After few hours of permeation, hydrogen flux decreased because of less permeable Pd-film formation.

According to Mardilovich et al. the densification occurred at the Pd/stainless steel interface [63]. Densification results in a loss of surface area and consequently hydrogen flux decreases. Grain agglomeration was promoted at this hydrogen atmosphere [67]. When uniform, smooth grain agglomerated Pd-film has been made, hydrogen flux became constant. Recrystallization occurs affecting the hydrogen permeability as well as membrane strength during annealing because the adsorption enthalpy of hydrogen as well as surface diffusion on palladium depends on orientation in some extent [55]. Figure 4.12 shows the change of helium flow rate during the cooling of the membrane from annealing temperature to room temperature.

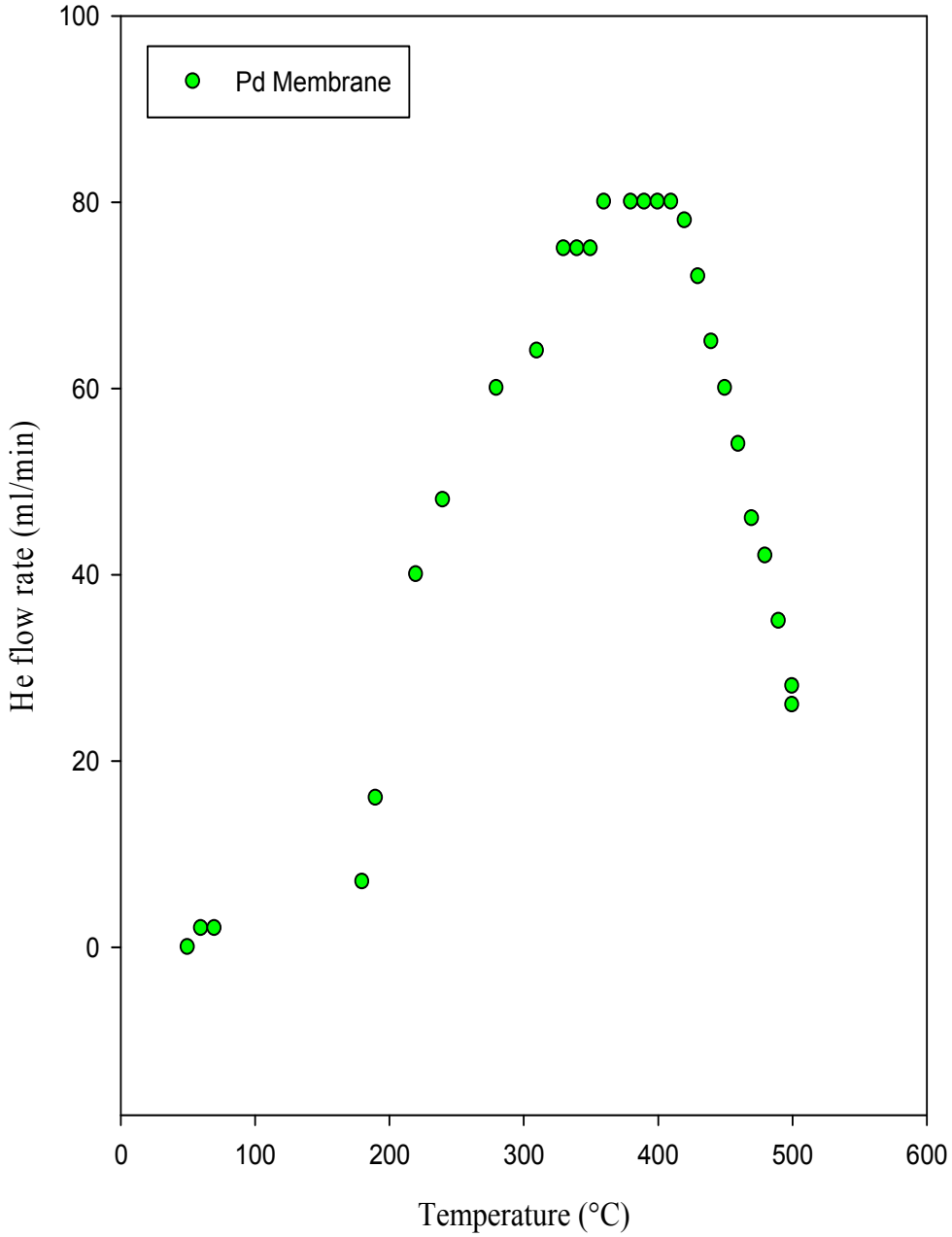

Figure 4.10. Change of helium flow rate during temperature increasing up to 500 °C for annealing Pd 20 MPSS membrane fabricated by SIEP process.

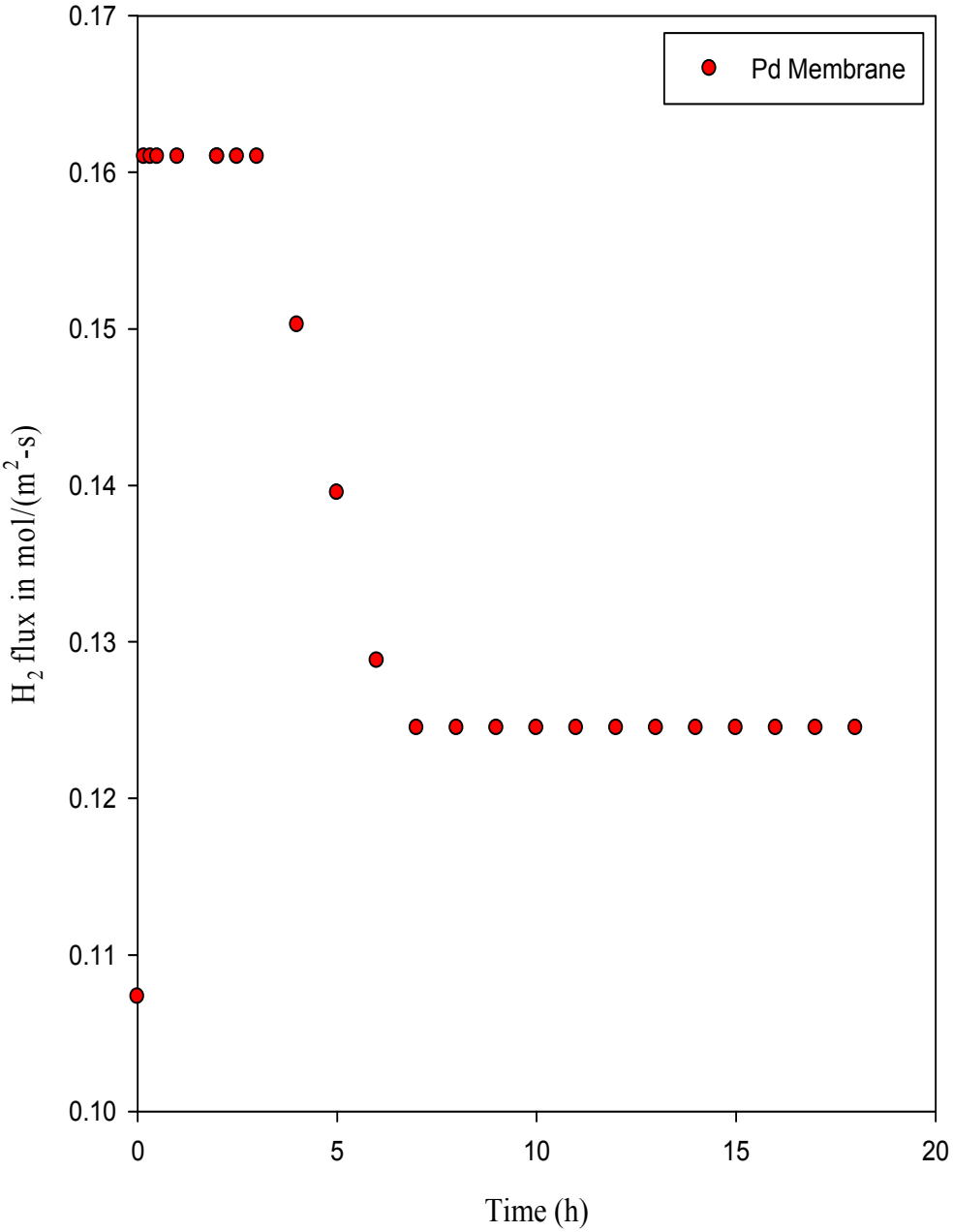

Figure 4.11. Changes in the hydrogen permeation flux for Pd 20 MPSS membrane during the annealing process at 500 °C with transmembrane pressure difference of 15 psi.

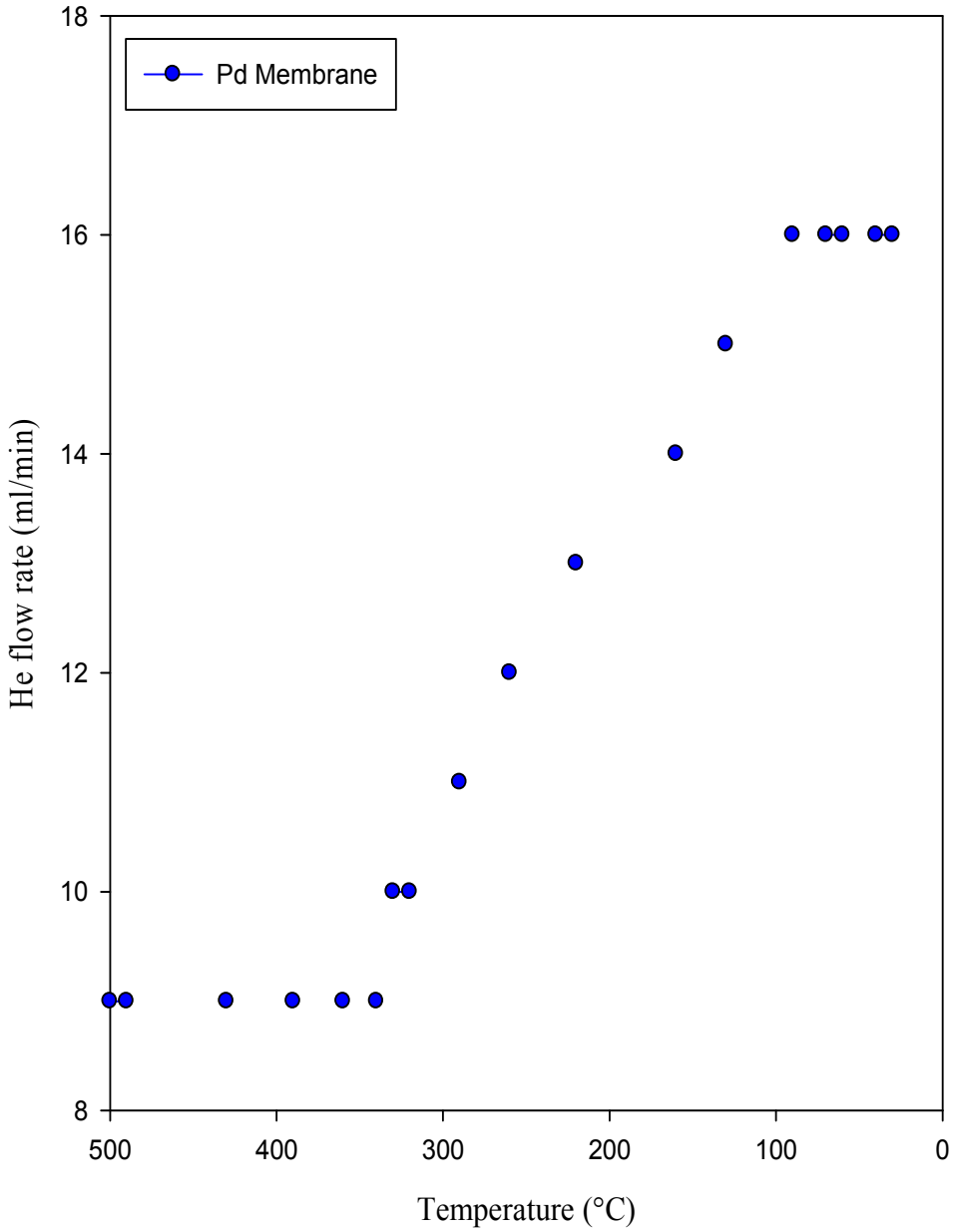

Figure 4.12. Change of helium flow rate during cooling from 500 to 30 °C after annealing of Pd 20 MPSS membrane.

Some hydrogen might be entrapped in the palladium layer during annealing. Once helium was introduced into the system, the helium flow rate was small. With running time, hydrogen was removed from the Pd layer by the helium pressure gradient resulting in increased helium flow rate and eventually helium flow rate became constant. Researchers also noted the increase and decrease of hydrogen or nitrogen permeation flux during palladium membrane operation [55]. An initial decrease in hydrogen flux that attained a steady state value after 80 hours and a decrease in nitrogen flux with increasing temperature were found by Wu et al [68]. According to them, the interactions between the Pd-film and the titania support or rearrangement of the Pd-film resulting in a decrease in the effective membrane area for hydrogen permeation causes these phenomena.

4.3.1 Effect of Heat Treatment on Microstructures

One of the major concerns about Pd-composite membrane is the microstructural changes in the Pd-film. During high temperatures operation, the thermodynamic instability happens due to free energy present in the large volume fraction of grain boundaries. As a result, the micro- and nanocrystalline grains of Pd-films sinter and conglomerate [68]. Figure 4.13 shows the XRD reflection patterns of Pd membrane before and after 18 hours heat treatment at 500 °C and one atmospheric pressure under hydrogen atmosphere. The reflection patterns for both before and after annealing of the membrane are similar. The characteristic planes found for this palladium in this XRD were [111], [200], [220] and [311], and the respective 2-theta values are 40.159, 46.924, 68.231 and 82.212. The 2-theta values for this membrane after heat treatment decreased in a little bit.

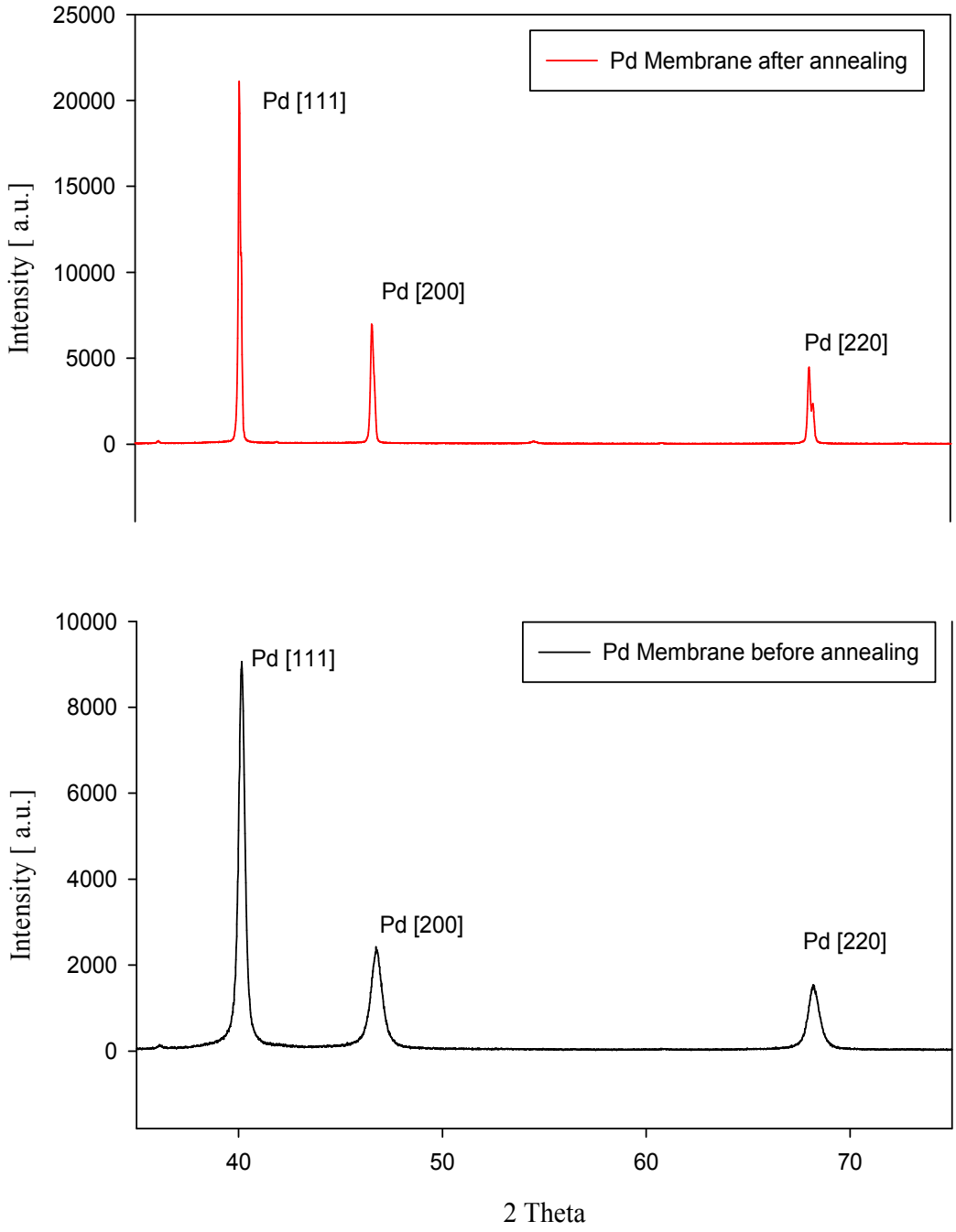

Figure 4.13. XRD patterns of Pd membrane fabricated by SIEP process at pre- and post-heat treatment.

After heat treatment, peaks gained more intensity which indicates that the crystals are well organized. In the XRD, more sharp peaks (more intensity) mean more crystalline. In the presence of hydrogen during heat treatment, crystals of palladium organize in a definite way. Grain growth during annealing of the Pd-film is confirmed by XRD. The d-spacing values are calculated using Bragg's law and shown in the Table 4.2 (as given in page 59) along with 2-theta values and lattice parameter calculated from the plane spacing equation. The lattice parameters for before and after heat treatment palladium found in the XRD are 3.8826 Å and 3.8885 Å, respectively. The little higher lattice parameter of the membrane after annealing than that of the membrane before annealing is the result of the migration of minute amount of Fe of the substrate into Pd-film which is consistent with the literatures [38, 65].

In the fabrication of Pd membrane by SIEP, Pd-film is deposited on MPSS substrate by multilayer deposition. This Pd-film contains small grains with large grain boundaries. This large grain boundaries reduces hydrogen selectivity [3]. Furthermore, pinholes originate from grain boundaries resulting in reduced selectivity. In order to improve the film quality, the Pd-film needs to be annealed. Upon annealing, Pd grains cluster fuses intimately with small grain boundaries. As a result, smooth and uniform Pd-film is produced. Figures 4.14 and 4.15 depict a representative surface morphology for Pd membrane before and after annealing at 1.00 K and 5.00 K magnifications, respectively. Clearly, it is recognizable from the images that the smaller grains agglomerated into larger grains with recognizable boundaries. Figure 4.16 shows some pinholes in the range of diameter of 50 - 200 nm on the surface of the membrane after heat treatment.

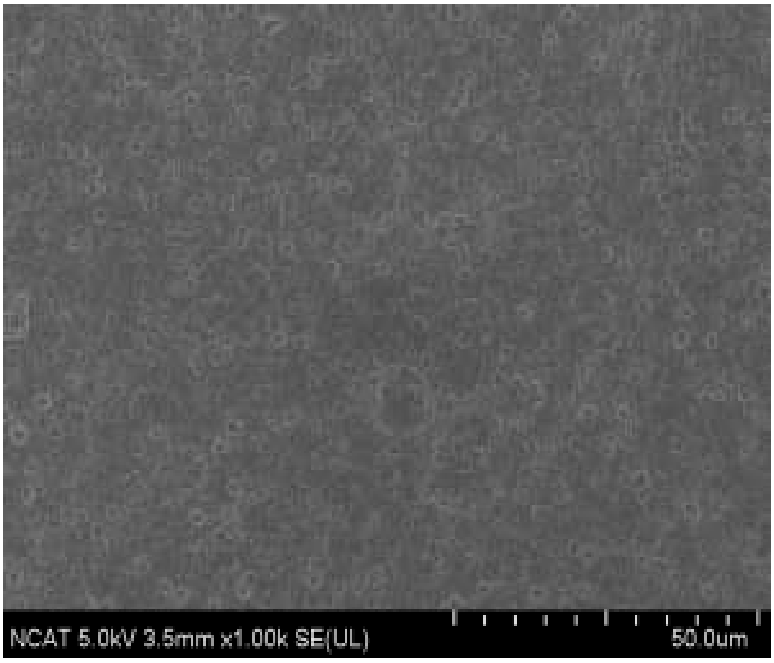

(a) Pd at 1.00 K (before heat treatment)

(b) Pd at 1.00 K (after heat treatment)

Figure 4.14. SEM images at 1.00 K magnification showing the effect of heat treatment on the Pd microstructure.

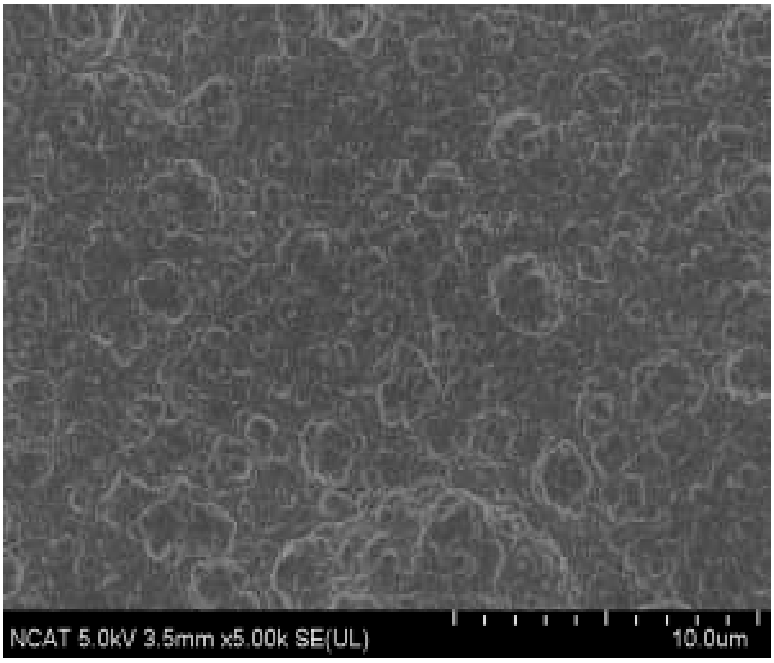

(a) Pd at 5.00 K (before heat treatment)

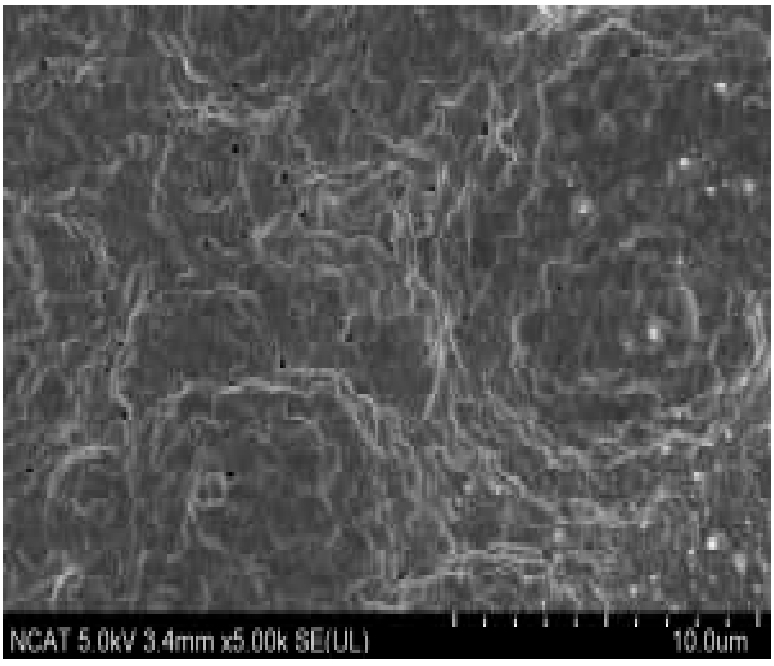

(b) Pd at 5.00 K (after heat treatment)

Figure 4.15. SEM images at 5.00 K magnification showing the effect of heat treatment on the Pd microstructure.

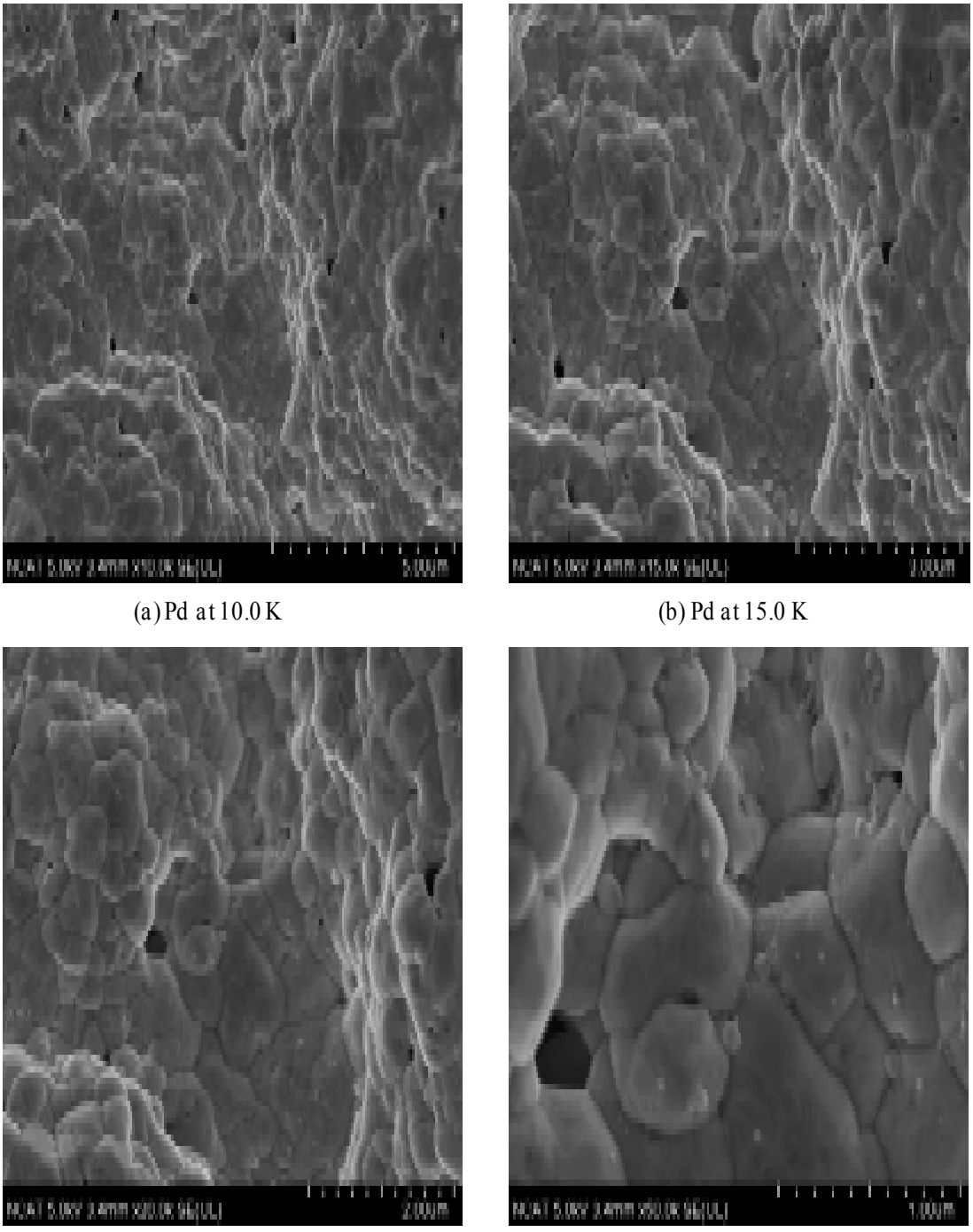

(a) Pd at 10.0 K

(b) Pd at 15.0 K

(c) Pd at 20.0 K

(d) Pd at 50.0 K

Figure 4.16. SEM images at 10.0 K, 15.0 K, 20.0 K and 50.0 K magnifications of Pd membrane at post-heat treatment.

Interstitial space might form during the multilayer deposition and drying steps. In the fabrication of the membrane, deposition was carried out by cycle. After each cycle of deposition, membrane was dried for 2 hours when an oxide layer might form. This oxide layer was reduced during annealing. Reduction of oxide layer formed some pinholes in the Pd-film. Reorientation of the crystals also occurs in the annealing period. The metals from the top are used up occupying the inter-granular spaces, and the interstitial spaces. While cooling starts after heat treatment, recrystalization occurs and diffusion ceases. Cooling step plays a significant role in the creation of pinholes. Figure 4.17 shows the comparison of surface of Pd-film of membrane before and after annealing at different magnifications. It reveals the effects of heat treatment on membrane. The surface topology of the permeability tested membrane is shown in Figure 4.18 at different resolution. The surface of membranes at pre- and post-heat treatment, post permeability test, and post 1200 hours of operation are shown in Figures 4.19, 4.20, 4.21 at 1.00 K, 10.0 K and 20.0 K magnifications, respectively.

4.3.2 Studies of Pd Membrane Cross-section

Several membranes were fabricated in the SIEP process. Among them, four membranes were annealed at 500 °C temperature and one atmospheric pressure for 18 hours under hydrogen environment. Permeability tests were taken for four membranes at 250 °C, 350 °C, 450 °C and 550 °C temperatures and 20 psi, 40 psi, 60 psi, 80 psi and 100 psi pressure drops. Then they were cut into pieces and metal polished for the investigation of microstructure of the membranes. One freshly prepared membrane sample Pd 31 was also cut into pieces and microstructure of the Pd-film was analyzed.

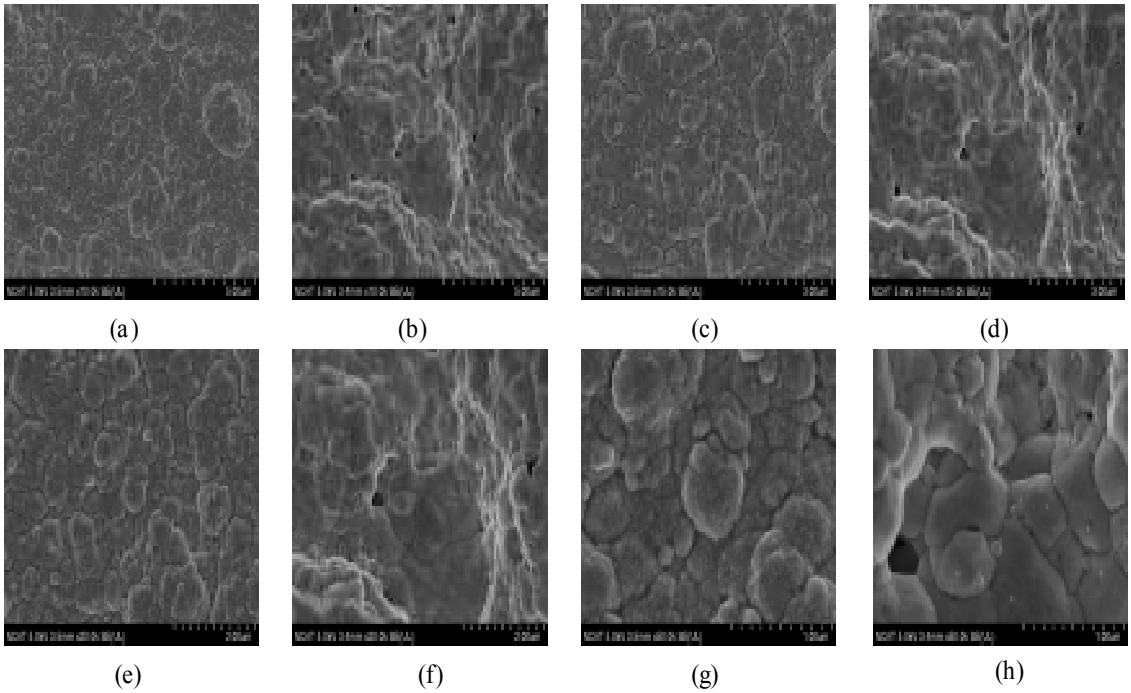

Figure 4.17. SEM images at different resolutions of Pd membrane at pre-heat treatment (HT) and post-heat treatment (HT), (a) Pd at 10.0 K (pre-HT), (b) Pd at 10.0 K (post-HT), (c) Pd at 15.0 K (pre-HT), (d) Pd at 15.0 K (post-HT), (e) Pd at 20.0 K (pre-HT), (f) Pd at 20.0 K (post-HT), (g) Pd at 50.0 K (pre-HT), and (h) Pd at 50.0 K (post-HT).

SEM images were taken for the cross-section of these membranes showed in the Figures 4.22 and 4.23. From the Figures 4.22 and 4.23, it is observed that before annealing, there is no intrusion of palladium inside the stainless steel but after annealing some palladium passed inside the substrate. SEM images also show that there is no nanoholes in the membrane before heat treatment but some nanoholes are seen after annealing through the cross-section of the membrane. The diffusion of metals into the substrate and the film is an important feature of membrane since this diffusion reduces the hydrogen permeability.

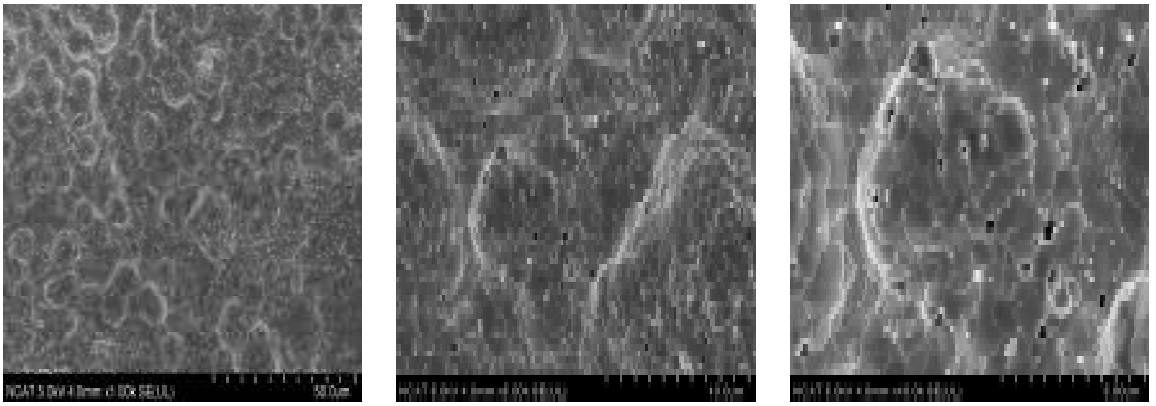

(a) Pd at 1.00 K (b) Pd at 5.00 K (c) Pd at 10.0 K

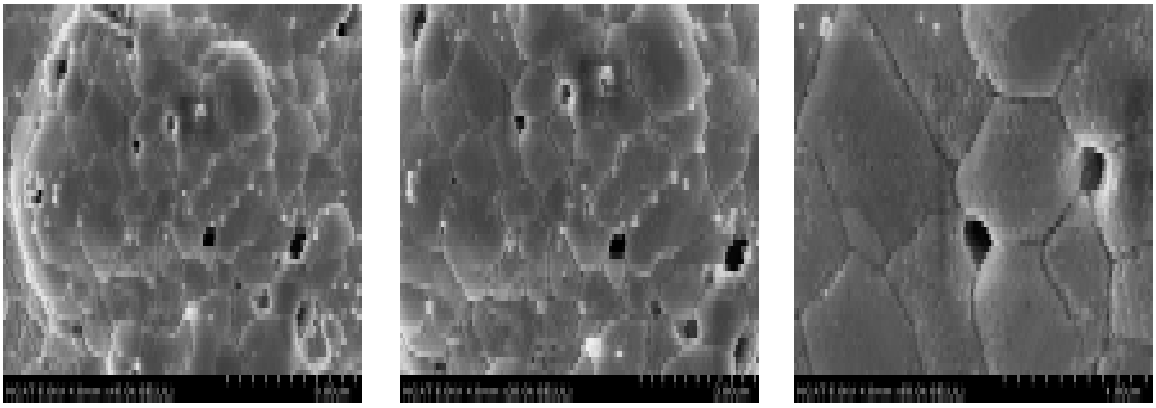

(d) Pd at 15.0 K (e) Pd at 20.0 K (f) Pd at 50.0 K

Figure 4.18. SEM images of Pd membrane after permeability test at different resolutions.

Film cross-sections were found to have all pores of the substrate surface plugged with the Pd metal. A deep penetration of the metals into the pores of the substrate was seen as well. A detail study was carried out on a single pore of the film from the pore mouth to the very deep inside of the pore to elucidate the behavior of metal deposition. Cross-sectional EDS line scans were performed for both membranes after H_2 permeation tests at temperatures of 250 - 550 °C to confirm the intermetallic diffusion and metal distribution.

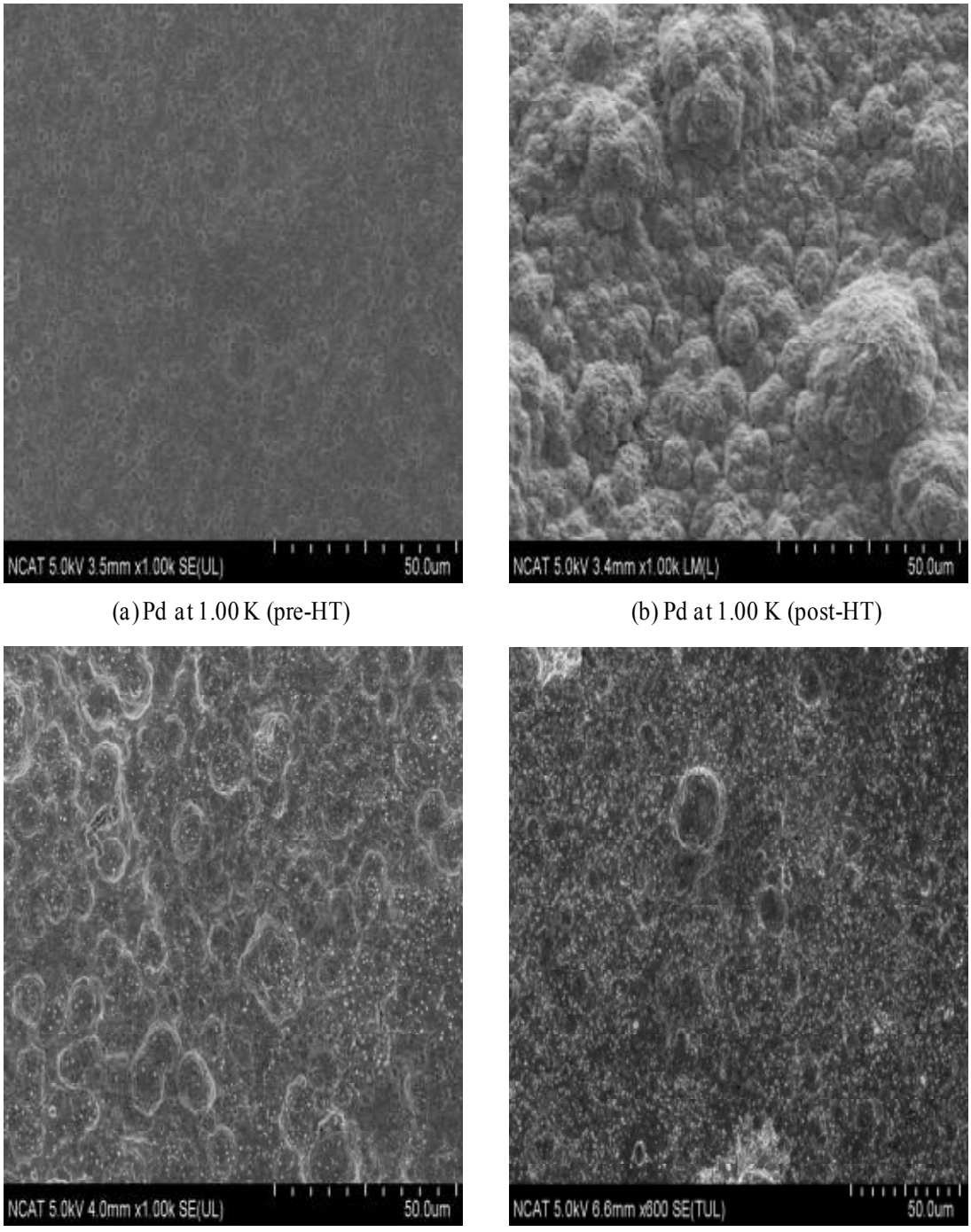

(a) Pd at 1.00 K (pre-HT)

(b) Pd at 1.00 K (post-HT)

(c) Pd at 1.00 K (after PT)

(d) Pd at 1.00 K (after 1200 hours test)

Figure 4.19. SEM images at 1.00 K magnification of Pd membrane at pre- and post-heat treatment (HT), after permeability test (PT), and after 1200 hours test.

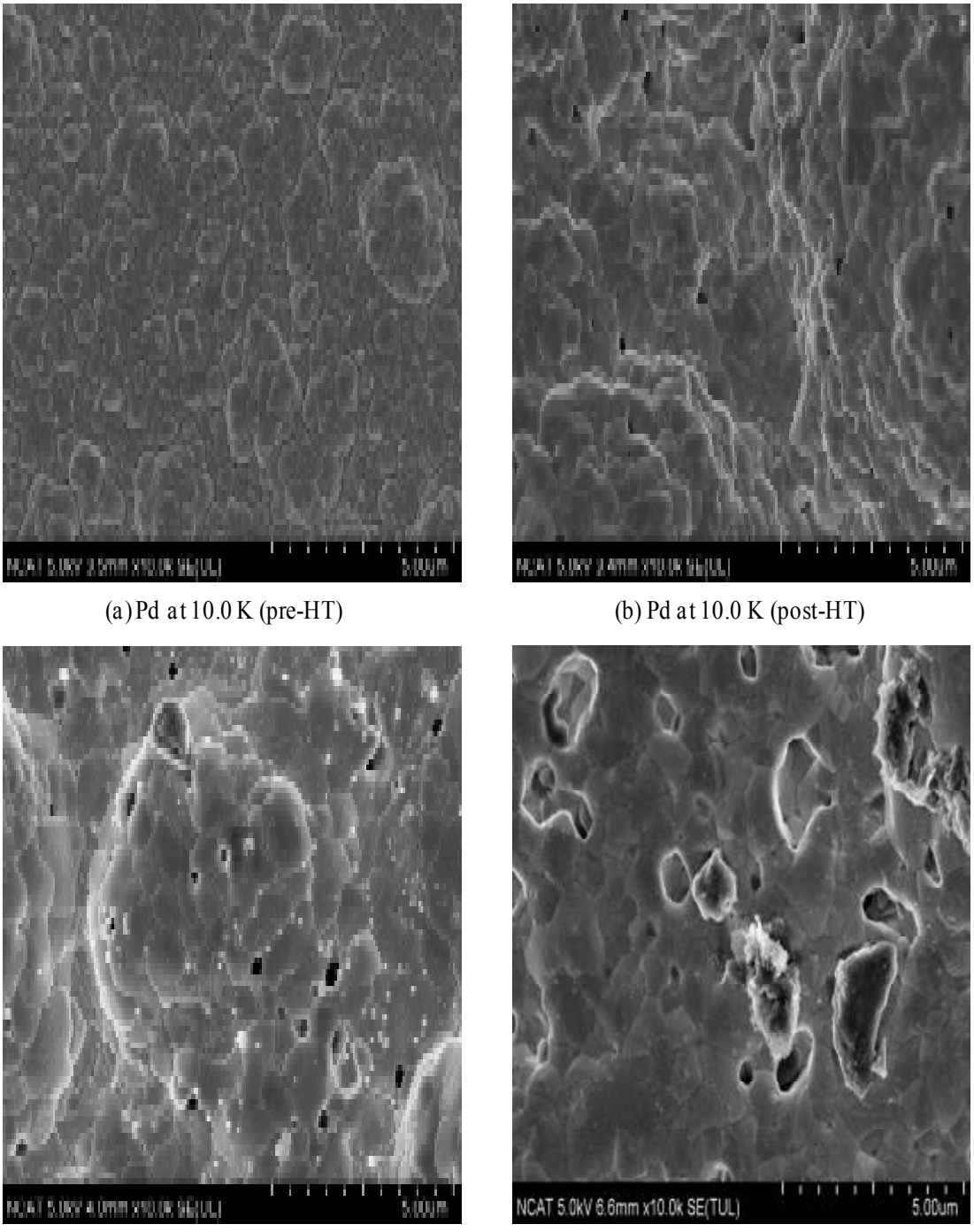

(a) Pd at 10.0 K (pre-HT)

(b) Pd at 10.0 K (post-HT)

(c) Pd at 10.0 K (after PT)

(d) Pd at 10.0 K (after 1200 hours test)

Figure 4.20. SEM images at 10.0 K magnification of Pd membrane at pre- and post-heat treatment (HT), after permeability test (PT), and after 1200 hours test.

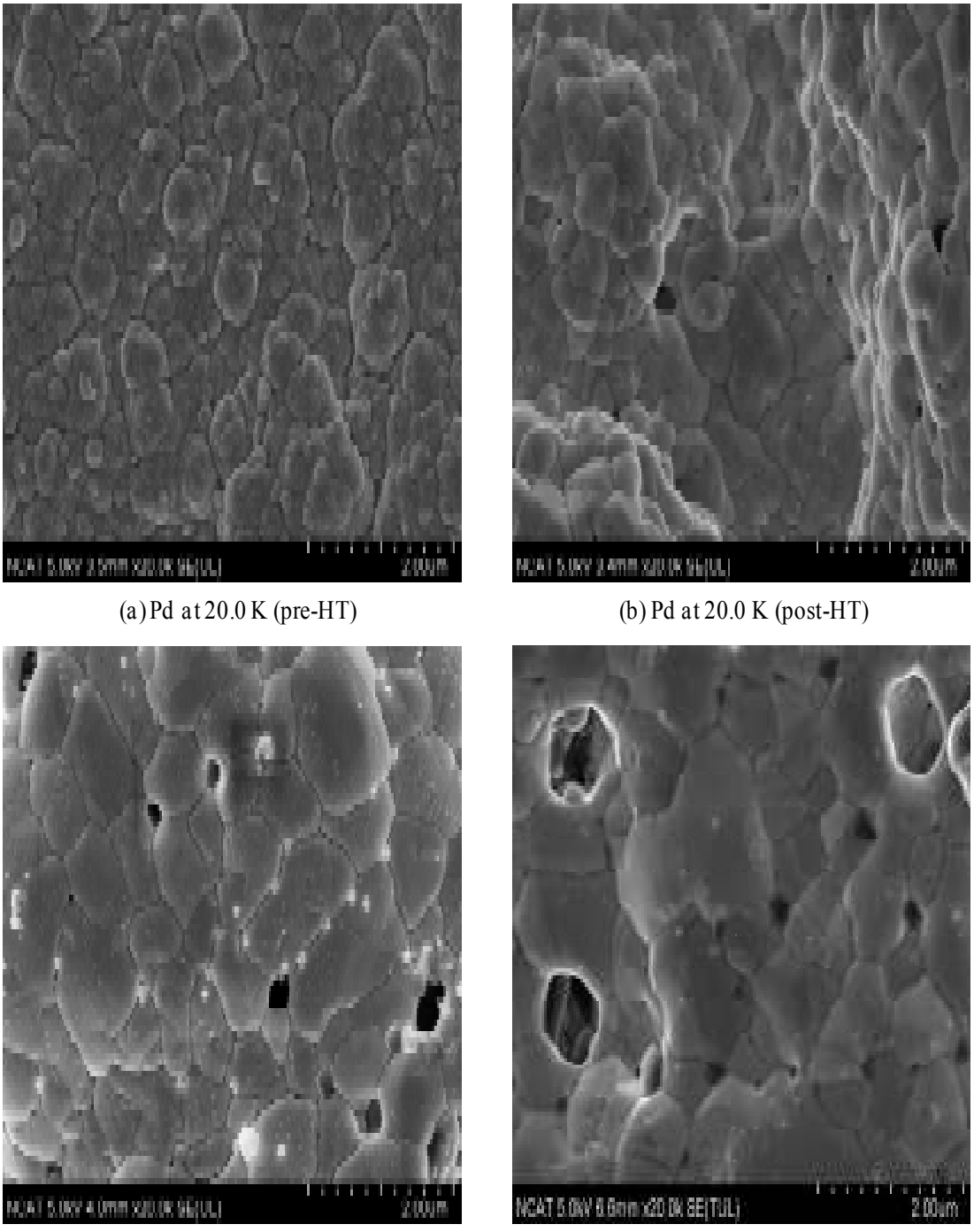

(a) Pd at 20.0 K (pre-HT)

(b) Pd at 20.0 K (post-HT)

(c) Pd at 20.0 K (after PT)

(d) Pd at 20.0 K (after 1200 hours test)

Figure 4.21. SEM images at 20.0 K magnification of Pd membrane at pre- and post-heat treatment (HT), after permeability test (PT), and after 1200 hours test.

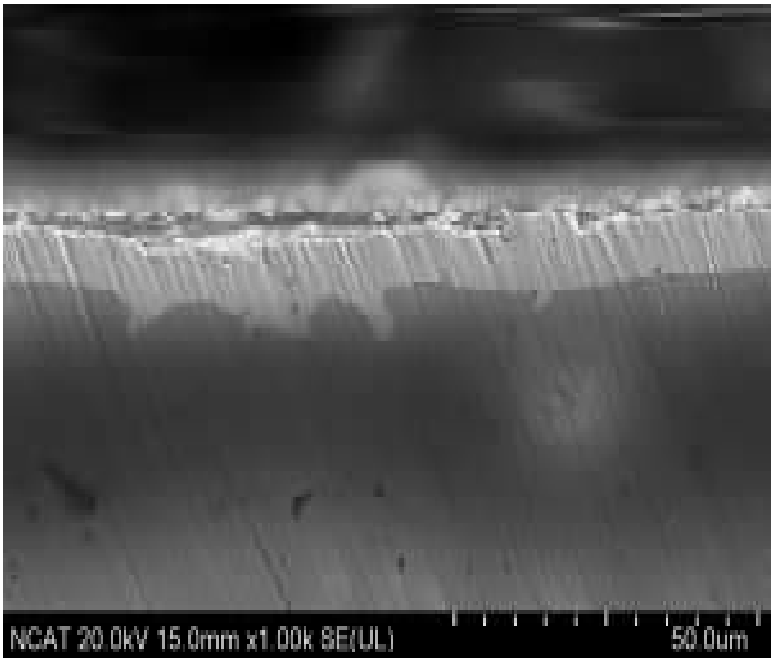

(a) Pd 31 film at 1.00 K (before-annealing)

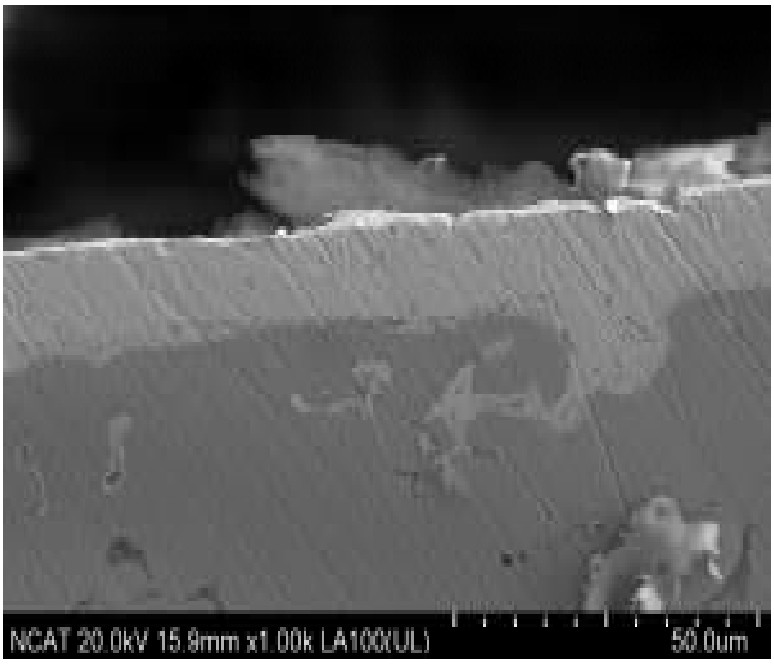

(b) Pd 19A film at 1.00 K (after-annealing)

Figure 4.22. Typical SEM images at 1.00 K magnification of Pd-film cross-section of two different membranes Pd 19A (after-annealing) and Pd 31(before-annealing).

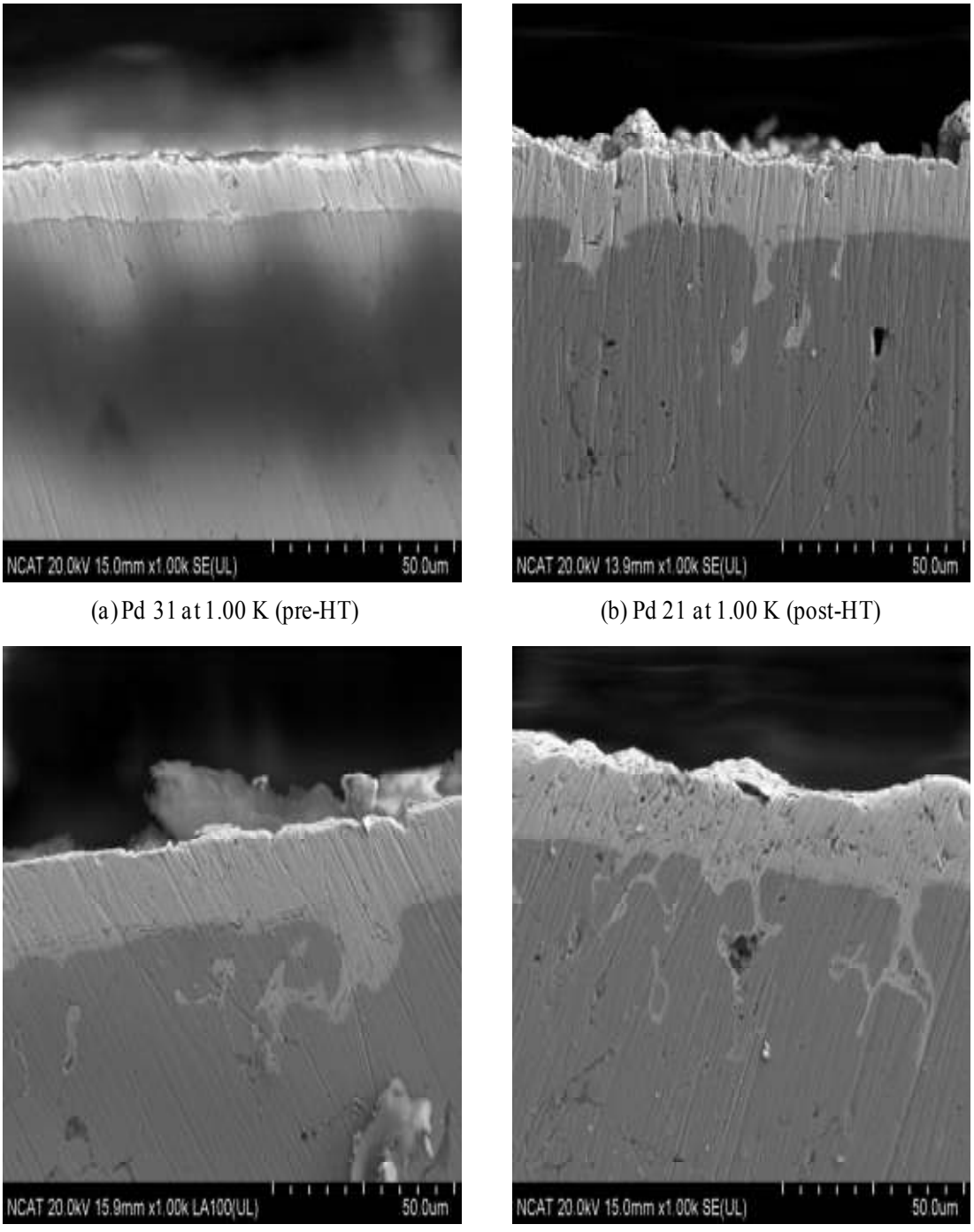

(a) Pd 31 at 1.00 K (pre-HT)

(b) Pd 21 at 1.00 K (post-HT)

(c) Pd 19A at 1.00 K (post-HT)

(d) Pd 26 at 1.00 K (post-HT)

Figure 4.23. SEM images at 1.00 K magnification of Pd-film cross-section of different membranes.

Cross-sectional EDS line scans were performed for both membranes after H_2 permeation tests at temperatures of 250 - 550 °C to confirm the intermetallic diffusion and metal distribution. The cross-sectional EDS line scans also give better understanding of the Pd deposition in the pores and on the surface of the substrate. EDS analysis was carried out from the pore mouth to a distance of 35 μm inside the interphase. A series of line scanning was carried out for Pd-film cross-section showed in Figure 4.24. The line scanning shows that in the palladium film, there were little peaks for elements such as Fe, Cr, and Ni and the highest peak was for Pd. After a certain level, the Pd peak drops sharply and the peaks for Fe, Cr and Ni peaks rise up. Figure 4.24 shows the intermetallic diffusion between Pd and MPSS elements dominated by Fe. Fe and Cr diffused into the Pd-film and Pd diffused into the stainless steel substrate in some extent.

EDS mapping was carried out for the Pd membrane cross-section to visualize the metal deposition and diffusion shown in the Figures 4.25 and 4.26. EDS mapping for Pd 31 at pre-heat treatment and Pd 26 at post-heat treatment are shown in Figures 4.25 and 4.26, respectively. Pd, Fe and Cr of membrane Pd 31 are highlighted in Figure 4.25 (a), (b) and (c) respectively. It is observed that Fe, Cr and Ni are found mainly in the substrate and a trace amount of these elements are found in the film. Since the cut piece of the membrane was needed to be polished before EDS analysis, some stainless steel particles containing Fe, Cr and Ni elements doped in the film during metal polishing for sample preparation. It is depicted in the EDS mapping shown in Figures 4.25 and 4.26 that Pd metal went far from the Pd-film and substrate interface inside the substrate. This diffused Pd blocked the pores of MPSS.

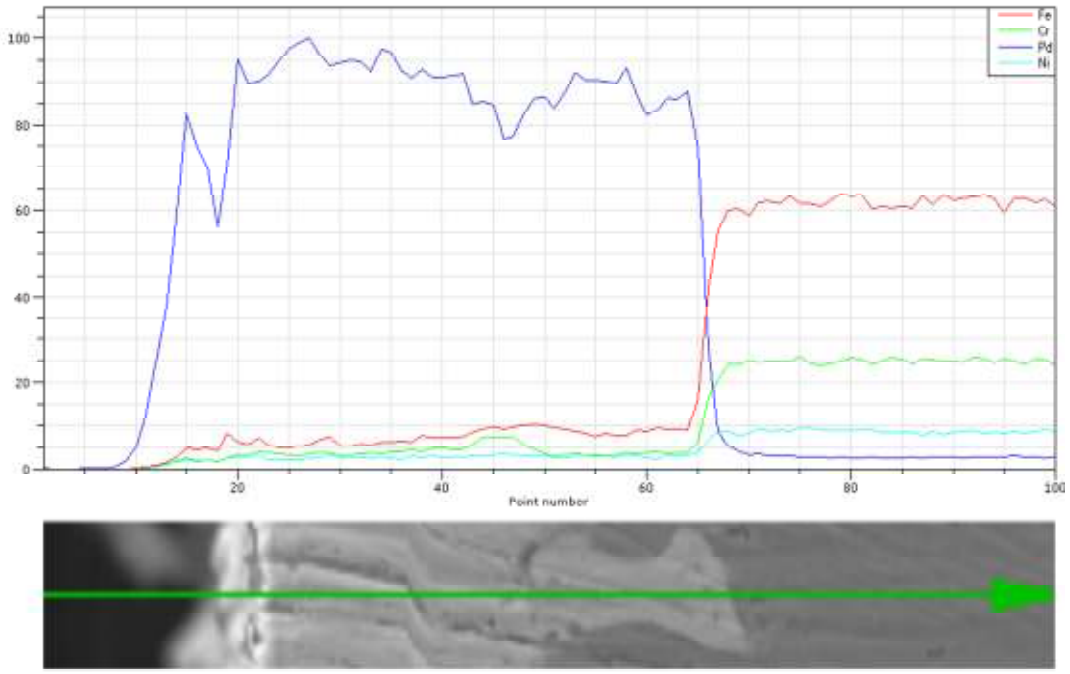

(a)

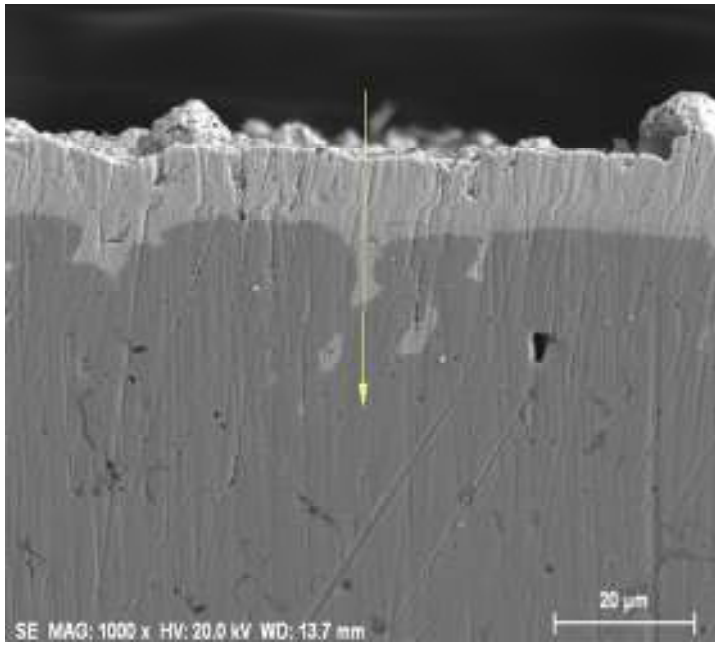

(b)

Figure 4.24. EDS line scanning of Pd-film cross-section [Scanning length 35 µm].

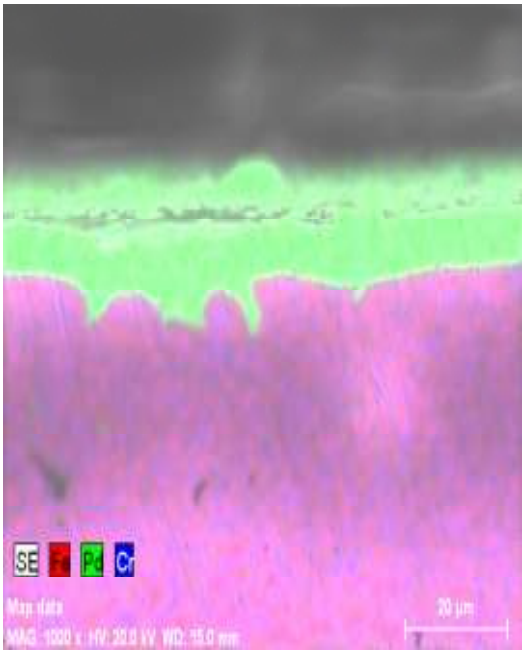

(a) X-section for EDS mapping

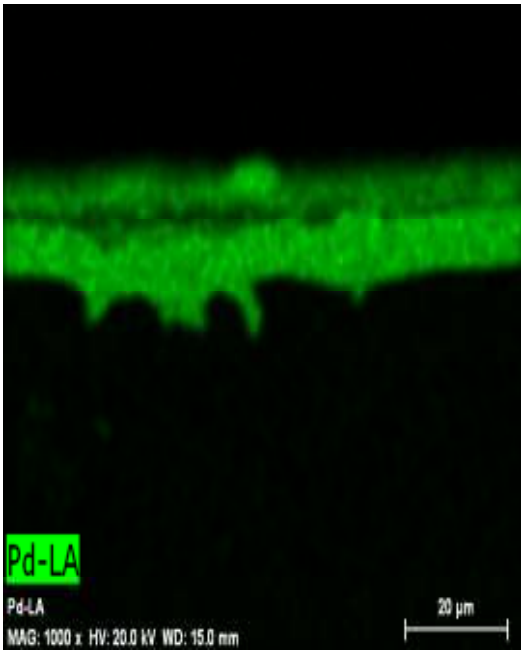

(b) Pd in EDS mapping

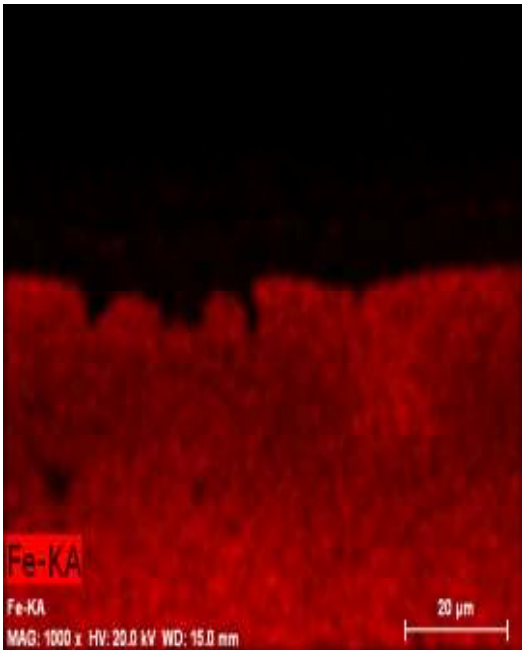

(c) Fe in EDS mapping

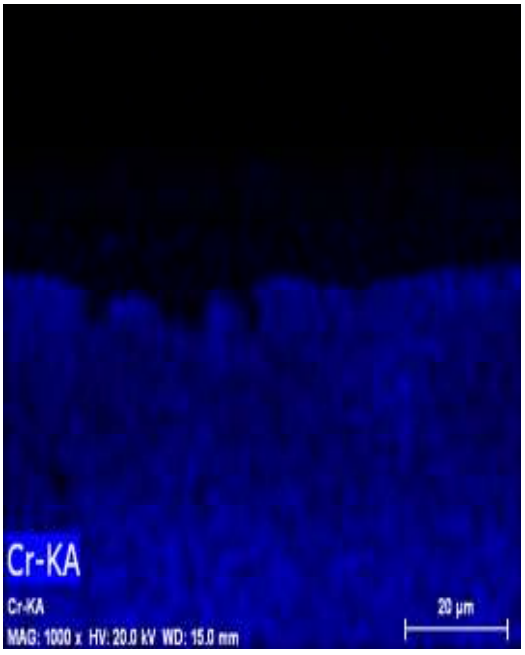

(d) Cr in EDS mapping

Figure 4.25. EDS mapping of Fe, Cr and Pd in Pd membrane fabricated by SIEP process showing the metal distribution in the Pd-film and substrate (before heat treatment).

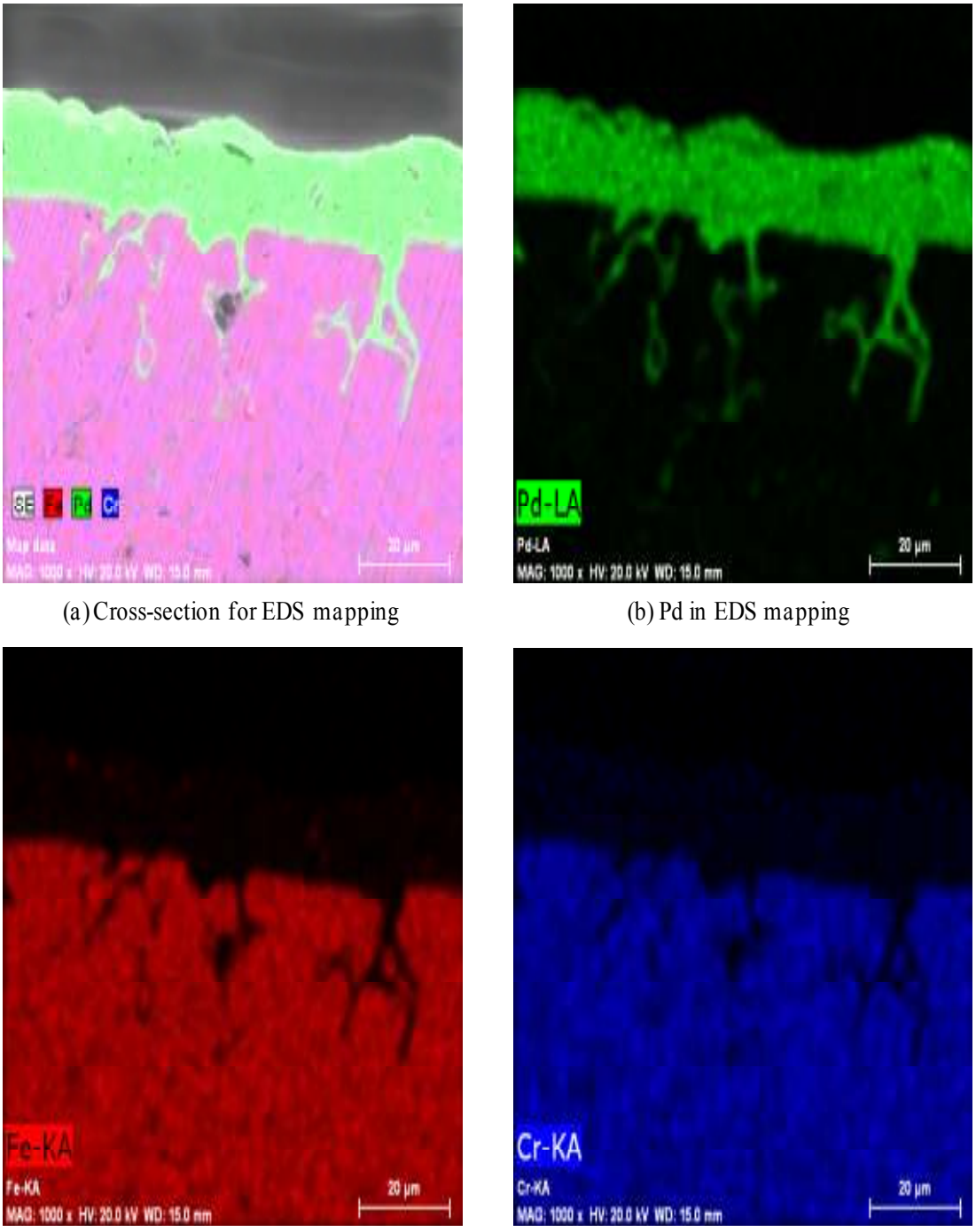

(a) Cross-section for EDS mapping

(b) Pd in EDS mapping

(c) Fe in EDS mapping

(d) Cr in EDS mapping

Figure 4.26. EDS mapping of Fe, Cr and Pd in Pd membrane fabricated by SIEP process showing the metal distribution in the Pd-film and substrate (after heat treatment).

4.4 Permeability Studies of Pd Membranes

The permeation tests were carried out with a H_2/N_2 single gas method. Each time, the membranes were assembled in a testing cell and sealed with graphite. The pressure on the permeate side was always ambient. Before testing, the membrane was heated up to 250 °C under nitrogen gas environment. The fluxes of pure nitrogen and pure hydrogen were measured as a function of their pressures on the membrane retentate side [49, 69]. After test, the membranes were thoroughly purged with nitrogen before cooling down to room temperature [69].

Membrane samples Pd 26 by using 4×CMC of DTAB, Pd 19A by using no DTAB, and Pd 21 and Pd 22 by using 1×CMC of DTAB were fabricated. From this study, we found that DTAB at 4×CMC was the most effective surfactant in SIEP process that enabled us to deposit integrated, defect free Pd-film on MPSS. We tested these Pd-MPSS membranes for gas-tightness and hydrogen perm-selectivity in our permeability measurement set-up shown in Figure 3.1 (as given in page 42). The thicknesses of the Pd-film on MPSS support were found to be 11.0 μm for Pd 26, 16.5 μm for Pd 19A, 12.4 μm for Pd 21 and 13 μm for Pd 22. Basically those membranes were fabricated using less thick Pd-film. Some pinholes were produced during heat treatment. To take the permeability test of these membranes, the membranes were needed more deposition to make it pinhole free again which increased the Pd-film thickness and decreased the hydrogen permeability and eventually increased the selectivity. Hydrogen permeance for the membrane sample Pd 26 was found to be 27.25 m^3/m^2-hr at 140 kPa and 550 °C. The selectivity of hydrogen with respect to nitrogen was about 330. This suggests the Pd-

MPSS membrane fabricated by SIEP technique was extremely gas-tight and essentially defect free at 11 μm Pd-film thickness. Shu et al. reported that at least 15 μm of metal deposited by an EP method is required to obtain a dense and defect free film when using 0.2 μm porous stainless steel supports [34]. So, the Pd-film thickness of Pd-composite membrane fabricated by SIEP process is much smaller than that for Pd-composite membrane fabricated by EP process.

The transport of hydrogen through dense Pd-film is a complex multistep process, which involves: (1) reversible dissociative chemisorptions of molecular hydrogen on the membrane surface; (2) reversible dissolution of atomic hydrogen in the bulk layers of the metal; (3) diffusion of atomic hydrogen through the bulk metal; and (4) association of hydrogen into hydrogen molecule. The hydrogen flux through dense Pd-film can be expressed in the form of Fick's first law as follows:

$$N_H = \frac{Q_H}{t}(P_f^n - P_p^n) \tag{4.1}$$

where Q_H is the hydrogen permeability (a product of solubility and diffusivity), t is the membrane thickness, and P_f and P_p are the partial pressures of hydrogen on the high and low pressure sides, respectively. When diffusion through the bulk metal is the rate limiting step and hydrogen atoms form an ideal solution in the metal, n is equal to 0.5, and then Equation. (4.1) becomes the Sievert's law.

The hydrogen permeability measurements were carried out in our permeation measurement set-up using pure hydrogen in the temperature range of 250 to 550 °C and in the pressure range of 20-100 psi. The measured data as a function of pressure

difference $(P_f - P_p)$ are presented in Figures 4.27, 4.28, 4.29 and 4.30 for samples Pd 26, Pd 19A, Pd 21 and Pd 22, respectively. The lines drawn in the figures are non-linear least-square fit with a power index, n = 0.82 for Pd 26, n = 0.85 for Pd 19A, n = 0.85 for Pd 22, and n = 0.84 for Pd 21 whereas for Pd-MPSS, Sievert's law index n is 0.5. The flux data in Figures 4.27, 4.28, 4.29, and 4.30 shows that with increasing temperature, hydrogen flux increases for a given transmembrane pressure difference. Further, hydrogen flux increases with increased pressure drop across the membrane. A value of n greater than 0.5 may result when surface processes influence the permeation rate [70]. The hydrogen diffusivity may become dependent on concentration of dissolved hydrogen and that may contribute to n values greater than 0.5 [37]. Leakage of hydrogen through defects in the metal film or membrane seals may also increase the value of n. Further, small resistance of the MPSS membrane support may also slightly increase the value of n. The deviation in the observed flux data from the idealized Sievert's law may be attributed to some of the contributing factors just discussed. Barbieri et al. reported that the index value (n) can be deviated from the Sievert's law for all reasons and the reasons cannot be concluded clearly [71]. The hydrogen flux of membrane samples Pd 26, Pd 19A, and Pd 21 are in the range of 0.161-1.7172 mol/m^2-s, 0.0142-0.2202 mol/m^2-s, 0.0601-0.4722 mol/m^2-s, respectively at temperatures of 250-550 °C and pressure drop of 20-100 psi. The flux of Pd 22 is in the range of 0.0.0429-0.1717 mol/m^2-s, at temperatures of 300 - 450 °C and pressure drop of 20-60 psi. Among all the membrane samples, Pd 26 fabricated by SIEP process using 4×CMC DTAB surfactant have shown best performance in permeability.

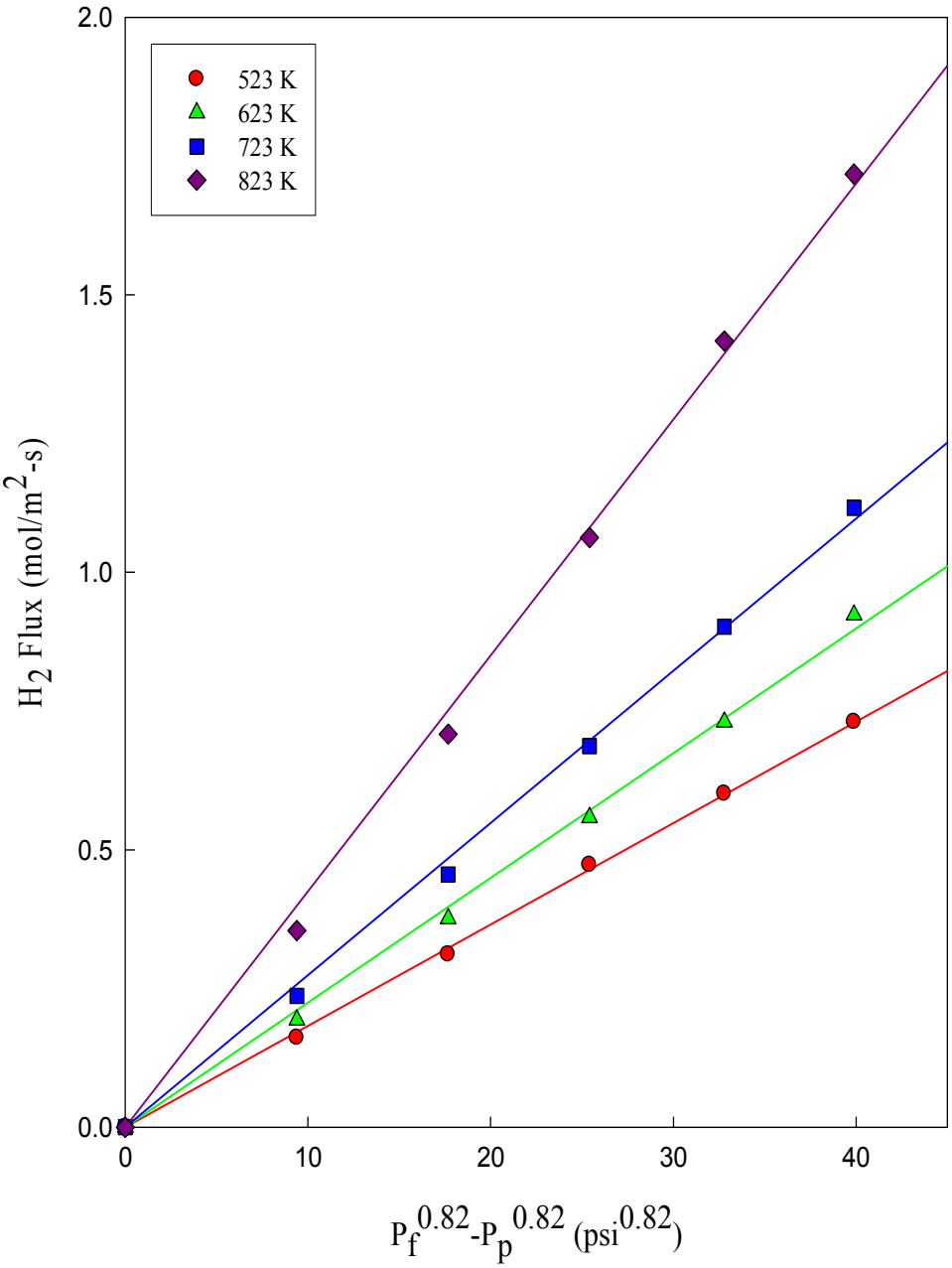

Figure 4.27. Hydrogen flux in Pd 26 MPSS membrane fabricated by SIEP process using 4×CMC of DTAB at different temperatures.

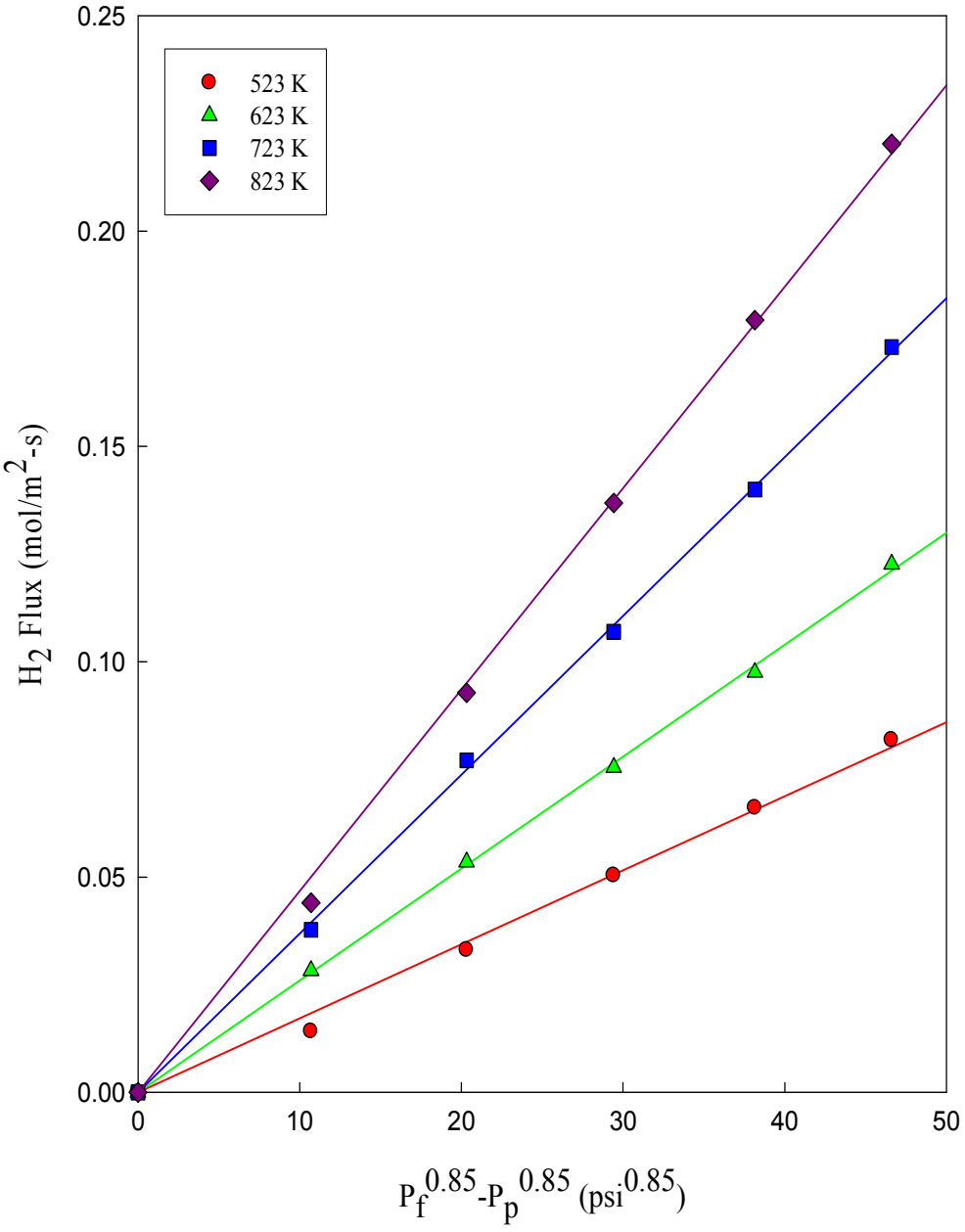

Figure 4.28. Hydrogen flux in Pd 19A MPSS membrane fabricated by CEP process.

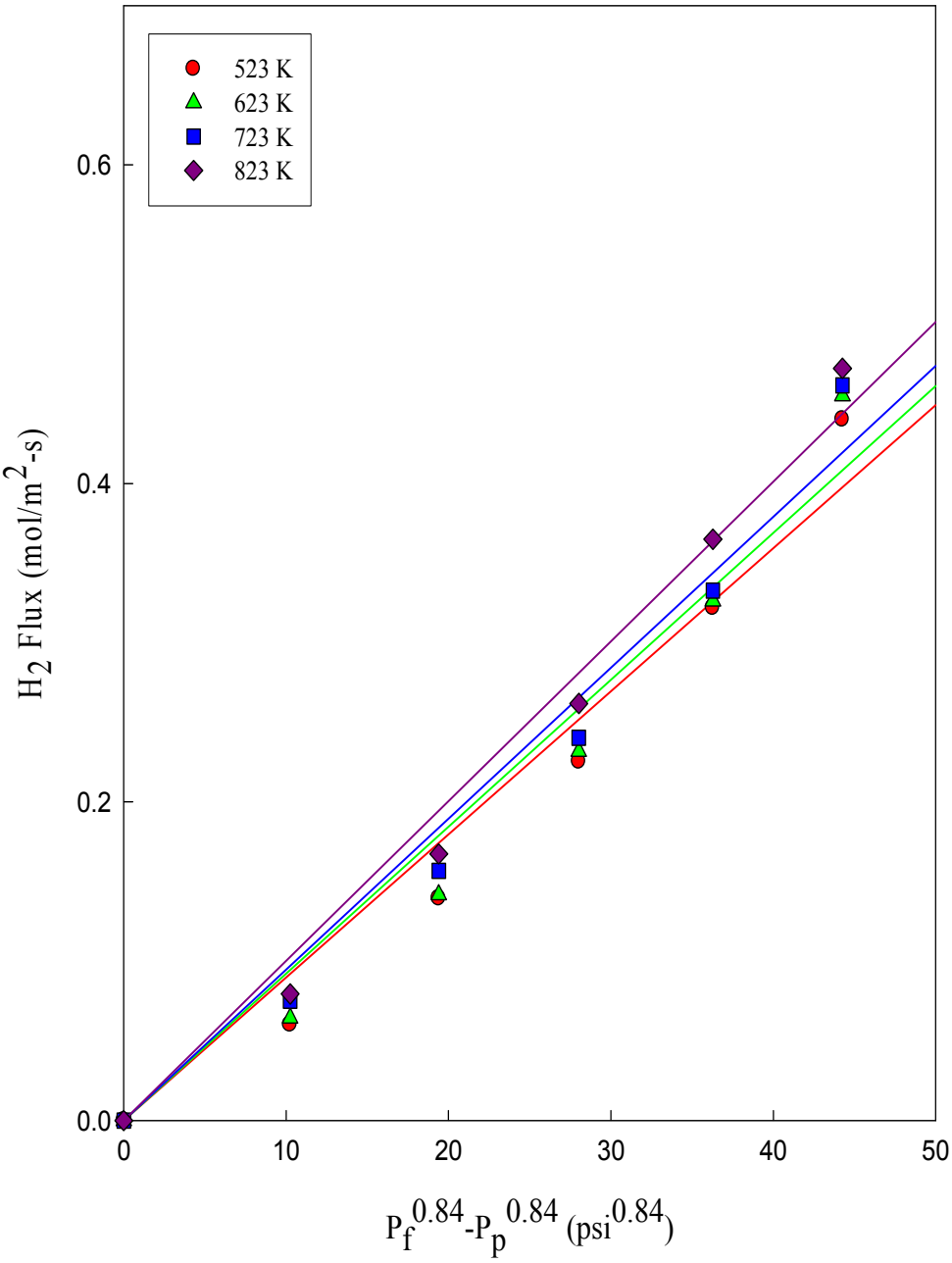

Figure 4.29. Hydrogen flux in Pd 21 MPSS membrane fabricated by SIEP process using 1×CMC of DTAB at different temperatures.

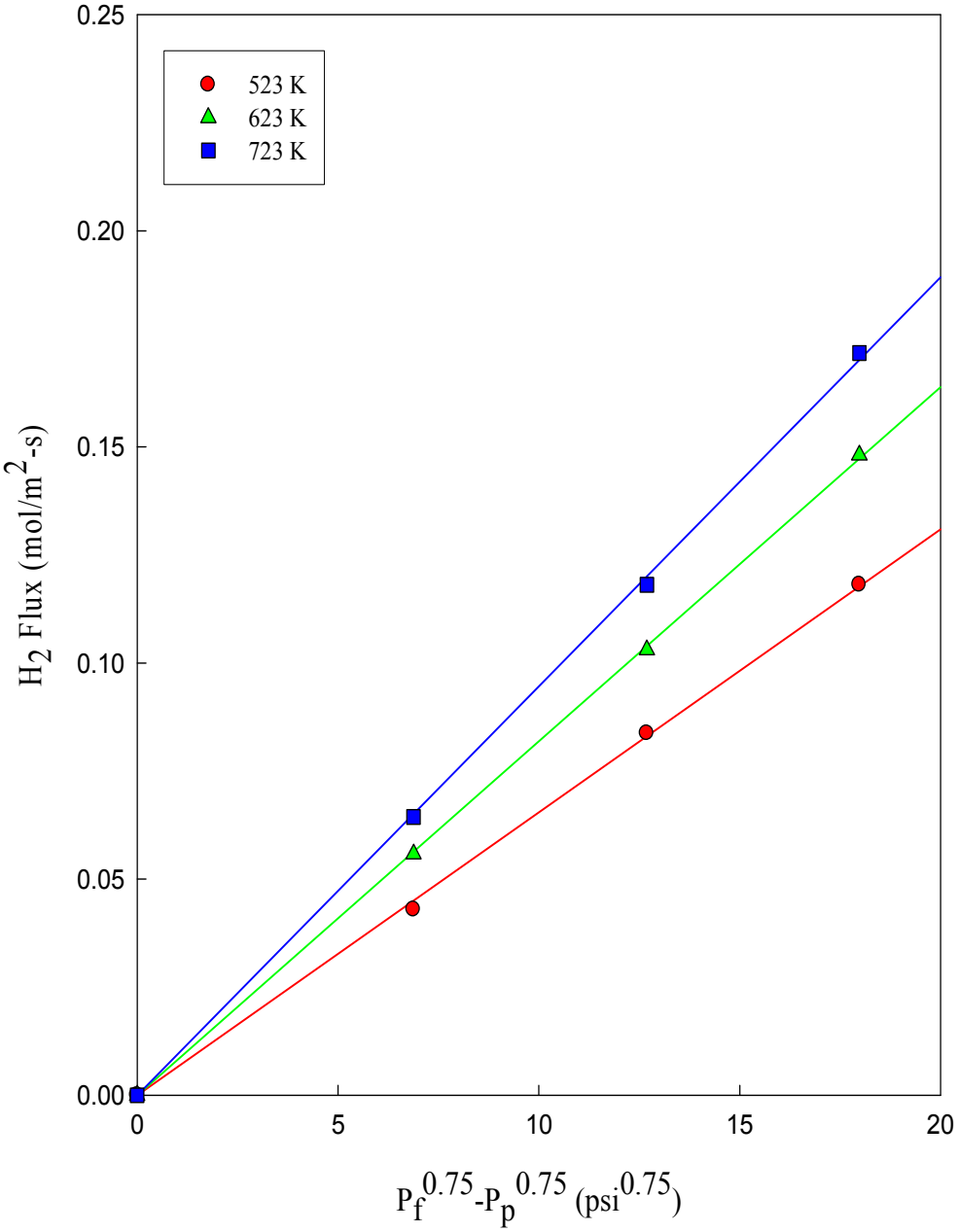

Figure 4.30. Hydrogen flux in Pd 22 MPSS membrane fabricated by SIEP process using 1×CMC of DTAB at different temperatures.

The membrane selectivity was defined as the ratio of hydrogen flux versus the nitrogen flux under identical conditions of temperature and pressure. The ability of a membrane to separate gases is characterized by the selectivity of the membrane. Ideal selectivity (or separation factor) is defined as the ratio of the permeability of the penetrants of interest.

Hydrogen to nitrogen selectivity data of samples Pd 26, Pd 19A, Pd 21 and Pd 22 are shown in Figures 4.31, 4.32, 4.33, and 4.34, respectively. These selectivity figures show that selectivity decreases with increasing pressure drop across the membrane exponentially at the same temperature and selectivity increases with increasing temperature at the same pressure drop. For all the membrane samples, regardless of concentration of used surfactant, selectivity is highest at the maximum temperature and minimum pressure drop and vise-versa. In this work, the maximum temperature and minimum pressure drop were 550 °C and 20 psi, respectively. The highest selectivity at 550 °C and 20 psi is 330 for Pd 26, 85 for Pd 19A, 207 for Pd 21 and 267 for Pd 22. Among these three membranes, Pd 26 fabricated by SIEP process using 4×CMC DTAB surfactant showed best selectivity and Pd 19A fabricated without surfactant showed least selectivity. The highest selectivity at 450 °C and 20 psi is 267 for Pd 22. The Pd-film thickness of Pd 22 (13 μm) is little higher than that for Pd 21 (12.4 μm) and Pd 26 (11 μm).

Grandjean et al. prepared Pd membranes supported on porous stainless steel disks by an EP method by modifying the substrates surface by shot peening treatment. They found that the H_2 permeance of their membranes was 5.8×10^{-7} $molm^{-2}$ s^{-1} Pa^{-1} [72].

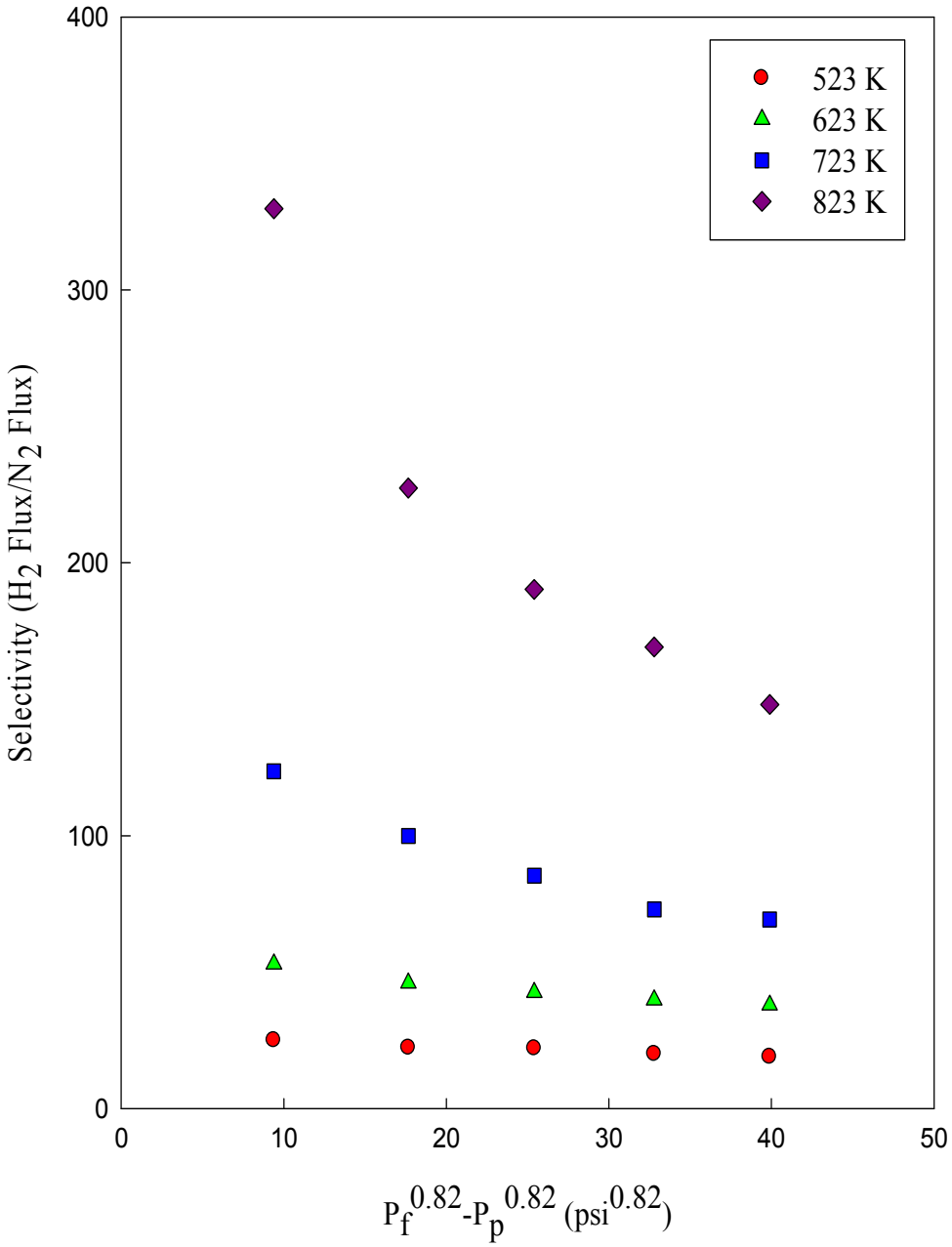

Figure 4.31. Hydrogen-to-nitrogen selectivity in Pd 26 MPSS membrane fabricated by SIEP process using 4×CMC of DTAB at different temperatures.

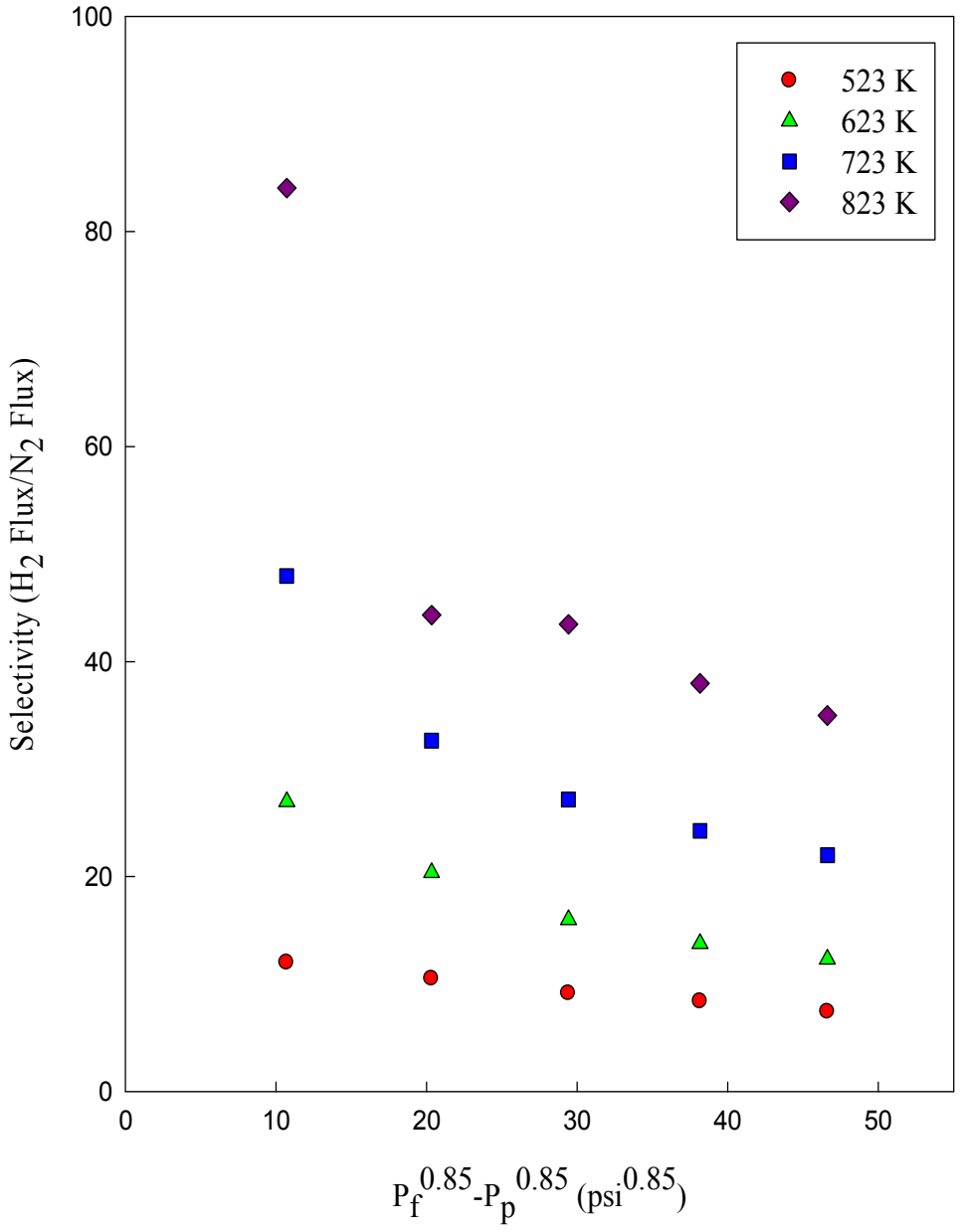

Figure 4.32. Hydrogen-to-nitrogen selectivity in Pd 19A MPSS membrane fabricated by CEP process.

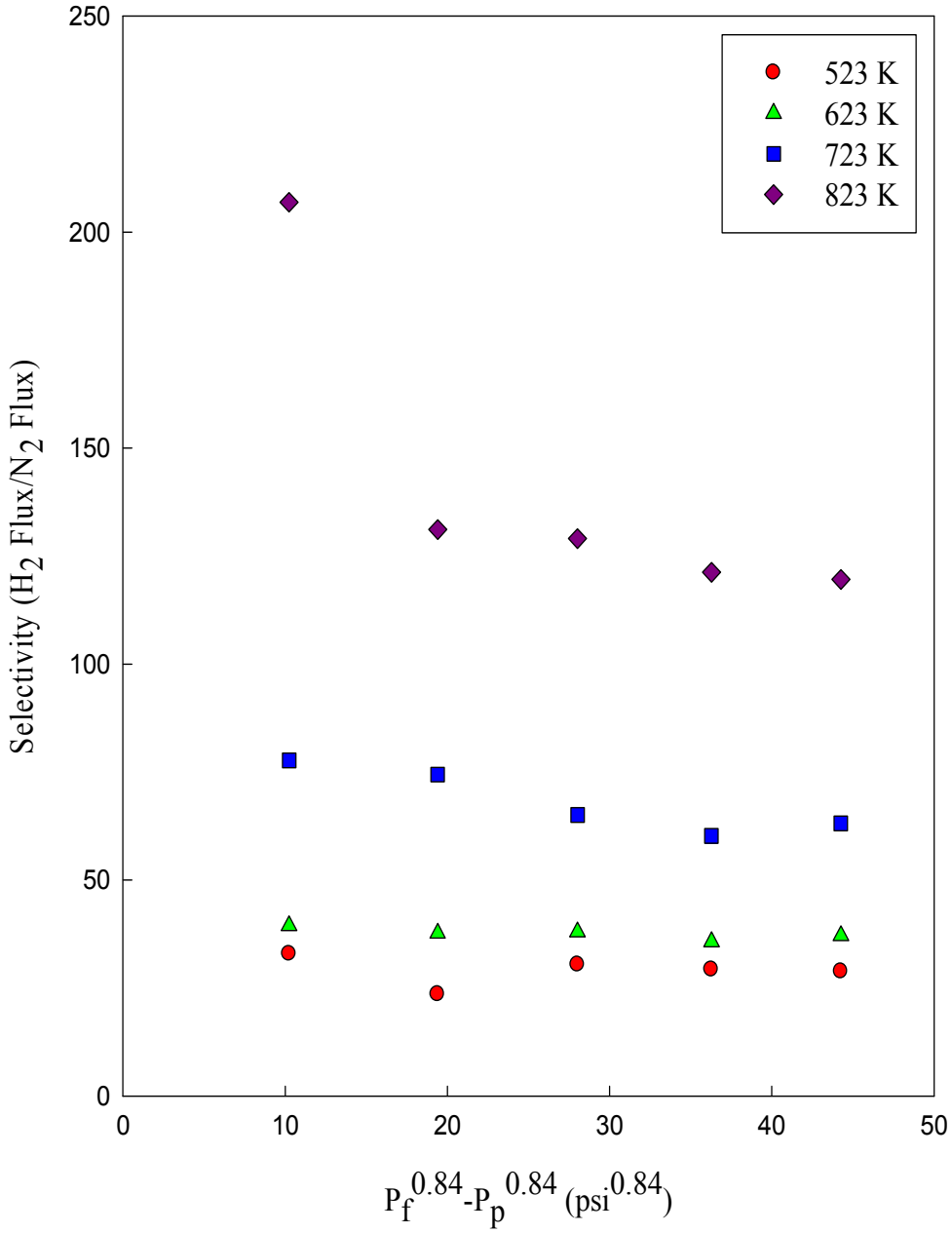

Figure 4.33. Hydrogen-to-nitrogen selectivity in Pd 21 MPSS membrane fabricated by SIEP process using 1×CMC of DTAB at different temperatures.

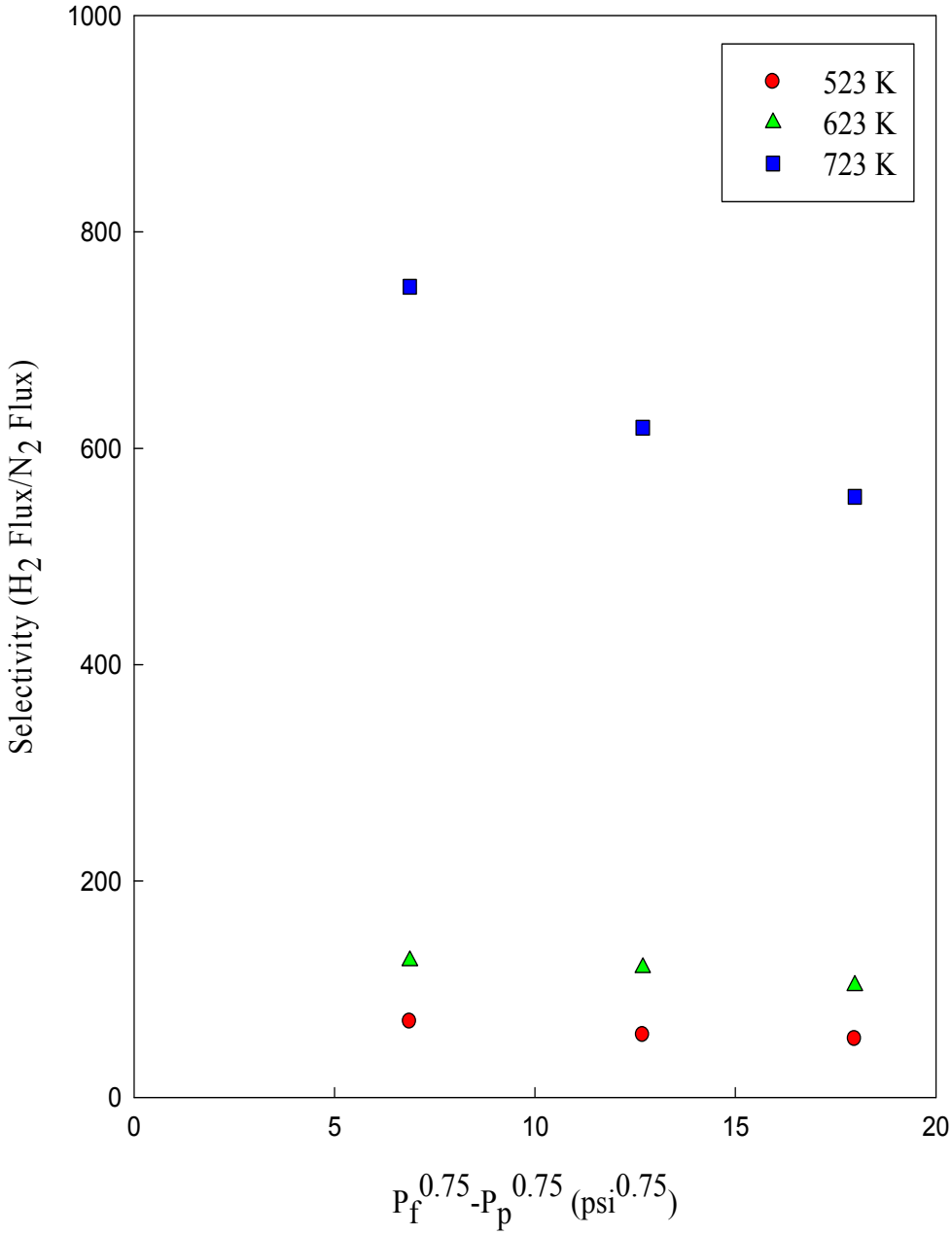

Figure 4.34. Hydrogen-to-nitrogen selectivity in Pd 22 MPSS membrane fabricated by SIEP process using 1×CMC of DTAB at different temperatures.

Tong et al. prepared Pd membranes with thickness of 2–3 μm by electroless plating of Pd or Pd/Ag layers with a thin diffusion barrier of silver by electro plating on a stainless steel substrate filled with aluminum hydroxide gel. Their best membrane showed H_2 permeance of 1.7×10^{-6} molm^{-2} s^{-1} Pa^{-1} with no N_2 permeance at 673 K [73]. Huang et al. produced Pd membranes on PSS by an EP method. Before coating they modified the substrate surface by coating with a porous yttria stabilized zirconia layer by atmospheric plasma spray. Huang group reported that the H_2 permeance of their membrane was 7.5×10^{-7} molm^{-2} s^{-1} Pa^{-1} at 673K with a H_2/N_2 selectivity of 700 [74].

Shi and Szpunar reported the fabrication of Pd membranes which showed a H_2 premeance of 6.5×10^{-7} molm^{-2} s^{-1} Pa^{-1} at 773K but did not mention the H_2 selectivity [75]. Ma et al. reported a preparation of Pd membrane on PSS with a chromium oxide layer as a diffusion barrier. Their best membrane showed H_2 permeance of 3.5×10^{-7} molm^{-2} s^{-1} Pa^{-1} with a very high H_2/He selectivity at 723 K [76]. Zhang et al. fabricated a Pd membrane of 11 μm thickness on PSS substrate modified with yttria stabilized zirconia layer as a diffusion barrier. This Pd membrane showed a permeance of 9.8×10^{-7} molm^{-2} s^{-1} Pa^{-1} at 773K with thermal stability to 923K [66]. A Pd membrane of 12 μm thickness on PSS with WO_3 intermediary layer was reported by Zahedi et al. [77]. They claimed that the membrane has permeance of 2.1×10^{-8} molm^{-2} s^{-1} Pa$^{0.5}$ with an exponent n = 0.5 and a N_2/H_2 selectivity of 10,000 at 723 K. Cornaglia and coworkers prepared a Pd membrane of 19 μm thickness on PSS with an effective diffusion barrier, NaA zeolite [78]. The membrane has permeance of 1.6×10^{-6} molm^{-2} s^{-1} Pa^{-1} with an exponent n = 0.5 and a N_2/H_2 selectivity of 608 at 723 K. Our Pd membrane fabricated by SIEP

method offers better H_2 flux data, with a film thickness of 11 μm over MPSS support. So fundamentally, this study is consistent with literature. From gas-tightness experiment, we are inclined to conclude that the Pd-MPSS (7.5 μm pd-film thickness) fabricated by DTAB induced SIEP is very much defect free. But, heat treatment produces pinholes. For the use of the membrane, repair deposition is required. So, the Pd-film thickness increases in some extent.

To illustrate the intrinsic membrane behavior of the SIEP Pd membranes, we computed the permeability coefficients Q_H using an Arrhenius plot (Q_H vs. 1/T). The Arrhenius plots of the four sample membranes are given in Figures 4.35, 4.36, 4.37 and 4.38. The data fits very well with the Arrhenius equation:

$$Q_H = Q_{Ho} \exp\left(-E / RT\right) \tag{4.2}$$

where Q_{Ho} is the reference permeance, E is the activation energy, T is the absolute temperature and R is the universal gas constant. We found, E = 8.83 KJ/mol for Pd 26 fabricated by SIEP using 4×CMC DTAB whereas E = 13.62 KJ/mol for Pd 19A fabricated by CEP process. The activation energy for Pd-film is lower than the reported results in literature. For Pd membrane, previously the reported activation energy was 14.45 KJ/mol for 17 μm Pd-film on ceramic substrate [70], and 19.7 KJ/mol was reported for a different membrane [63].

Table 4.3 shows different properties of the membranes such as membrane thickness, Sieverts'law index, activation energy, and pre-exponential index. The Pd-film thickness, Sieverts'law index and activation energy for Pd 26 is less than that for Pd 19A.

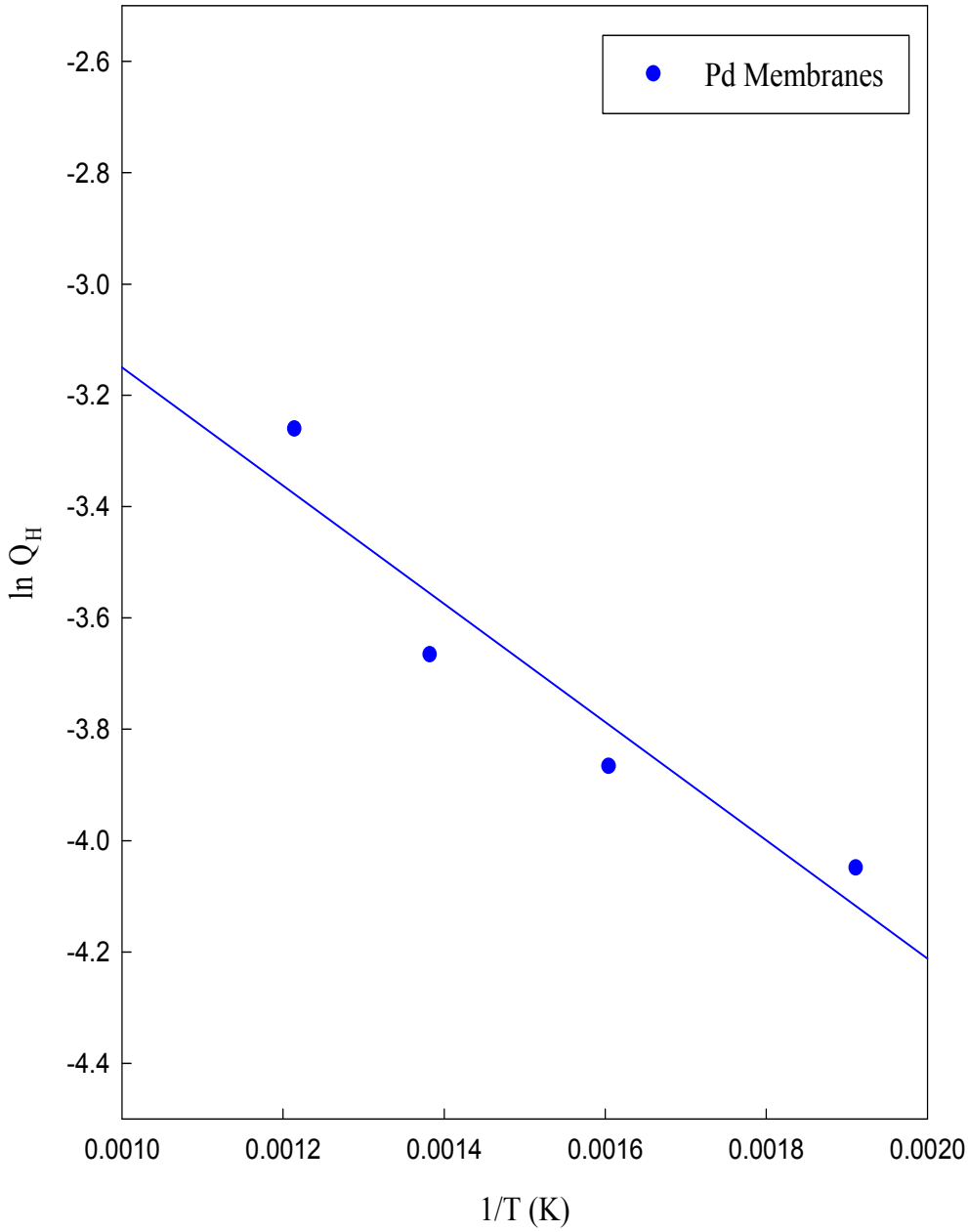

Figure 4.35. Arrhenius plot of H_2 permeability coefficients of Pd 26 MPSS membrane fabricated by SIEP process using 4×CMC of DTAB.

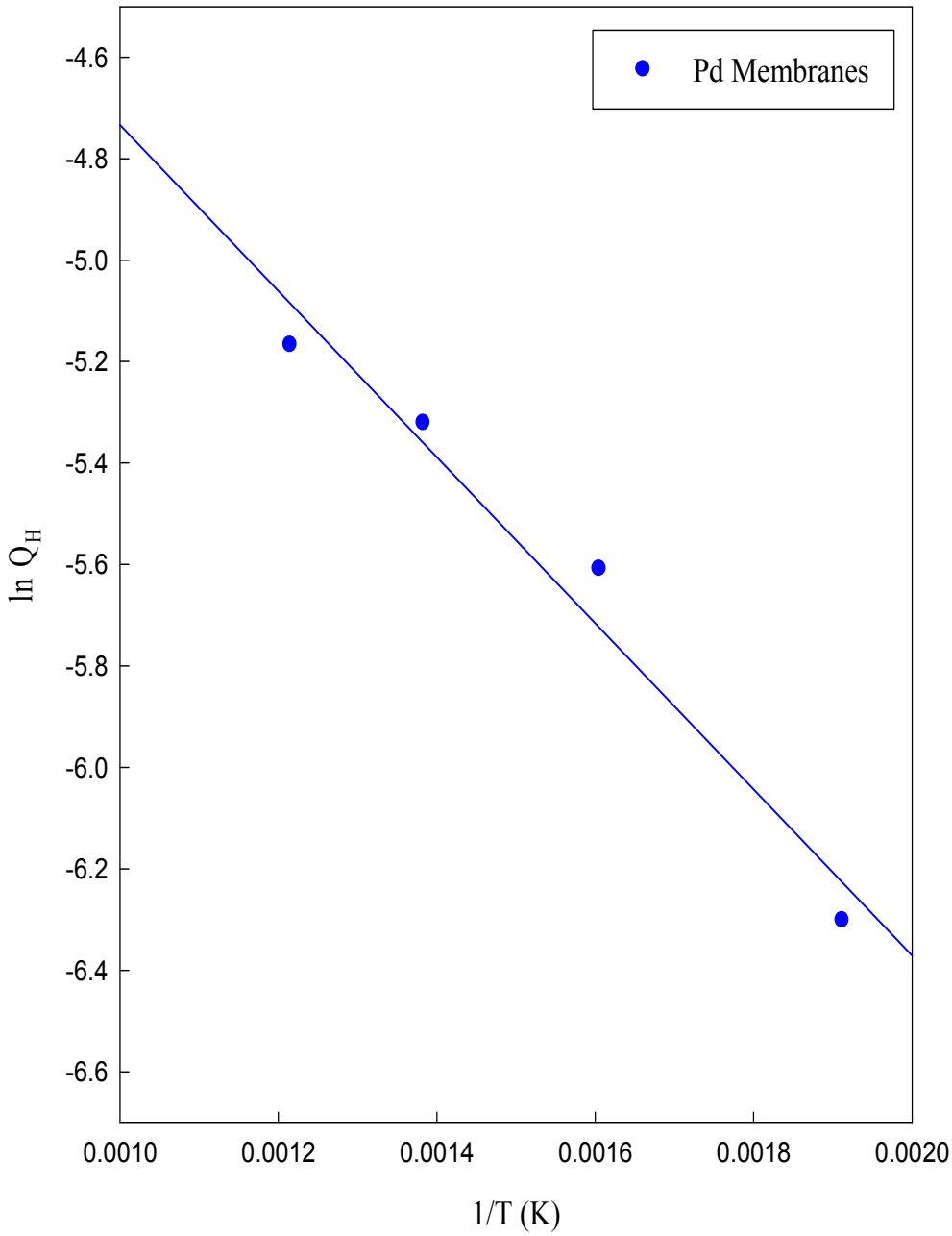

Figure 4.36. Arrhenius plot of H_2 permeability coefficients of Pd 19A MPSS membrane fabricated by CEP process.

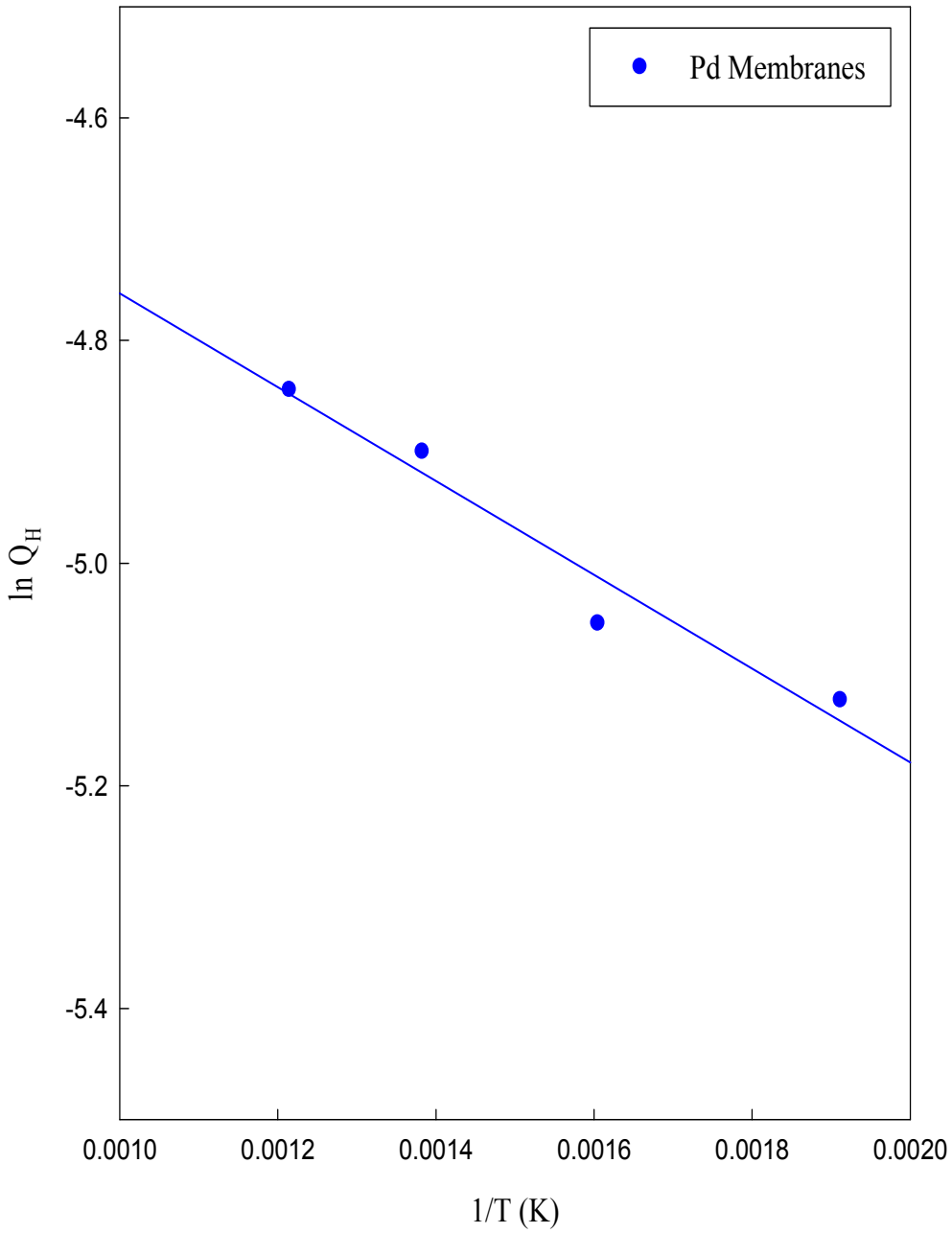

Figure 4.37. Arrhenius plot of H_2 permeability coefficients of Pd 21 MPSS membrane fabricated by SIEP process using 1×CMC of DTAB.

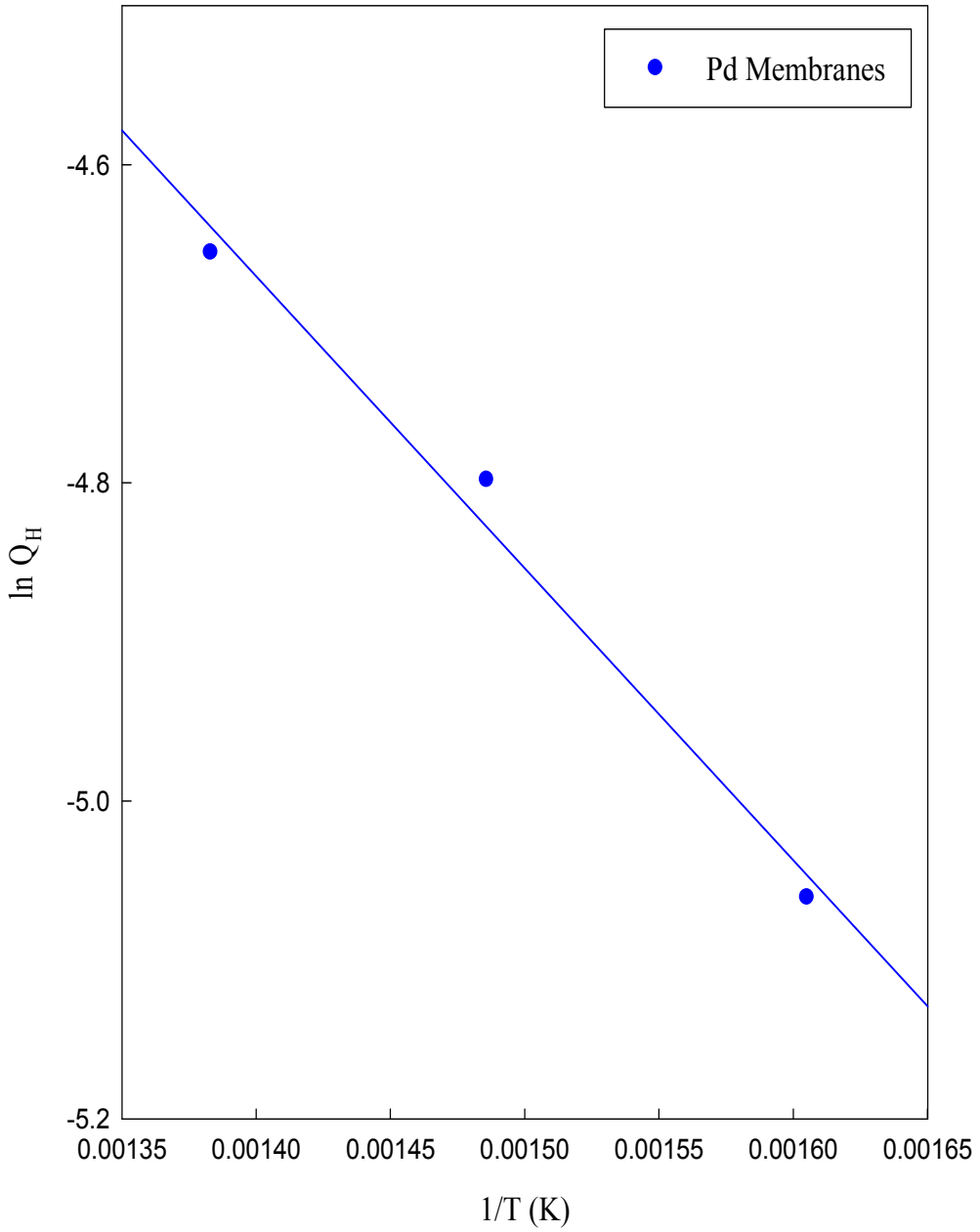

Figure 4.38. Arrhenius plot of H_2 permeability coefficients of Pd 22 MPSS membrane fabricated by SIEP process using 1×CMC of DTAB.

Table 4.3. Comparison of values of activation energy, Sieverts's law and Pre-exponential factor of different membranes fabricated by SIEP method

Membrane	DTAB (CMC)	Thickness by SEM (μm)	Sieverts' Law Power Index	Pre-exponential Factor Q_o	Activation Energy KJ/mol
Pd 19A	0	16.5	0.85	0.045	13.62
Pd 21	1	12.4	0.84	0.013	3.5
Pd 22	1	13	0.85	0.08	15.27
Pd 26	4	11	0.82	0.124	8.83
Pd 30	4	7.5	-	-	-
Pd 31	4	11.6	-	-	-
Pd 32	4	13.49	-	-	-

The pre-exponential index is greater than that for Pd 19A. From the values of the activation energy (*E*), we see that with increase in film thickness of membranes, value of activation energy decreases, which suggests that the surface phenomena of dissociative adsorption and recombinative desorption do not provide significant influence on permeation process of our fabricated Pd membranes. Activation energy for diffusion can be increased because of lattice defects, grain boundaries, and micro voids [55]. Membranes Pd 21 and Pd 22 did not give consistent results of different properties. So they could not be compared.

4.5 Long Term Performance

The long term stability of Pd-MPSS composite membranes was examined in H_2 and N_2 gases as a function of temperature. Defects may develop in the thin Pd-film at high temperatures [79, 80]; membrane Pd 30 was intentionally prepared with a relatively

thick film than usual pinhole-free membrane. This membrane needed 11.6 μm thick Pd-film to be helium gas tight. Pd 30 membrane was subjected to thermal cycling to check its performance. For a period of 1200 hours, H_2 flux of the membrane was recorded under thermal cycling of 300 – 450 – 300 °C, and at 15 psi pressure in our permeability test set-up. On each day of testing, the membrane underwent a couple of thermal cycles. During the 1200 hours hydrogen gas permeation test of the membrane, nitrogen leak test was carried out almost every 72 hours by switching hydrogen gas to nitrogen gas to check the integrity of the Pd membrane. During continuous operation, the membrane showed a good stability while the N_2 leakage was zero.

The Figure 4.39 shows that the hydrogen fluxes at 300 °C and 450 °C were 0.0150 and 0.0215 mol/(m^2-s), respectively. The hydrogen flux was increasing till almost 850 hours. After almost 850 hours of operation, flux became 0.0301 and 0.0365 mol/(m^2-s) at 300 °C and 450 °C temperatures, respectively. The increase in hydrogen flux up to 850 hours operation is attributed to the peeling off certain layer of the Pd-film. This peeling off made the Pd-film thinner, resulting in increasing hydrogen flux. As of 1200 hours of permeability test, the membrane remained stable. Over the period of 1200 hours of operation, there was no leakage of nitrogen indicating that H_2/N_2 permselectivity was infinite. However, after 1200 hours, the N_2 flux became 0.00215 mol/m^2-s, and the selectivity came to almost 18, based on the H_2 flux, 0.0365 mol/m^2-s at 450 °C. This indicates that in the temperature range of 300 – 450 °C, up to the 1200 hours test, there was no pinhole in the Pd-film. So, it can be assumed that some layers of the Pd-film were peeled off and all of a sudden, some of these peeled off spots became pinholes.

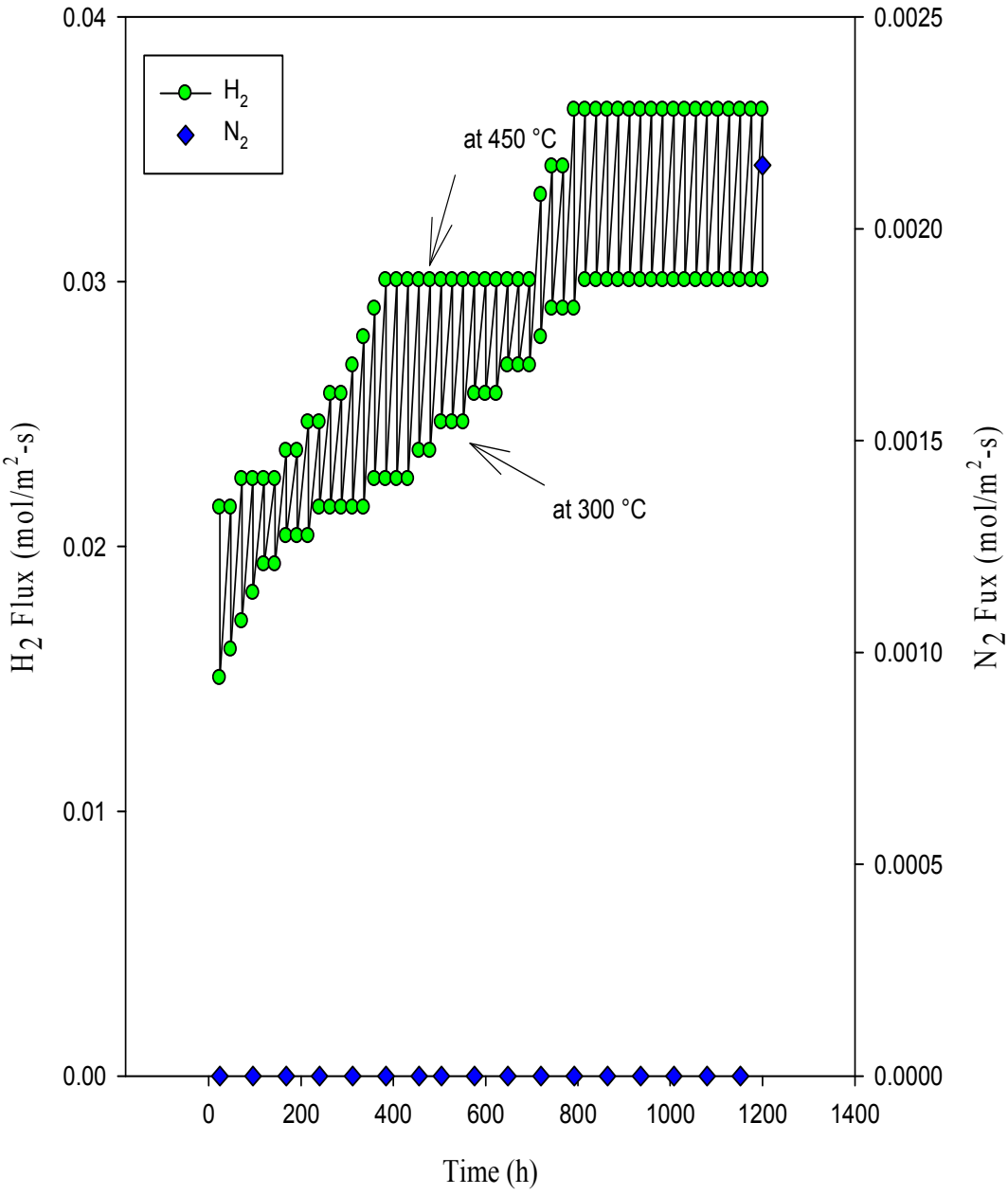

Figure 4.39. H_2 and N_2 flux data of Pd 30 composite MPSS membrane fabricated by SIEP method under thermal cycling at 15 psi transmembrane pressure.

Another membrane Pd 32 was fabricated by SIEP process, but an oxide layer as an intermetallic diffusion barrier was produced on the substrate surface prior to the application of the dense hydrogen selective Pd skin layer. For the oxide layer, the cleaned stainless steel substrate was heated at 600 °C for 12 hours in the presence of air. Instrumental analysis was not carried out for the confirmation of forming of the oxide layer. This membrane needed 13.49 μm thick Pd-film to be helium gas tight. The oxide surface is rougher. The Pd membrane needed thicker Pd-film to be helium gas tight due to having rougher oxide surface on the substrate surface. After heat treatment, Pd 32 membrane was tested for thermal cycling to check its performance and thermal stability. For a period of 408 hours, H_2 flux of the membrane was recorded under thermal cycling of 350 – 450 – 350 °C, and at 15 psi pressure in our permeability set-up.

Hydrogen and nitrogen flux data of Pd 32 composite MPSS membrane fabricated by SIEP method under thermal cycling are placed in the Figure 4.40. The Figure 4.40 shows that the hydrogen fluxes at 350 °C and 450 °C were 0.062 and 0.0773 mol/ (m^2-s), respectively after 408 hours. The hydrogen flux of membrane Pd 32 is about double than that of membrane 30. Over the 408 hours testing period, nitrogen flux was found to be zero. So the Pd 32 membrane performed thermal cycling for 408 hours with infinite selectivity. As of 408 hours of permeability test, the permeability remained stable. Though the thickness of the Pd 32 membrane is higher than that of the Pd 30 membrane, the hydrogen flux of membrane Pd 32 is about double than that of membrane Pd 30. Because Pd 32 membrane had an oxide film as a diffusion barrier on the substrate what prevented the metal diffusion.

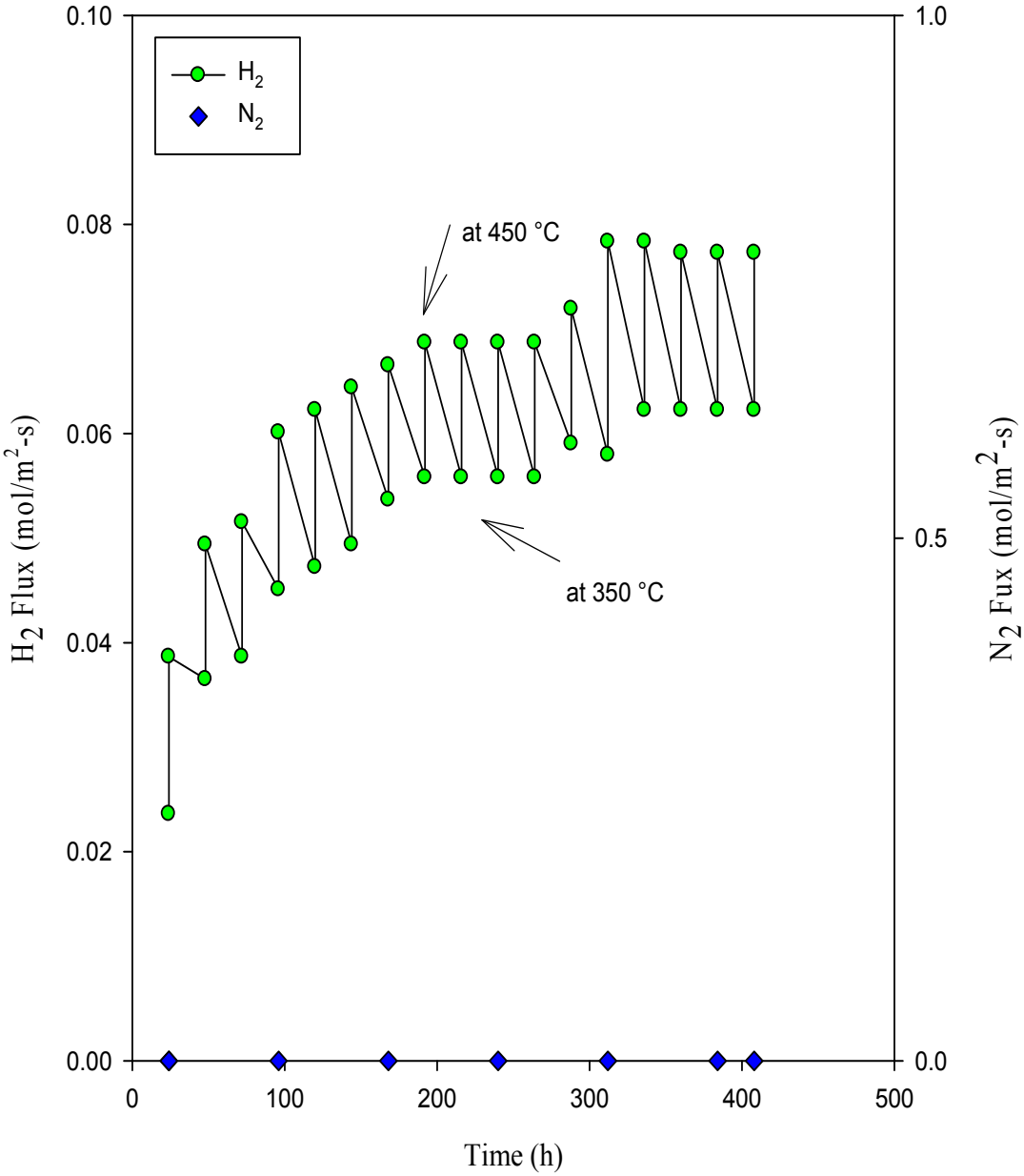

Figure 4.40. H_2 and N_2 flux data of Pd 32 composite MPSS membrane fabricated by SIEP method under thermal cycling at 15 psi transmembrane pressure.

Metal such as Fe, Cr or Ni of stainless steel diffuses into the Pd-film during annealing at 500 °C temperature under hydrogen atmosphere. In the absence of diffusion barrier, Pd-film and stainless steel elements produce a less permeable alloy during annealing. From Figures 4.39 and 4.40, it can be observed that both Pd 30 and Pd 32 have shown similar behavior in permeability and selectivity during the long term thermal stability test. The horizontal blue dashed line merged with abscissa in Figures 4.39 and 4.40 refers the introduction of N_2 for several minutes to check the integrity of the Pd membrane during H_2 permeation tests. No N_2 gas was observed passing through the membrane, indicating the absence of defects formed during performance tests. Once H_2 gas was introduced again in the system, H_2 flux decreased for both membranes but returned back to normal in few hours.

Lin et al. fabricated a Pd membrane with oxidized porous stainless steel. It was found that the minimum thickness of Pd membrane required for gas-tightness was 25 μm on oxidized PSS support [66]. Lin et al. also reported the fabrication of Pd membrane of 20 μm thickness on PSS support [81]. The final selectivity (H_2/N_2) and H_2 permeance of this membrane were 4000 and 5.0 m^3/m^2-h-$bar^{0.5}$, respectively after 900 hours test. Shirasaki et al. fabricated Pd/rare earth membrane of less than 20 μm thickness on PSS support [82]. This membrane showed selectivity (H_2/N_2) greater than 10000 after 3300 hours of test. Yi Hua Ma et al. claimed that they prepared Pd membrane of 4 μm thickness on hastelloy [83]. This membrane was tested for 2200 hours and the final selectivity (H_2/He) and H_2 permeance were found 22000 and 42.8 m^3/m^2-h-$bar^{0.5}$, respectively. 90%Pd/10%Cu membrane of 1.5 μm thickness on ZnO_2/porous alumina

support was reported by J. Douglas Way et al. [84]. The membrane prepared by J. Douglas Way et al. showed 7000 selectivity (H_2/N_2) and 12.6 m^3/m^2-h-bar H_2 permeance after 4100 hours operation. J. Douglas Way's group also reported fabrication of Pd 75%/Cu 25% membrane of 3 μm thickness on ZnO_2/porous alumina support [85]. Pd 75%/Cu 25% membrane performed 340 hours with 8.85 m^3/m^2-h-bar H_2 permeance and end selectivity 11 (H_2/N_2). Ronald hughes et al. reported the preparation of Pd/Ag membrane of 5.5 μm thickness on porous alumina support having 15.4 m^3/m^2-h-$bar^{0.61}$ H_2 permeance and 4500 selectivity (H_2/N_2) after 960 hours of testing period [86]. X.L. Pan et al. claimed that they prepared 3 μm thick Pd membranes which showed 16.4 m^3/m^2-h-bar H_2 permeance and 1300 selectivity (H_2/N_2) after 800 hours of testing period [87]. H. Li et al. reported the preparation of 10.9-13.8 μm thick Pd membrane on porous alumina substrate [88]. This Pd membrane performed 120 hours with 18 m^3/m^2-h-bar H_2 permeance whereas selectivity of this membrane was not mentioned. From the literature review, it is seen that no author reported any membrane performed long term thermal stability test with infinite selectivity. Our membranes fabricated by SIEP showed excellent long term thermal stability with comparable H_2 flux and infinite selectivity.

4.5.1 Post Process Characterization

The Pd 30 membrane fabricated by SIEP process using 4×CMC of DTAB was tested for thermal cycling (300 - 450 - 300 °C) for 1200 hours. After 1200 hours of performance, nitrogen gas started to leak, indicating some pinholes were created in the Pd-film of the membrane. This tested membrane was characterized by SEM analysis. Post-process characterization shows a considerable grain growth and micro-strain

relaxation in the Pd membrane after the prolonged permeation experiment. Changes in surface area are relatively small. The formation of pinholes is identified as the main source of the N_2 leakage during the testing at higher temperature.

Figures 4.41 and 4.42 show SEM images at 600 X, 1.00 K, 5.00 K, and 10.0 K and at 15.0 K, 20.0 K, 50.0 K, and 100 K magnifications, respectively of the surface topology of Pd 30 membrane at post 1200 hours performance and thermal stability test. It is seen from the SEM images taken after 1200 hours of operation that there are some pinholes on the surface of the membrane. In Figures 4.41 and 4.42, the morphology of the tested membrane shows that pinholes are over the whole membrane surface, indicating that pinhole formation is not a localized phenomenon but affects the whole surface. The pits have the average diameter about 0.67 μm. From the SEM images, it is seen that all of the pinholes did not penetrate the palladium layer with same diameter. Although selectivity came down all of a sudden, it is clear from the SEM image that all of the pinholes have not been created suddenly but these pinholes did not penetrate through the Pd-film. Peeling of the Pd layer occurred during the thermal cycling. The peeling made the Pd-film thinner. After 1200 hours of operation, some spots of the peeled off area passed through the Pd-film and became pinholes. Since 0.2 – 0.4 times of the melting point of nanocrystalline metal is the sintering temperature, sintering plays an important role in the formation of leak and leak growth [89]. Pd cluster sintering is one of the reasons for leak formation. Increased surface roughness is observed by SEM for which there may be several possible causal roots; lattice stress relaxation, BCC/FCC phase transition in the Pd alloy, Pd grain coalescence, or Pd grain sintering.

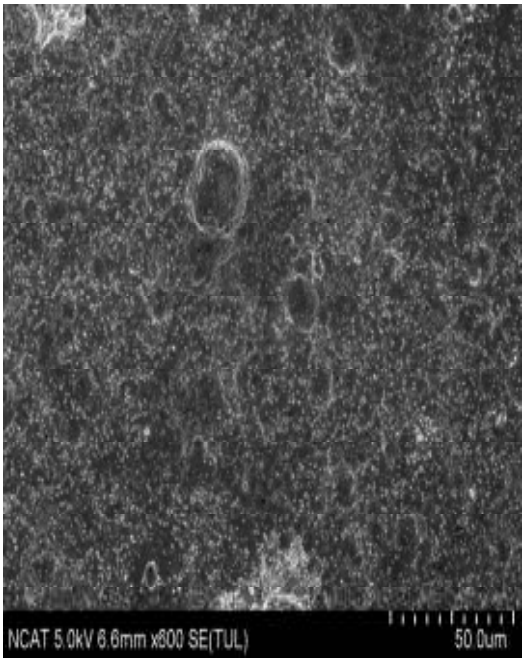

(a) Pd at 600 X

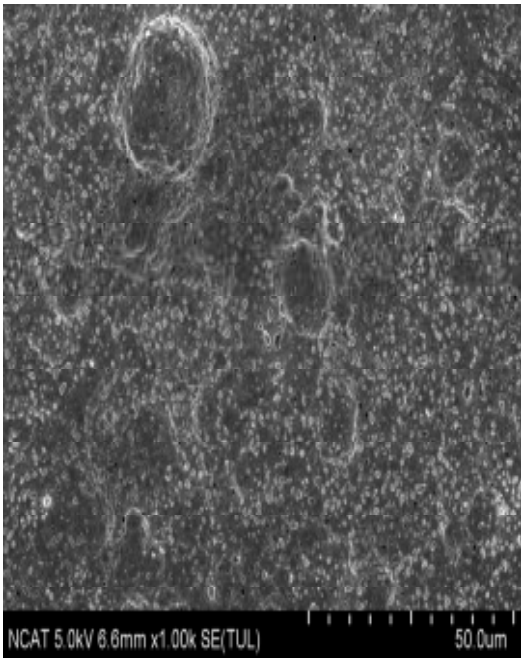

(b) Pd at 1.00 K

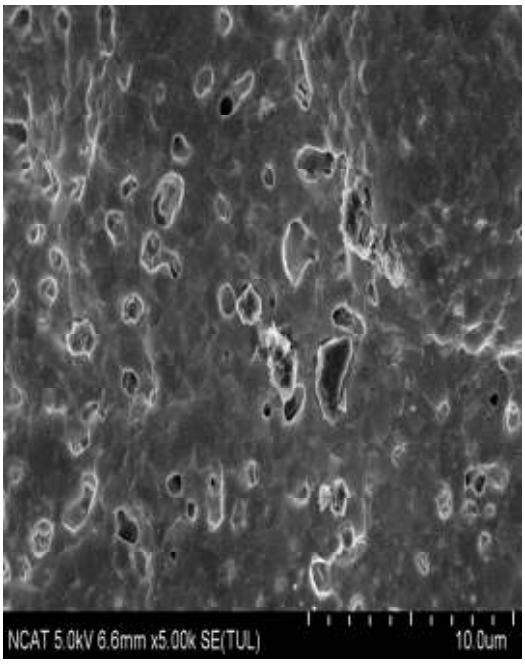

(c) Pd at 5.00 K

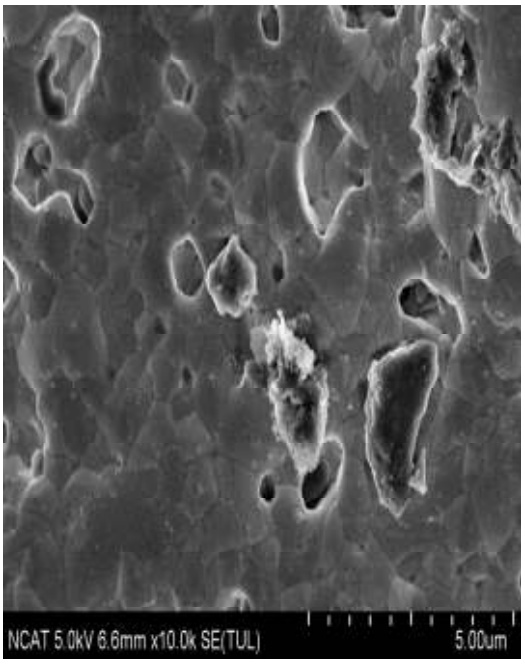

(d) Pd at 10.0 K

Figure 4.41. SEM images at 600 X, 1.00 K, 5.00 K and 10.0 K magnifications of Pd 30 membrane after 1200 hours of operation in the temperature range of 300 – 450 °C at 15 psi transmembrane pressure.

(e) Pd at 15.0 K

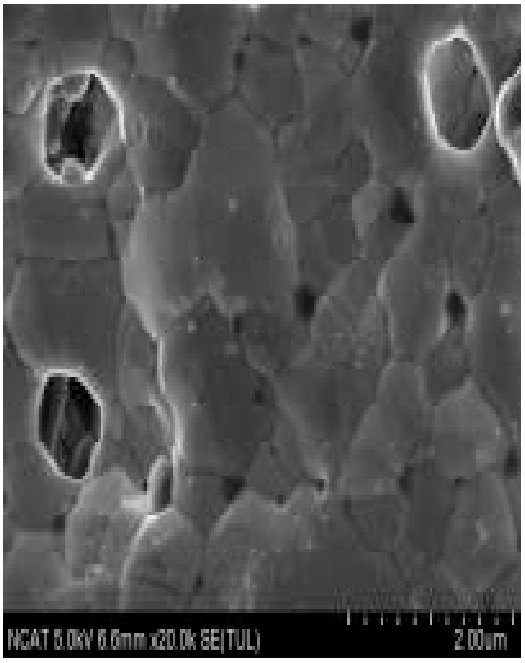

(f) Pd at 20.0 K

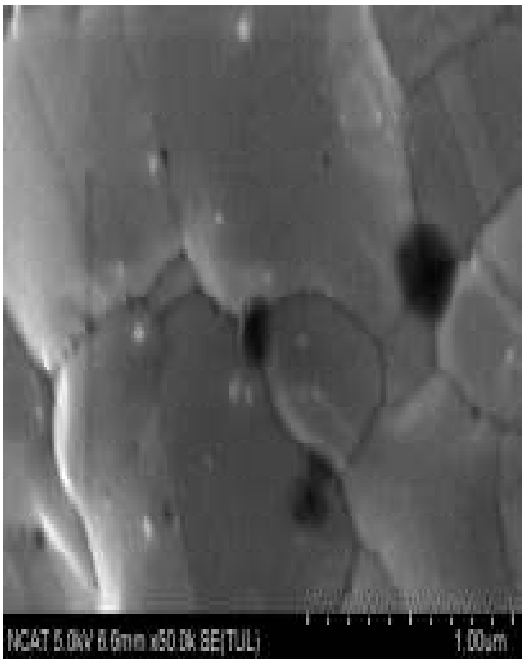

(g) Pd at 50.0 K

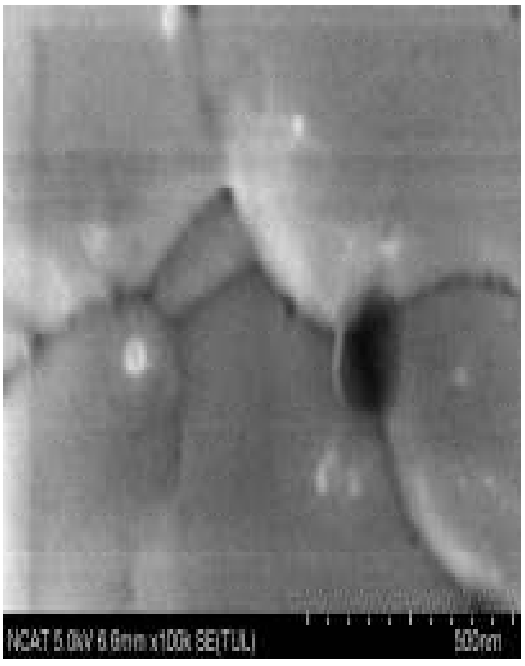

(h) Pd at 100 K

Figure 4.42. SEM images at 15.0 K, 20.0 K, 50.0 K, and 100 K magnifications of Pd 30 membrane after 1200 hours of operation in the temperature range of 300 - 450 °C at 15 psi transmembrane pressure.

Figures 4.41 and 4.42 show that some grains of the membrane top surface took shape of cauliflower. It looks like that the cauliflower shaped Pd grain was about to get off the membrane surface. It can be guessed that before peeling off, the Pd grain takes the cauliflower shape for some reasons.

The Pd 32 membrane with a diffusion barrier fabricated by SIEP process using 4×CMC of DTAB was tested for thermal cycling (350 – 450 – 350 °C) for 408 hours. Nitrogen gas did not leak through the membrane over the testing period. After 408 hours thermal stability test, the membrane was characterized by SEM analysis. Figures 4.43 and 4.44 show SEM images at 700 X, 1.00 K, 5.00 K, and 10.0 K and at 15.0 K, 20.0 K, 25.0 K, and 50.0 K magnifications, respectively of the surface topology of Pd 32 membrane at post 408 hours performance and thermal stability test. Figures 4.43 and 4.44 show that no significant number of pinholes has been created in the Pd-film of the membrane. Pd membrane permeating hydrogen gas is prone to have pinholes or defects operated below 350 °C temperature. Since Pd 32 membrane was not operated below 350 °C temperature, pinholes could not form. Though some very micropits are seen on the top surface of the Pd-film, these micropits did not go through the whole Pd layer to allow nitrogen gas to pass the membrane. The Pd 32 membrane contains infinitesimal sized and white colored spots over the whole surface area and some black spots in the agglomerated and clustered Pd grain boundaries. These spots might come from impurities present on the Pd layer. Pinholes might originate from the black spots. Figure 4.45 shows the SEM images at the resolutions of 5.00 K, 10.0 K and 15.0 K of Pd membranes at pre-heat treatment, after 408 hours test, and after 1200 hours test.

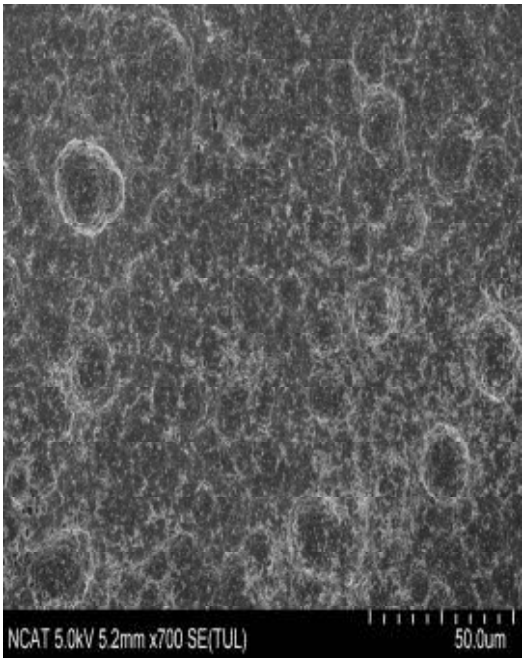

(a) Pd at 700 X

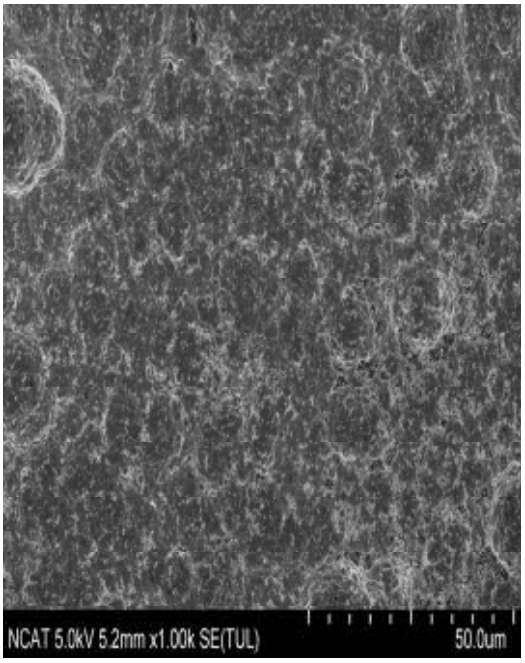

(b) Pd at 1.00 K

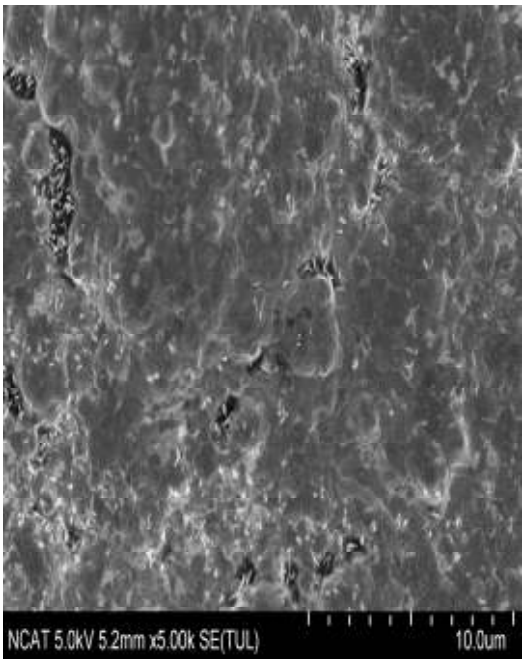

(c) Pd at 5.00 K

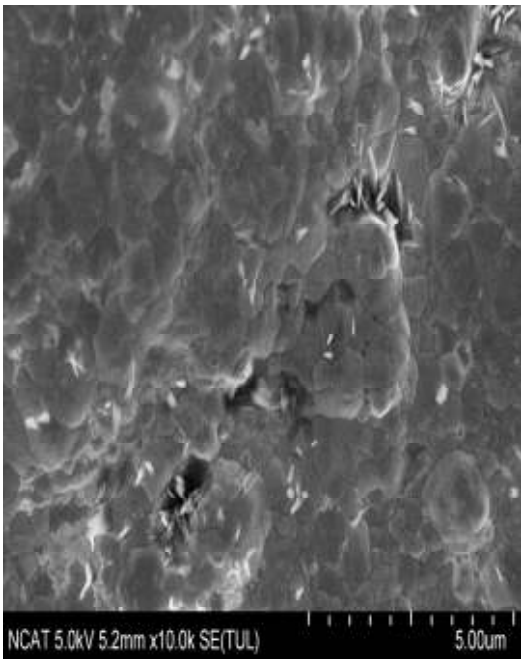

(d) Pd at 10.0 K

Figure 4.43. SEM images at 600 X, 1.00 K, 5.00 K and 10.0 K magnifications of Pd 32 membrane after 408 hours of operation in the temperature range of 350 – 450 °C at 15 psi transmembrane pressure.

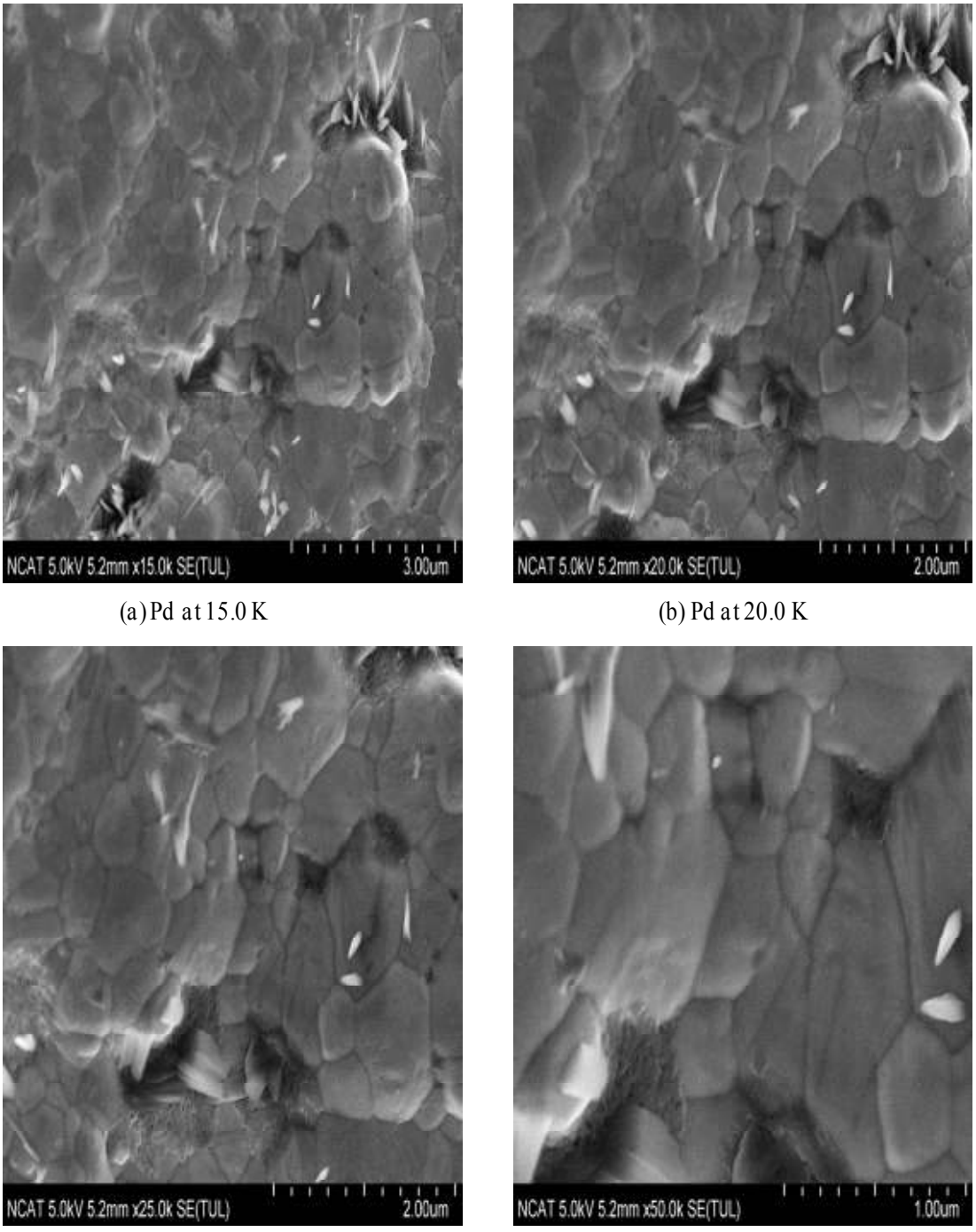

(a) Pd at 15.0 K

(b) Pd at 20.0 K

(c) Pd at 25.0 K

(d) Pd at 50.0 K

Figure 4.44. SEM images at 15.0 K, 20.0 K, 25.0 K and 50.0 K magnifications of Pd 32 membrane after 408 hours of operation in the temperature range of 350 – 450 °C at 15 psi transmembrane pressure.

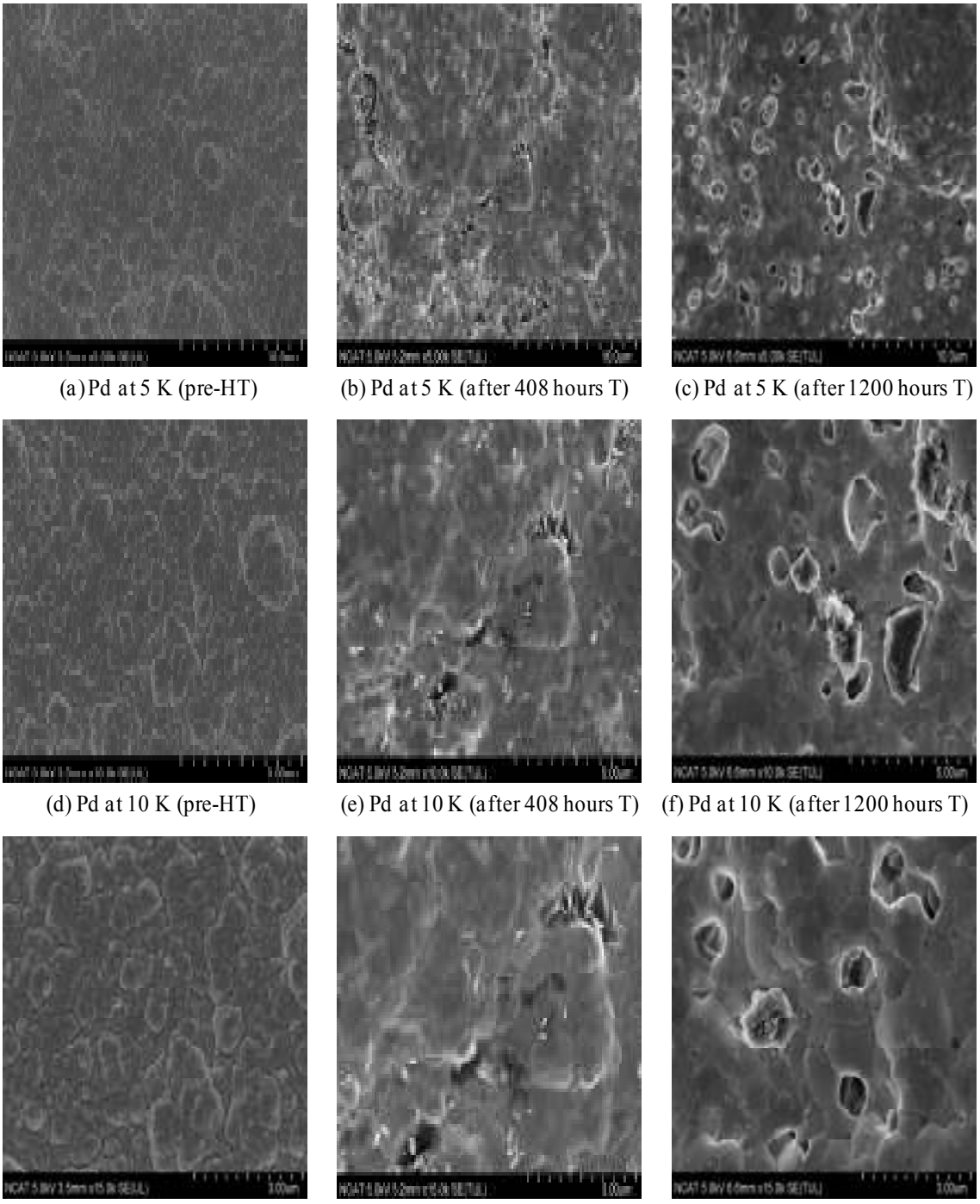

(a) Pd at 5 K (pre-HT) (b) Pd at 5 K (after 408 hours T) (c) Pd at 5 K (after 1200 hours T)

(d) Pd at 10 K (pre-HT) (e) Pd at 10 K (after 408 hours T) (f) Pd at 10 K (after 1200 hours T)

(g) Pd at 15 K (pre-HT) (h) Pd at 15 K (after 408 hours T) (i) Pd at 15 K (after 1200 hours T)

Figure 4.45. SEM images of Pd membranes at pre-heat treatment (HT), and after 408 and 1200 hours test (T).

CHAPTER 5

CONCLUSIONS

This work encompasses the fabrication of Pd-composite membrane on MPSS substrate by SIEP process as well as the investigation of thermal stability of the fabricated membranes. Membrane structure has a significant effect on hydrogen permeance and selectivity of Pd membranes [10]. In this study, we used a cationic surfactant, DTAB at different concentrations, which enables the deposition of a robust thin-film of Pd with excellent grain structures on stainless steel substrate. The surfactant, DTAB at concentration of 4×CMC controls the Pd grain size and grain size distribution effectively. The particle sizes were found in the range of 0.05-1.00 μm. Addition of DTAB in Pd plating bath helped the Pd membrane become helium gas tight with shorter plating time and relatively smooth, uniform, and thinner Pd-film. Upon heat treatment, excellent grain agglomeration was observed in the SIEP membrane with significant grain fusion. Cross-sectional EDS analysis of the SIEP Pd membrane shows deep penetration of metals in the pores of up to 25 μm. XRD spectra confirmed the polycrystalline structure of the Pd-film after 18 hours of annealing at 500 °C under a hydrogen environment. Pd-composite membranes showed excellent permeability and selectivity for hydrogen with thermal stability under operation at 250 - 550 °C temperature. Moreover, one membrane, Pd 30, had undergone the thermal durability tests for over 1200 hours under H_2 atmosphere for temperature cycles at 300 - 450 °C and 15 psi transmembrane pressure drop. N_2 gas was introduced periodically to check whether any pinhole has

formed in the membrane. Up to 1200 hours, the membrane performed with infinite selectivity, but all of a sudden, the membranes selectivity came down to 18. Post process characterization was carried out with SEM analysis, which showed some pinholes on the membrane surface. Another membrane, P 32 with a diffusion barrier on the substrate surface performed 408 hours with good hydrogen permeability and infinite selectivity. SEM images of post tested Pd 32 membrane show that there is no pinhole on the surface of the Pd-film.

5.1 Future Works and Recommendations

Membranes fabricated by SIEP technique give better permeability, selectivity, and long term thermal stability. These membranes require thinner Pd-film. SIEP process also requires considerable reduced fabrication cost. It is time now to identify the actual surfactant concentration which will provide the optimum surface activity. To demonstrate the technical viability of the Pd membrane, the following works are suggested to be carried out:

1. Fundamental studies on bath kinetics would be helpful to choose suitable complexing agent, operating conditions and appropriate bath recipe during Pd membrane development, which will ultimately results a thin film Pd membrane with superior selectivity under extreme process conditions. Co-ordination of Pd^{+2}/EDTA could be extended to understand the actual grain growth kinetics in presences of different complexes during surfactant induced electroless process. It is also necessary to reveal the role of pH on complexation and further bath stabilization process. Study of bath kinetics for Pd-bath will give important clues

how the surfactant interacts with other chemicals during deposition period. Intermediate SEM and XRD analysis of Pd membrane morphology deposited at shorter time intervals would further explain the effect of complex on in-situ grain formation and grain distribution.

2. The SIEP process can be applied to the Pd-alloy films, such as, Pd-Ni and Pd-Au and some tertiary palladium alloys such as Pd-Ru-In, Pd-Ag-Ru and Pd-Ag-Rh should be fabricated with proper alloy compositions that would be thermally stable and resist H_2 embrittlement during long term thermal cycling operation in extreme conditions.
3. Gas transport mechanism of the membrane can be modeled using Aspen plus software.
4. The determination of cause of pinhole formation and leak growth rates under pure H_2 testing is essential for the Pd membrane. Molecular simulation can be applied to investigate the pinhole formation with time in the Pd-film of the membranes.
5. Monte Carlo simulations can be used to observe the grain growth of thin Pd-films.
6. Finally, scale up of our work has to be under taken for proto type development.

REFERENCES

[1] Chen, C. and Gobina, E., "Ultra-thin palladium technologies enable future commercial deployment of PEM fuel cell systems," *Membrane Technology,* **2010**, 8 (2010).

[2] Kitiwan, M. and Atong, D., "Effects of porous alumina support and plating time on electroless plating of palladium membrane," *Journal of Materials Science & Technology,* **26**, 1148 (2009).

[3] Rahman, M. M., "Fabrication of Pd and Pd-Ag membranes by surfactant induced electroless plating (SIEP)," MS Thesis, Chemical and Bioengineering, North Carolina A & T State University, Greensboro, NC (2010).

[4] Adhikari, S. and Fernando, S., "Hydrogen membrane separation techniques," *Industrial & Engineering Chemistry Research,* **45**, 875 (2006).

[5] Ayturk, M. E., Mardilovich, I. P., Engwall, E. E., and Ma, Y. H., "Synthesis of composite Pd-porous stainless steel (PSS) membranes with a Pd/Ag intermetallic diffusion barrier," *Journal of Membrane Science,* **285**, 385 (2006).

[6] Yan, H. and Roland, D., "Preparation and characterization of palladium alloy composite membranes with a diffusion barrier for hydrogen separation," *Journal of Membrane Science,* **282**, 15 (2006).

[7] Gao, H., Lin, Y. S., Li, Y., and Zhang, B., "Chemical stability and its improvement of palladium based metallic membranes," *Industrial & Engineering Chemistry Research,* **43**, 11 (2004).

[8] Timothy, L. and Ward, T. D., "Model of hydrogen permeation behavior in palladium membranes," *Journal of Membrane Science,* **153**, 21 (1999).

[9] Li, X., Liu, T. M., Huang, D., Fan, Y. Q., and Xu, N. P., "Preparation and characterization of ultrathin palladium membranes," *Industrial & Engineering Chemistry Research,* **48**, 5 (2009).

[10] Yun, S. and Oyama, T. S., "Correlations in palladium membranes for hydrogen separation: A review," *Journal of Membrane Science,* **375**, 28 (2011).

[11] Islam, M. S., Rahman, M. M., and Ilias, S., "Characterization of Pd–Cu membranes fabricated by surfactant induced electroless plating (SIEP) for hydrogen separation," *International Journal of Hydrogen Energy,* **37**, 3477 (2012).

[12] Roland, D., Volker, H., and Kristian, D., "Membrane reactors for hydrogenation and dehydrogenation processes based on supported palladium," *Journal of Molecular Catalysis A,* **173**, 50 (2001).

[13] Gimeno, M. P., Wu, Z. T., Soler, J., Herguido, J., Li, K., and Menéndez, M., "Combination of a two-zone fluidized bed reactor with a Pd hollow fibre membrane for catalytic alkane dehydrogenation," *Chemical Engineering Journal,* **155**, 298 (2009).

[14] Bi, Y., Xu, H., Li, W., and Goldbach, A., "Water–gas shift reaction in a Pd membrane reactor over $Pt/Ce0.6ZrO.4O_2$ catalyst," *International Journal of Hydrogen Energy,* **34**, 2965 (2009).

[15] Shi, L., Goldbach, A., Zeng, G., and Xu, H., "Direct H_2O_2 synthesis over Pd membranes at elevated temperatures," *Journal of Membrane Science,* **348**, 160 (2010).

[16] Tong, J., Matsumura, Y., Suda, H., and Haraya, K., "Experimental study of steam reforming of methane in a thin (6 μm) Pd-based membrane reactor," *Industrial & Engineering Chemistry Research,* **44**, 12 (2005).

[17] Ilias, S. and Islam, M. A., "Methods of preparing thin films by electroless plating," United States Patent, (2010).

[18] Grashoff, G. J., Pilkington, C. E., and Corti, C. W., "The purification of hydrogen," *Platinum Metals Review,* **27**, 157 (1983).

[19] Ho, W. S. W. and Sirkar, K. K., Membrane Handbook, New York, Chapman & Hall, (1992).

[20] Islam, M. A., "The development of improved electroless plating in fabricating Pd-based membrane and membrane reactor application for hydrogen separation," PhD Dissertation, Energy and Environmental Studies, North Carolina A & T State University, Greensboro, NC (2008).

[21] Hsieh, H. P., Inorganic Membranes for Separation and Reaction, New York, ELSEVIER, (1996).

[22] Lu, G. Q., Costa, J. C. D. D., Duke, M., Giessler, S., Socolow, R., Williams, R. H., and Kreutz, T., "Inorganic membranes for hydrogen production and purification: a critical review and perspective," *J Colloid Interface Sci,* **314**, 589 (2007).

[23] Razima, S. S., Alexander, S. M., and Arvind, V., "Pd-composite membranes prepared by electroless plating and osmosis: synthesis, characterization and properties," *Separation and Purification Technology,* **25**, 18 (2001).

[24] Bose, A. C., Inorganic membranes for energy and fuel applications, Springer, (2009).

[25] Ismail, A. F. and David, L. I. B., "A review on the latest development of carbon membranes for gas separation," *Journal of Membrane Science,* **193**, 18 (2001).

[26] Shu, J., Grandjean, B. P. A., Neste, A. V., and Kaliaguine, S., "Catalytic palladium-based membrane reactors: A review," *The Canadian Journal of Chemical Engineering,* **69**, 1036 (1991).

[27] Lewis, F. A., The Palladium Hydrogen System, New York, Academic Press, (1967).

[28] Ayturk, M. E., "Synthesis, annealing strategies and in-situ characterization of thermally stable composite thin Pd/Ag alloy membranes for H_2 separation," PhD Dissertation, Department of Chemical Engineering, Worcester Polytechnic Institute, Worcester, MA 01609 (2007).

[29] William D. Callister, I., Materials science and engineering an introduction, John Wiley & Sons, (1994).

[30] Massalski, T. B., Okamoto, H., Subramanian, P. R., and Kacprzak, L., in *Binary Alloy Phase Diagrams*. vol. 3, ed: ASM International, (1990).

[31] Chen, Y., Atago, T., and Mohri, T., "First-principles study for ordering and phase separation in the Fe-Pd system," *Journal of Physics: Condensed Matter,* **14**, 1903 (2002).

[32] Ayturk, M. E., Engwall, E. E., and Ma, Y. H., "Microstructure analysis of the intermetallic diffusion-induced alloy phases in composite Pd/Ag/porous stainless steel membranes," *Industrial and Engineering Chemistry Research,* **46**, 4295 (2007).

[33] Bryden, K. J. and Ying, J. Y., "Nanostructured palladium-iron membranes for hydrogen separation and membrane hydrogenation reactions," *Journal of Membrane Science,* **203**, 29 (2002).

[34] Shu, J., Adnot, A., Grandjean, B. P. A., and Kaliaguine, S., "Structurally stable composite Pd-Ag alloy membranes: introduction of a diffusion barrier," *Thin Solid Films,* **286**, 72 (1996).

[35] Nam, S. E. and Lee, K. H., "Hydrogen separation by Pd alloy composite membranes: introduction of diffusion barrier," *Journal of Membrane Science,* **192**, 177 (2001).

[36] Rosenthal, P. A., Duncan, W. M., and Woollam, J. A., "In situ process diagnostics and intelligent materials processing. symposium," in *In Situ Process Diagnostics and Intelligent Materials Processing. Symposium,*, Warrendale, PA, USA, (1998).

[37] Uemiya, S., Sato, N., Ando, H., Kude, Y., Matsuda, T., and Kikuchi, E., "Separation of hydrogen through palladium thin film supported on a porous glass tube," *Journal of Membrane Science,* **56**, 303 (1991).

[38] Ma, Y. H., Mardilovich, I. P., Engwall, E. E., Ceylan, A. B., Ayturk, M. E., and Guazzone, F., "Characterization of intermetallic diffusion barrier and alloy formation for Pd/Cu and Pd/Ag porous stainless steel composite membranes," *Industrial and Engineering Chemistry Research,* **43**, 2936 (2004).

[39] Uemiya, S., Matsuda, T., and Kikuchi, E., "Hydrogen permeable palladium-silver alloy membrane supported on porous ceramics," *Journal of Membrane Science,* **56**, 315 (1991).

[40] Shu, J., Bongondo, B. E. W., Grandjean, B. P. A., Adnot, A., and Kaliaguine, S., "Surface segregation of Pd-Ag membranes upon hydrogen permeation," *Surface Science,* **291**, 129 (1993).

[41] Li, A., Liang, W., and Hughes, R., "Characterisation and permeation of palladium/stainless steel composite membranes," *Journal of Membrane Science,* **149**, 259 (1998).

[42] Cheng, Y. S. and Yeung, K. L., "Palladium-silver composite membranes by electroless plating technique," *Journal of Membrane Science,* **158**, 127 (1999).

[43] Keuler, J. N. and Lorenzen, L., "Developing a heating procedure to optimise hydrogen permeance through Pd-Ag membranes of thickness less than 2.2 μm," *Journal of Membrane Science,* **195**, 203 (2002).

[44] Huang, T. C., Wei, M. C., and Chen, H. I., "Preparation of hydrogen-permselective palladium-silver alloy composite membranes by electroless co-deposition," *Separation and Purification Technology,* **32**, 239 (2003).

[45] Ma, Y. H., Mardilovich, P. P., and She, Y., "Hydrogen gas-extraction module and method of fabrication," United States Patent, (2000).

[46] Ma, Y. H., Mardilovich, I. P., and Engwall, E. E., "Composite gas separation modules having intermediate porous metal layers," United States Patent, (2007).

[47] Tong, J., Shirai, R., Kashima, Y., and Matsumura, Y., "Preparation of a pinhole-free Pd-Ag membrane on a porous metal support for pure hydrogen separation," *Journal of Membrane Science,* **260**, 84 (2005).

[48] Ma, Y. H., Mardilovich, I. P., and Engwall, E. E., "Thin composite palladium and palladium/alloy membranes for hydrogen separation," *Annals of the New York Academy of Sciences,* **984**, 346 (2003).

[49] Islam, M. A. and Ilias, S., "Characterization of Pd-composite membrane fabricated by surfactant induced electroless plating (SIEP): Effect of grain size on hydrogen permeability," *Separation Science and Technology,* **45**, 1886 (2010).

[50] Mallory, G. O. and Hajdu, J. B., Electroless plating: fundamentals and applications, New York, William Andrew Publishing/Noyes, (1990).

[51] Rhoda, R. N. and Madison, A. M., "Palladium plating by chemical reduction," United States Patent, (1959).

[52] Ayturk, M. E. and Ma, Y. H., "Electroless Pd and Ag deposition kinetics of the composite Pd and Pd/Ag membranes synthesized from agitated plating baths," *Journal of Membrane Science,* **330**, 233 (2009).

[53] Ayturk, M. E., Mardilovich, I. P., Engwall, E. E., and Ma, Y. H., "Synthesis of composite Pd-porous stainless steel (PSS) membranes with a Pd/Ag intermetallic diffusion barrier," *Journal of Membrane Science,* **285**, 385 (2006).

[54] Yeung, K. L., Sebastian, J. M., and Varma, A., "Novel preparation of Pd/Vycor composite membranes," *Catalysis Today,* **25**, 231 (1995).

[55] Paglieri, S. and Way, J., "Innovations in palladium membrane research," *Separation & Purification Methods,* **31**, 1 (2002).

[56] Muller, K. H., "Dependence of thin-film microstructure on deposition rate by means of a computer simulation," *Journal of Applied Physics,* **58**, 2573 (1985).

[57] Kirchheim, R., Muetschele, T., Kieninger, W., Gleiter, H., Birringer, R., and Koble, T. D., "Hydrogen in amorphous and nanocrystalline metals," *Materials science and engineering,* **99**, 457 (1988).

[58] Gleiter, H., "Nanocrystalline materials," *Progress in Materials Science,* **33**, 223 (1989).

[59] Chen, B. H., Hong, L., Ma, Y., and Ko, T. M., "Effects of surfactants in an electroless nickel-plating bath on the properties of Ni-P alloy deposits," *Industrial and Engineering Chemistry Research,* **41**, 2668 (2002).

[60] Nwosu, N., Davidson, A., Hindle, C., and Barker, M., "On the influence of surfactant incorporation during electroless nickel plating," *Industrial & Engineering Chemistry Research,* **51**, 5635 (2012).

[61] Koji, O. and Shigeru, T., "Micellar electrokinetic chromatography," *Bull. chem. Soc. Jpn,* **71**, 17 (1998).

[62] Aixing, F., Somasundaran, P., and Turro, N. J., "Adsorption of alkyltrimethylammonium bromides on negatively charged alumina," *Langmuir,* **13**, (1997).

[63] Mardilovich, P. P., She, Y., Ma, Y. H., and Rei, M. H., "Defect-free palladium membranes on porous stainless-steel support," *AIChE Journal,* **44**, 310 (1998).

[64] Li, A., Grace, J. R., and Lim, C. J., "Preparation of thin Pd-based composite membrane on planar metallic substrate," *Journal of Membrane Science,* **306**, 159 (2007).

[65] Ayturk, M. E., Engwall, E. E., and Ma, Y. H., "Microstructure analysis of the intermetallic diffusion-induced alloy phases in composite Pd/Ag/porous stainless steel membranes," *Industrial & Engineering Chemistry Research,* **46**, 4295 (2007).

[66] Zhang, K., Gao, H., Rui, Z., Liu, P., Li, Y., and Lin, Y. S., "High-temperature stability of palladium membranes on porous metal supports with different intermediate layers," *Industrial & Engineering Chemistry Research,* **48**, 1880 (2009).

[67] Okazaki, J., Ikeda, T., Tanaka, D. P., Sato, K., Suzuki, T. M., and Mizukami, F., "An investigation of thermal stability of thin palladium–silver alloy membranes for high temperature hydrogen separation," *Journal of Membrane Science,* **366**, 212 (2011).

[68] Wu, L. Q., Xu, N., and Shi, J., "Preparation of a palladium composite membrane by an improved electroless plating technique," *Industrial & Engineering Chemistry Research,* **39**, 7 (2000).

[69] Hu, X., Yu, J., Song, J., Wang, X., and Huang, Y., "Toward low-cost Pd/ceramic composite membranes for hydrogen separation: A case study on reuse of the recycled porous Al_2O_3 substrates in membrane fabrication," *International Journal of Hydrogen Energy,* **36**, 15794 (2011).

[70] Collins, J. P. and Way, J. D., "Preparation and characterization of a composite palladium-ceramic membrane," *Industrial and Engineering Chemistry Research,* **32**, 3006 (1993).

[71] Caravella, A., Barbieri, G., and Drioli, E., "Modelling and simulation of hydrogen permeation through supported Pd-alloy membranes with a multicomponent approach," *Chemical Engineering Science,* **63**, 2149 (2008).

[72] Jemaa, N., Shu, J., Kaliaguine, S., and Grandjean, B. P. A., "Thin palladium film formation on shot peening modified porous stainless steel substrates," *Industrial & Engineering Chemistry Research,* **35**, 5 (1996).

[73] Tong, J., Shirai, R., Kashima, Y., and Matsumura, Y., "Preparation of a pinhole-free Pd–Ag membrane on a porous metal support for pure hydrogen separation," *Journal of Membrane Science,* **260**, 84 (2005).

[74] Huang, Y. and Dittmeyer, R., "Preparation of thin palladium membranes on a porous support with rough surface," *Journal of Membrane Science,* **302**, 160 (2007).

[75] Shi, Z. and Szpunar, J. A., "Synthesis of an ultra-thin palladium membrane for hydrogen extraction," *Rev.Adv.Mater.Sci. ,* **15**, 9 (2007).

[76] Samingprai, S., Tantayanon, S., and Ma, Y. H., "Chromium oxide intermetallic diffusion barrier for palladium membrane supported on porous stainless steel," *Journal of Membrane Science,* **347**, 8 (2010).

[77] Zahedi, M., Afra, B., Mobarake, M. D., and Bahmani, M., "Preparation of a Pd membrane on a WO_3 modified porous stainless steel for hydrogen separation," *Journal of Membrane Science,* **333**, 45 (2009).

[78] Bosko, M. L., Ojeda, F., Lombardo, E. A., and Cornaglia, L. M., "NaA zeolite as an effective diffusion barrier in composite Pd/PSS membranes," *Journal of Membrane Science,* **331**, 57 (2009).

[79] Peters, T. A., Tucho, W. M., Ramachandran, A., Stange, M., Walmsley, J. C., Holmestad, R., Borg, A., and Bredesen, R., "Thin Pd–23%Ag/stainless steel composite membranes: long-term stability, life-time estimation and post-process characterisation," *Journal of Membrane Science,* **326**, 572 (2009).

[80] Bosko, M. L., Miller, J. B., Lombardo, E. A., Gellman, A. J., and Cornaglia, L. M., "Surface characterization of Pd–Ag composite membranes after annealing at various temperatures," *Journal of Membrane Science,* **369**, 267 (2011).

[81] Lin, Y. M. and Rei, M. H., "Study on the hydrogen production from methanol steam reforming in supported palladium membrane reactor," *Catalysis Today* **67**, 8 (2001).

[82] Shirasaki, Y., Tsuneki, T., Ota, Y., Yasuda, I., Tachibana, S., Nakajima, H., and Kobayashi, K., "Development of membrane reformer system for highly efficient hydrogen production from natural gas," *International Journal of Hydrogen Energy,* **34**, 4482 (2009).

[83] Guazzone, F. and Ma, Y. H., "Leak growth mechanism in composite Pd membranes prepared by the electroless deposition method," *AIChE Journal,* **54**, 487 (2008).

[84] Roa, F. and Way, J. D., "Influence of alloy composition and membrane fabrication on the pressure dependence of the hydrogen flux of palladium-copper membranes," *Industrial & Engineering Chemistry Research,* **42**, (2003).

[85] Kulprathipanja, A., Alptekin, G. O., Falconer, J. L., and Way, J. D., "Effects of water gas shift gases on Pd-Cu alloy membrane surface morphology and separation properties," *Industrial & Engineering Chemistry Research,* **43**, 4188 (2004).

[86] Hou, K., "Preparation of thin and highly stable Pd/Ag composite membranes and simulative analysis of transfer resistance for hydrogen separation," *Journal of Membrane Science,* **214**, 43 (2003).

[87] Pan, X. L., Stroh, N., Brunner, H., Xiong, G. X., and Sheng, S. S., "Pd/ceramic hollow fibers for H_2 separation," *Separation and Purification Technology,* **32**, 265 (2003).

[88] Li, H., Pieterse, J. Z., Dijkstra, J. W., Haije, W. G., Xu, H. Y., Bao, C., Van Den Brink, R. W., and Jansen, D., "Performance test of a bench-scale multi-tubular membrane reformer," *Journal of Membrane Science,* **373**, 43 (2011).

[89] Koch, C. C., Nanostructured materials processing, properties and potential applications, Willian Andrew publishing, (2006).